

CAPITAL UNIVERSITY OF SCIENCE AND
TECHNOLOGY, ISLAMABAD



Numerical Simulations of Heat and Mass Transfer Flows utilizing Nanofluid

by

Faisal Shahzad

A thesis submitted in partial fulfillment for the
degree of Doctor of Philosophy

in the

Faculty of Computing

Department of Mathematics

2020

**Numerical Simulations of Heat and Mass Transfer Flows
utilizing Nanofluid**

By

Faisal Shahzad
(DMT-143019)

Dr. Noor Fadiya Mohd Noor, Assistant Professor
University of Malaya, Kuala Lumpur, Malaysia
(Foreign Evaluator 1)

Dr. Fatma Ibrahim, Scientific Engineer
Technische Universität Dortmund, Germany
(Foreign Evaluator 2)

Dr. Muhammad Sagheer
(Thesis Supervisor)

Dr. Muhammad Sagheer
(Head, Department of Mathematics)

Dr. Muhammad Abdul Qadir
(Dean, Faculty of Computing)

DEPARTMENT OF MATHEMATICS
CAPITAL UNIVERSITY OF SCIENCE AND TECHNOLOGY
ISLAMABAD
2020

Copyright © 2020 by Faisal Shahzad

All rights reserved. No part of this thesis may be reproduced, distributed, or transmitted in any form or by any means, including photocopying, recording, or other electronic or mechanical methods, by any information storage and retrieval system without the prior written permission of the author.

Dedicated to my beloved father and adoring mother who remain alive within my
heart



CAPITAL UNIVERSITY OF SCIENCE & TECHNOLOGY ISLAMABAD

Expressway, Kahuta Road, Zone-V, Islamabad
Phone: +92-51-111-555-666 Fax: +92-51-4486705
Email: info@cust.edu.pk Website: <https://www.cust.edu.pk>

CERTIFICATE OF APPROVAL

This is to certify that the research work presented in the thesis, entitled “**Numerical Simulations of Heat and Mass Transfer Flows Utilizing Nanofluid**” was conducted under the supervision of **Dr. Muhammad Sagheer**. No part of this thesis has been submitted anywhere else for any other degree. This thesis is submitted to the **Department of Mathematics, Capital University of Science and Technology** in partial fulfillment of the requirements for the degree of Doctor in Philosophy in the field of **Mathematics**. The open defence of the thesis was conducted on **October 07, 2020**.

Student Name : Faisal Shahzad
(DMT143019)

The Examining Committee unanimously agrees to award PhD degree in the mentioned field.

Examination Committee :

(a) External Examiner 1: Dr. Saeed Islam, Professor
Abdul Wali Khan University,
Mardan

(b) External Examiner 2: Dr. Masood Khan,
Professor
QAU, Islamabad

(c) Internal Examiner : Dr. Muhammad Afzal
Assistant Professor
CUST, Islamabad

Supervisor Name : Dr. Muhammad Sagheer
Professor
CUST, Islamabad

Name of HoD : Dr. Muhammad Sagheer
Professor
CUST, Islamabad

Name of Dean : Dr. Muhammad Abdul Qadir
Professor
CUST, Islamabad

AUTHOR'S DECLARATION

I, **Faisal Shahzad (Registration No. DMT-143019)**, hereby state that my PhD thesis entitled, '**Numerical Simulations of Heat and Mass Transfer Flows Utilizing Nanofluid**' is my own work and has not been submitted previously by me for taking any degree from Capital University of Science and Technology, Islamabad or anywhere else in the country/ world.

At any time, if my statement is found to be incorrect even after my graduation, the University has the right to withdraw my PhD Degree.



(Faisal Shahzad)

Dated: 07 October, 2020

Registration No : DMT-143019

PLAGIARISM UNDERTAKING

I solemnly declare that research work presented in the thesis titled “**Numerical Simulations of Heat and Mass Transfer Flows Utilizing Nanofluid**” is solely my research work with no significant contribution from any other person. Small contribution/ help wherever taken has been duly acknowledged and that complete thesis has been written by me.

I understand the zero tolerance policy of the HEC and Capital University of Science and Technology towards plagiarism. Therefore, I as an author of the above titled thesis declare that no portion of my thesis has been plagiarized and any material used as reference is properly referred/ cited.

I undertake that if I am found guilty of any formal plagiarism in the above titled thesis even after award of PhD Degree, the University reserves the right to withdraw/ revoke my PhD degree and that HEC and the University have the right to publish my name on the HEC/ University Website on which names of students are placed who submitted plagiarized thesis.



(Faisal Shahzad)

Dated: 07 October, 2020

Registration No : DMT-143019

List of Publications

It is certified that following publication(s) have been made out of the research work that has been carried out for this thesis:-

1. **F. Shahzad**, M. Sagheer, and S. Hussain, “Numerical simulation of magnetohydrodynamic Jeffrey nanofluid flow and heat transfer over a stretching sheet considering Joule heating and viscous dissipation,” *AIP Advances*, vol. 8, pp. 065316 (2018), DOI: 10.1063/1.5031447.
2. **F. Shahzad**, M. Sagheer, and S. Hussain, “MHD tangent hyperbolic nanofluid with chemical reaction, viscous dissipation and Joule heating effects,” *AIP Advances*, vol. 9, pp. 025007 (2019), DOI: 10.1063/1.5054798.
3. **F. Shahzad**, M. Sagheer, and S. Hussain, “Numerical solution of rotating flow of a nanofluid over a stretching surface in the presence of magnetic field,” *Journal of Nanofluids*, vol. 8, no 2, pp. 359-370 (2019), DOI: 10.1166/jon.2019.1578.

Faisal Shahzad

DMT-143019

Acknowledgements

I begin with the name of almighty **ALLAH**, who bestowed countless blessings upon me to accomplish the requirements for this thesis. Over and above everything else, it gives the greatest satisfaction as I offer my humblest words to thank the almighty ALLAH and millions of Darood-o-Salaam on the Holy Prophet **Hazrat Muhammad (Sallallahu AlaihayWa'alihi wasalam)** who is always a torch of guidance for humanity.

I really feel great honour to manifest my immense gratitude as well as profound thanks to my learned and worthy supervisor **Prof. Dr. Muhammad Sagheer** for his guidance, assistance, continuous encouragement, enthusiastic interest and constructive criticism throughout this research. Indeed, it is a matter of pride and privilege for me to be his PhD student. Without his generous help, the completion of this work would not have been possible. I would like to express my earnest thanks and incalculable respect to **Dr. Shafqat Hussain**. His valuable advice, learned guidance and timely suggestions helped me to bring my thesis into this final form.

I would like to extend my appreciation to **Dr. Rashid Ali, Dr. Abdur Rehman Kashif** and the rest of the faculty members of mathematics department for their moral support during my stay.

My most sincere and warm wishes to my friends especially Aftab, Yasir, Tahir, Junaid, Khalid, Tanveer and Atif. Honest and heartiest salutations are due to my **Parents** and siblings whose life long toil and nature made me what I am today. And last but not least the support, sacrifice and sharing of difficult moments from my wife is unforgettable. May Almighty Allah shower his blessings and prosperity on all those who assisted me during the completion of this thesis.

Abstract

In this dissertation, the nanofluid flow with the heat and mass transfer for various models of fluids is analyzed. The flows are induced over stretching sheet and two infinite plates. The important quantities such as magneto hydrodynamics, viscous dissipation, Joule heating, chemical reaction, Brownian motion and thermophoresis are incorporated for physical consideration. The MHD Jeffrey nanofluid flow and heat transfer over a stretching sheet considering the Joule heating and viscous dissipation is analyzed. The motion of a non-Newtonian tangent hyperbolic nano fluid past a stretching sheet is also investigated. Further, the effects of chemical reaction, viscous dissipation and Joule heating are also contemplated for the problem. Magnetic field is implemented in vertical direction under the assumption of low magnetic Reynolds number. Moreover, an elaborated evaluation is presented for the stratified MHD Jeffrey nanofluid flow towards a stretching surface in the presence of gyrotactic micro-organisms. And finally the numerical solution of rotating flow of a nanofluid over a stretching surface in the presence of magnetic field. To model the system of partial differential equations, different emerging laws of Physics are used. To convert the system of partial differential equations into the ordinary differential equations, some suitable transformations named as the similarity transformations are utilized. Further, utilizing the Keller box method and shooting technique, the system of ordinary differential equations has been solved with the help of the computational software MATLAB to compute the numerical results. The numerical solution obtained for the velocity, temperature, concentration and density of the motile micro-organisms profiles has been presented through graphs for different choices of the physical parameters. The numerical values of the skin friction, Nusselt, Sherwood and local density number of the motile micro-organisms have also been presented and analyzed through tables. A comparison with the previously available literature in limiting cases is also performed to strengthen the reliability of the code. To further strengthen the reliability of our MATLAB code, the results presented in the previously published articles are reproduced successfully.

Contents

Author’s Declaration	v
Plagiarism Undertaking	vi
List of Publications	vii
Acknowledgements	viii
Abstract	ix
List of Figures	xiii
List of Tables	xvi
Abbreviations	xvii
Symbols	xviii
1 Introduction	1
1.1 Introduction	1
1.2 Background	1
1.3 Problem Identification	9
1.4 Research Objectives	10
1.5 Scope of Research	10
1.6 Significance of Research	11
1.7 Thesis Outline	11
2 Fundamental Laws and Solution Methodology	13
2.1 Introduction	13
2.2 Types of Fluid Flow [87, 88]	13
2.2.1 Steady and Unsteady Flows	14
2.2.2 Uniform and Non-uniform Flows	14
2.2.3 Laminar and Turbulent Flows	14
2.2.4 One Two and Three Dimensional Flow	15
2.2.5 Compressible and Incompressible Flows	15

2.2.6	Rotational and Irrotational Flows	15
2.3	Boundary Layer Theory [89]	16
2.4	Significant Dimensionless Numbers [90–92]	17
2.4.1	Reynolds Number	18
2.4.2	Prandtl Number	18
2.4.3	Lewis Number	19
2.4.4	Eckert Number	19
2.4.5	Skin Friction Coefficient	19
2.4.6	Nusselt Number	20
2.4.7	Sherwood Number	20
2.4.8	Weissenberg Number [93]	21
2.4.9	Deborah Number	21
2.5	Heat Transfer [94]	21
2.5.1	Convection	22
2.5.2	Conduction	22
2.5.3	Radiation	22
2.6	Mass Transfer [94]	23
2.7	Classification of Fluids [95]	23
2.7.1	Ideal Fluid	23
2.7.2	Real Fluid	24
2.7.3	Newtonian Fluid	24
2.7.4	Non-Newtonian Fluid	25
2.8	Nanofluids [96]	27
2.9	Brownian Motion	28
2.10	Thermophoresis	28
2.11	Viscous Dissipation [97]	28
2.12	Joule Heating [98]	29
2.13	Magnetohydrodynamics [99, 100]	29
2.14	Basic Laws	30
2.14.1	Conservation of Mass [101]	30
2.14.2	Momentum Equation	30
2.14.3	Energy Conservation	31
2.14.4	Conservation Law of Concentration	32
2.14.5	Microorganism Transport Equation	32
2.15	Mathematical Description of some Fluid Models [101, 102]	33
2.15.1	Viscous Fluid	33
2.15.2	Jeffrey Fluid [103]	33
2.15.3	Tangent Hyperbolic Fluid [104]	34
2.16	Solution Methodologies	35
2.16.1	Keller Box Method [105–107]	35
2.16.2	Shooting Method [108]	42
3	Numerical Simulation of MHD Jeffrey Nanofluid Flow and Heat Transfer over a Stretching Sheet	45

3.1	Introduction	45
3.2	Mathematical Formulation	46
3.3	Solution Methodology	49
3.4	Results and Discussions	54
3.5	Concluding Remarks	62
4	MHD Tangent Hyperbolic Nanofluid with Chemical Reaction, Viscous Dissipation and Joule Heating Effects	64
4.1	Introduction	64
4.2	Mathematical Formulation	65
4.3	Numerical Procedure	67
4.4	Results and Discussions	73
4.5	Concluding Remarks	80
5	Stratified MHD Jeffrey Nanofluid Flow with Gyrotactic Microorganisms past a Stretching Surface	82
5.1	Introduction	82
5.2	Mathematical Formulation	83
5.3	Numerical Solution by Keller Box Method	86
5.4	Results and Discussions	92
5.5	Concluding Remarks	101
6	MHD Rotating Flow of Nanofluid past a Stretching Sheet	103
6.1	Introduction	103
6.2	Mathematical Formulation	104
6.3	Solution Methodology	108
6.4	Results and Discussion	109
6.5	Conclusions	119
7	Conclusion	121
7.1	Conclusion	121
7.2	Future Recommendations	123
	Bibliography	124

List of Figures

2.1	The blowup of the boundary layer shows the flow's velocity profile above the separation point.	16
2.2	Rheological behaviour of materials.	24
2.3	Rheological behaviour of non-Newtonian fluids.	26
2.4	Flow diagram of the present technique.	36
2.5	Grid structure for difference approximations.	37
3.1	Geometry of the problem.	46
3.2	Typical grid structure for difference approximations.	50
3.3	Velocity field for various types of nanofluids.	58
3.4	Temperature field for various types of nanofluids.	58
3.5	Velocity field corresponding to various values of ϕ	58
3.6	Temperature field corresponding to various values of ϕ	58
3.7	Velocity profile corresponding to various values of Deborah number β	59
3.8	Temperature profile corresponding to various values of Deborah number β	59
3.9	The velocity profile $f''(0)$ for various values of β	59
3.10	The temperature profile θ for different values of Pr and β	59
3.11	Temperature distribution for different values of Ec and β	60
3.12	variation of the local Nusselt number against Ec for various values of β	60
3.13	Variation of Nusselt number against β for various values of M	60
3.14	Variation of skin friction coefficient against β for various values of M	60
3.15	Variation of skin friction coefficient against ϕ for various values of M	61
3.16	Variation of skin friction coefficient against ϕ for various values of β	61
3.17	Variation of Nusselt number against ϕ for various values of Ec	61
3.18	Variation of Nusselt number against ϕ for various values of Pr	61
3.19	Variation of skin friction coefficient against ϕ for various values of M	62
3.20	Variation of skin friction coefficient against ϕ for various values of β	62
4.1	Geometry of the problem.	65
4.2	Velocity plot $f'(\eta)$ for assorted values of magnetic parameter M	76
4.3	Velocity plot $f'(\eta)$ for assorted values of power-law index n	76
4.4	Velocity plot $f'(\eta)$ for assorted values of Weissenberg number We	76
4.5	Temperature plot $\theta(\eta)$ for assorted values of magnetic parameter M	76

4.6	Temperature plot $\theta(\eta)$ for assorted values of Prandtle Pr .	77
4.7	Temperature plot $\theta(\eta)$ for assorted values of Eckert Ec .	77
4.8	Temperature plot $\theta(\eta)$ for assorted values of Nt .	77
4.9	Temperature plot $\theta(\eta)$ for assorted values of Nb .	77
4.10	Concentration plot $\phi(\eta)$ for assorted values of Nb .	78
4.11	Concentration plot $\phi(\eta)$ for assorted values of Nt .	78
4.12	Concentration plot $\phi(\eta)$ for assorted values of Le .	78
4.13	Concentration plot $\phi(\eta)$ for assorted values of $\gamma > 0$.	78
4.14	Concentration plot $\phi(\eta)$ for assorted values of $\gamma < 0$.	78
4.15	Influence of M and We on drag coefficient.	79
4.16	Influence of M and n on drag coefficient.	79
4.17	Influence of Nb and Pr on local Nusselt number $-\theta'(0)$.	79
4.18	Influence of Nt and Pr on local Nusselt number $-\theta'(0)$.	79
4.19	Influence of Nt and Le on local Sherwood number $-\phi'(0)$.	79
4.20	Influence of Nb and Le on local Sherwood number $-\phi'(0)$.	79
5.1	Physical model of the flow.	83
5.2	Influence of M on $f'(\eta)$.	97
5.3	Influence of β on $f'(\eta)$.	97
5.4	Influence of λ_1 on $f'(\eta)$.	97
5.5	Influence of Pr on $\theta(\eta)$.	97
5.6	Influence of Ec on $\theta(\eta)$.	97
5.7	Influence of β on $\theta(\eta)$.	97
5.8	Influence of Nt on $\theta(\eta)$.	98
5.9	Influence of Nb on $\theta(\eta)$.	98
5.10	Influence of St on $\theta(\eta)$.	98
5.11	Influence of Nb on $\phi(\eta)$.	98
5.12	Influence of Nt on $\phi(\eta)$.	98
5.13	Influence of Le on $\phi(\eta)$.	98
5.14	Influence of Sc on $\phi(\eta)$.	99
5.15	Influence of Pe on $\chi(\eta)$.	99
5.16	Influence of Lb on $\chi(\eta)$.	99
5.17	Influence of σ on $\chi(\eta)$.	99
5.18	Influence of Sm on $\chi(\eta)$.	99
5.19	Influence of β on $f''(0)$ for different values of M .	99
5.20	Influence of Ec on $-\theta'(0)$ for different values of β .	100
5.21	Influence of Nt on $-\phi'(0)$ for different values of Nb .	100
5.22	Influence of Le on $-\phi'(0)$ for different values of Nb .	100
5.23	Variation of $-\chi'(0)$ against Lb for different values of Pe .	100
5.24	Variation of $-\chi'(0)$ against Lb for different values of σ .	100
6.1	Geometry of the problem.	104
6.2	Impact of ϕ on $f'(\eta)$ when $\delta_1 = \delta_2 = \delta_3 = 2, S = 1$.	114
6.3	Impact of ϕ on $g(\eta)$ when $\delta_1 = \delta_2 = \delta_3 = 2, S = 1$.	114
6.4	Impact of ϕ on $\theta(\eta)$ when $\delta_1 = \delta_2 = \delta_3 = 2, S = 1$.	114

6.5	Impact of S on $f'(\eta)$ for copper-water nanofluid when $\delta_1 = \delta_2 = \delta_3 = 2, \phi = 0.2$.	114
6.6	Impact of S on $g(\eta)$ for copper-water nanofluid when $\delta_1 = \delta_2 = \delta_3 = 2, \phi = 0.2$.	114
6.7	Impact of S on $\theta(\eta)$ for copper-water nanofluid when $\delta_1 = \delta_2 = \delta_3 = 2, \phi = 0.2$.	114
6.8	Impact of δ_1 on $f'(\eta)$ for copper-water nanofluid when $\delta_2 = 0.2, \delta_3 = 0, \phi = 0.2, S = 5$.	115
6.9	Impact of δ_1 on $g(\eta)$ for copper-water nanofluid when $\delta_2 = 0.2, \delta_3 = 0, \phi = 0.2, S = 5$.	115
6.10	Impact of δ_1 on $\theta(\eta)$ for copper-water nanofluid when $\delta_2 = 0.2, \delta_3 = 0, \phi = 0.2, S = 5$.	115
6.11	Impact of δ_2 on $f'(\eta)$ for copper-water nanofluid when $\delta_1 = 0.2, \delta_3 = 0, \phi = 0.2, S = -3$.	115
6.12	Impact of δ_2 on $g(\eta)$ for copper-water nanofluid when $\delta_1 = 0.2, \delta_3 = 0, \phi = 0.2, S = -3$.	115
6.13	Impact of δ_2 on $\theta(\eta)$ for copper-water nanofluid when $\delta_1 = 0.2, \delta_3 = 0, \phi = 0.2, S = -3$.	115
6.14	Impact of δ_3 on $f'(\eta)$ for copper-water nanofluid when $\delta_1 = 2, \delta_2 = 2, \phi = 0.2, S = -1$.	116
6.15	Impact of δ_3 on $g(\eta)$ for copper-water nanofluid when $\delta_1 = 2, \delta_2 = 2, \phi = 0.2, S = -1$.	116
6.16	Impact of δ_3 on $\theta(\eta)$ for copper-water nanofluid when $\delta_1 = 2, \delta_2 = 2, \phi = 0.2, S = -1$.	116
6.17	Streamlines plot when $S = -1$.	116
6.18	Streamlines plot when $S = 0$.	116
6.19	Streamlines plot when $S = 1$.	116
6.20	Effects of ϕ and S on C_f at $\eta = 0$ when $\delta_1 = \delta_2 = \delta_3 = 0.5$.	117
6.21	Effects of ϕ and δ_1 on C_f at $\eta = 0$ when $\delta_2 = \delta_3 = 1.5, S = 1$.	117
6.22	Effects of ϕ and δ_2 on C_f at $\eta = 0$ when $\delta_1 = 2, \delta_3 = 1.5, S = 1$.	117
6.23	Effects of ϕ and δ_2 on C_f at $\eta = 0$ when $\delta_1 = 2, \delta_1 = 1, S = 1$.	117
6.24	Effects of ϕ and S on C_f at $\eta = 1$ when $\delta_1 = \delta_2 = \delta_3 = 0.5$.	117
6.25	Effects of ϕ and δ_1 on C_f at $\eta = 1$ when $\delta_2 = \delta_3 = 1.5, S = 1$.	117
6.26	Effects of ϕ and δ_2 on C_f at $\eta = 1$ when $\delta_1 = 2, \delta_3 = 1.5, S = 1$.	118
6.27	Effects of ϕ and δ_2 on C_f at $\eta = 1$ when $\delta_1 = 2, \delta_1 = 1, S = 1$.	118
6.28	Effects of ϕ and S on Nu_x at $\eta = 0$ when $\delta_1 = \delta_2 = \delta_3 = 0.5$.	118
6.29	Effects of ϕ and δ_1 on Nu_x at $\eta = 0$ when $\delta_2 = \delta_3 = 2, S = -1$.	118
6.30	Effects of ϕ and δ_2 on Nu_x at $\eta = 0$ when $\delta_1 = \delta_3 = 2, S = -1$.	118
6.31	Effects of ϕ and δ_3 on Nu_x at $\eta = 0$ when $\delta_1 = \delta_2 = 2, S = -1$.	118
6.32	Effects of ϕ and S on Nu_x at $\eta = 1$ when $\delta_1 = \delta_2 = \delta_3 = 0.5$.	119
6.33	Effects of ϕ and δ_1 on Nu_x at $\eta = 1$ when $\delta_2 = \delta_3 = 2, S = -1$.	119
6.34	Effects of ϕ and δ_2 on Nu_x at $\eta = 1$ when $\delta_1 = \delta_3 = 2, S = -1$.	119
6.35	Effects of ϕ and δ_3 on Nu_x at $\eta = 1$ when $\delta_1 = \delta_2 = 2, S = -1$.	119

List of Tables

3.1	Thermophysical properties of the base fluid and different nanoparticles[113].	48
3.2	Comparison of $-f''(0)$ with various values of M	54
3.3	Numerical values of $C_f Re_x^{1/2}$ and $Nu_x Re_x^{-1/2}$ for various values of parameters.	55
4.1	Comparison of $-f''(0)$ with various values of M	73
4.2	Values of $C_f Re_x^{1/2}$, $Nu_x^{-1/2}$ and $Sh_x^{-1/2}$ for various sorts of parameters in flow.	80
5.1	Variation of $-\theta'(0)$, $-\phi'(0)$ and $-\chi'(0)$ for different sorts of parameters in flow.	101
6.1	Thermophysical attributes of water, silver and copper nanoparticles[132].	106
6.2	Variation of $-g'(0)$ for different values of Ω at $Re = 1$ in case of $S_1 = S_2 = 0$	109
6.3	Values of skin friction coefficient and Nusselt number for the different values of rising parameters at lower/upper surface.	109
6.4	Values of C_f for the different values of rising parameters at lower surface.	110
6.5	Values of C_f for the different values of rising parameters at upper surface.	110
6.6	Values of Nu_x for the different values of rising parameters at lower surface.	111
6.7	Values of Nu_x for the different values of rising parameters at upper surface.	111

Abbreviations

IVP	initial value problem
BVP	boundary value problem
ODEs	ordinary differential equations
PDEs	partial differential equations
UCM	upper-convected Maxwell
MHD	Magnetohydrodynamics

Symbols

a	stretching rate
b	chemotaxis constant
B_0	strength of magnetic field
C	concentration
C_0	reference concentration
C_w	surface concentration
C_f	skin friction coefficient
c_p	specific heat
C_∞	ambient concentration
D	mass diffusivity
Dm	diffusivity of microorganisms
D_B	Brownian motion coefficient
D_T	thermophoresis diffusion coefficient
Ec	Eckert number
f	dimensionless stream function
$f'(\eta)$	non-dimensional velocity
$g(\eta)$	dimensionless velocity
Gr	mixed convection parameter
k	thermal conductivity
k_1	chemical reaction parameter
Le	Lewis number
Lb	bioconvection Lewis number
L	characteristic length

M	magnetic parameter
n	power law index
N	concentration of micro-organism
Nt	thermophoresis parameter
Nb	Brownian motion parameter
Nr	buoyancy ratio parameter
N_w	wall density of micro-organism
N_∞	ambient density of micro-organism
N_0	reference density of micro-organisms
Nu_x	Nusselt number
Pr	Prandtl number
Pe	bioconvection Peclet number
p^*	modified pressure
p	pressure
q_m	wall mass flux
q_w	wall heat flux
q_n	wall motile microorganisms flux
Re_x	Reynold number
Rb	bioconvection Rayeigh number
S	extra stress tensor
Sh_x	local Sherwood number
St	thermal stratification parameter
Sc	mass stratification parameter
Sm	motile density stratification parameter
T	temperature
T_o	reference temperature
T_w	surface temperature
T_∞	ambient temperature
T_0	lower temperture at upper wall
T_h	higher temperture at lower wall
U_w	stretching velocity

u, v, w	velocity components in x, y and z directions respectively
\mathbf{V}	velocity field
V_0	suction/injection velocity
We	Weissenberg number
W_c	constant maximum cell swimming speed
x, y, z	Cartesian coordinate
β	Deborah number
β^*	volume expansion coefficient
λ	relaxation time
λ_1	ratio of relaxation to retardation time
λ_2	retardation time
Γ	time constant
τ_w	shear stress
μ	dynamic viscosity
ν	kinematic viscosity
τ	heat capacity ratio
τ_{ij}	stress tensor
$\dot{\gamma}$	shear rate
γ	chemical reaction parameter
γ^*	average volume of microorganisms
σ_f	electrical conductivity
σ	bioconvection concentration difference
ρ	density
ρ_f	density of nanofluid
ρ_p	density of nanoparticles
ρ_m	density of microorganism
η	similarity variable
ψ	stream function
θ	dimensionless temperature
Ω	angular velocity
ϕ	rescaled nanoparticle volume fraction

χ	dimensionless density of micro-organism
Cu	copper
Ag	silver
H_2O	water
$C_2H_6O_2$	ethylene glycol
Al_2O_3	aluminium oxide
TiO_2	titanium dioxide

Subscripts

f	fluid phase
s	solid phase
nf	nanofluid

Chapter 1

Introduction

1.1 Introduction

This Chapter incorporates some necessary review associated with the Newtonian as well as non-Newtonian nanofluids over different sort of geometries. A brief background and significance of boundary layer nanofluid flow for a Jeffrey fluid, tangent hyperbolic fluid, rotating flow, magnetohydrodynamic flows, viscous dissipation and Joule heating effects, suction and injection effects, stretching sheet and bioconvection for heat and mass transport is given. Moreover it features a comprehensive literature review based on the problems taken into account in succeeding chapters. The problem identification, research objectives, scope, significance of research and the outline of all the chapters are also given within this chapter.

1.2 Background

The developments in the field of nanofluids have potential importance due to its excessive utilization in the real life and in modern heat and mass transport processes including domestic refrigerators, machining, hybrid-powered engines, microelectronics, grinding, heat exchangers, solar water heating, fuel cells, nuclear reactors, chillers, improving efficiency of diesel generators and pharmaceutical processes etc [1, 2]. Maxwell [3] added solid micrometer sized particles to the base fluids to enhance the thermal conductivity but it caused the

clogging, erosion in the pipes and rise in the pressure drop. The term nanofluid was first coined by Choi and Eastman [4–6]. These fluids are engineered by dispersing nanoparticles in the traditional fluids to boost the fluid's thermal conductivity. Nanoparticles have been formed from metals such as *Cu*, *Ag*, metal nitrides such as *SiN*, *AlN*, oxide ceramics such as *PbO*, *CuO*, carbide ceramics such as *CaC₂*, *TiC* and allotropes of carbon such as graphite, diamond, fullerene etc. To examine the heat transport enhancement by fine particles mounted in a fluid, many mathematical models can be formed in the literature. One of these is the Buongiorno model [7] that considers the fluids as well as the solid phase in the heat transport method. It is a non-homogeneous nanofluids equilibrium model which illustrates that the thermophoresis diffusion and Brownian movement are responsible for the rise in thermal conductivity. Another widely used model is the two-phase Tiwari and Das model [8] wherein the fluid phase as well as solid particles have been in equilibrium state having the similar local velocity. A number of issues arise while analyzing the heat transport enhancement employing the nanofluids. Such complications include the Brownian motion, gravity, layering at the boundary between solid and fluid, clustering of the particles and friction between the solid and liquid particles. Nanofluids are implemented to further improve the thermal conductivity of base liquids like water, glycerin, ethylene glycol and oil etc. Many researchers have investigated nanofluids for thermal conductivity enhancement [9–16]. Experimental study conducted by Lomascolo et al. [17] revealed that the thermal conductivity also depends on the concentration, size, shape and material of the nanoparticles.

The mathematical models for the motion of an incompressible Newtonian fluids [18] are catching the interest of a number of mathematicians over the time. The Newtonian fluids can be studied using the Navier-Stokes equations. They behave based on the law that shear stress is linearly related to rate of deformation. The viscosity of Newtonian fluids altered solely with temperature. The most familiar applications of Newtonian fluids are related to thin motor oil, alcohol, gasoline

and water etc. The last few decades, the non-Newtonian fluids have obtained an appreciable importance because the Navier-Stokes equations do not describe all the rheological properties of these fluids used in technology and industrial areas. However, the constitutive equations of these fluids are very complicated as compared with the Newtonian fluids. Accordingly, the non-Newtonian governing equations are highly non-linear than the Navier-Stokes equations and a single constitutive equation cannot describe all the properties of these kind of fluids. The flow behavior of non-Newtonian fluids has captivated the engineers and investigators in the past few decades in industrial sciences as well as engineering. Different from Newtonian fluids, these rheological fluids have been comprehensively utilized in many manufacturing and engineering processes. These processes include biomechanics, polymer processes, food production and enhanced oil recovery etc. Many constitutive equations are reported in literature to predict the features of non-Newtonian fluids. The non-Newtonian fluids have been divided into three categories namely the differential type, the rate type, and the integral type. The rate type of fluid models signifies the effect of relaxation and retardation time.

Among the non-Newtonian fluid models, the tangent hyperbolic fluids model [19] is capable of predicting the shear thinning (pseudo-plastic) phenomenon. It is a type of fluids which determines the fluid resistance having dominant rate of shear stress. These fluids include ketchup, paints, blood, nail polish and whipped cream etc. A number of researchers have already reported valuable analysis of the tangent hyperbolic fluid model keeping different flow phenomena. Abbas et al. [20] highlighted the pressure driven flow of tangent hyperbolic fluid inside a variable channel with flexible walls. Ibrahim [21] disclosed the magnetic effects on the slip flow of convectively heated and concentrated tangent hyperbolic nanoliquid over a stretchable surface. Kothandapani and Prakash [22] exposed the combined impacts of thermal radiation and heat source on peristaltic tangent hyperbolic fluid flow with the magnetic field. Shafiq et al. [23] exhibited the bio-convective effects on hydro-magneto tangent hyperbolic nanomaterial

flow with Newtonian heating. Mahanthesh et al. [24] illustrated the radiative flow of convectively heated tangent hyperbolic material flow over a stretched sheet with non-linear convection. Gaffar et al. [25] depicted the Biot number effects on the heat transfer flow of tangent hyperbolic fluid through a sphere. Kumar et al. [26] described the variable thermal conductivity effects on squeezed tangent hyperbolic fluid flow induced by a sensor surface. Nagendramma et al. [27] explored the stratification impacts on tangent hyperbolic nanomaterial flow induced via stretchable cylinder. Nagaraja et al. [28] illustrated the impact of suction/injection on magnetohydrodynamics flow of tangent hyperbolic fluid due to porous plate. Zakir and Gul [29] investigated the thermal slip effect on tangent hyperbolic fluid flow past a stretching surface.

Jeffrey fluids are amongst the rate type models. These fluids have acquired a notable attention of researchers in the current era. A Jeffrey fluid exhibits the linear viscoelastic feature and has numerous applications in polymer sector. The Jeffrey model [30] is the most simple and common among the non-Newtonian fluids which has the time derivative rather the convective derivative. The Jeffrey fluid model possesses two time representations, specifically the relaxation time and the retardation time. The retardation concept was originally introduced by Jeffrey to analyze the wave propagation occurrence in the earth's mantle and eventually in the description of the Jeffrey temperature flux model. Relaxation time describes the time used by the fluid to restore from the deformed position to their primary stability state. There are a number of applications of Jeffrey fluid model for instance dilute polymer solution. Andersson et al. [31] explored the MHD impact on the flow of power-law fluid past a stretching surface with a constant transverse magnetic field. Ahmad et al. [32] executed the numerical evaluation of the mixed convective flow of a Jeffrey fluid past an exponentially stretching sheet with magnetohydrodynamic impact. Narayana et al. [33] analyzed the MHD flow of a Jeffrey fluid due to a stretching surface by considering Dufour and Soret effects in the presence of heat source and chemical reaction. Jena et al. [34] found the exact solution of flow through

porous medium past a stretching sheet considering the chemical reaction and heat generation/absorption effects by making use of the Jeffery fluid model.

The fluid flow over a stretching sheet is of crucial importance from both the theoretical and the practical viewpoints because of its wide applications in the plastic engineering and metallurgy. Stretching sheet flows are important in various applications including paper production, aluminum bottle manufacturing processes, drawing of copper wires, metallurgical processes, spinning of fibers, production of rubber and plastic sheets, film coatings and crystal growing. During the process of extrusion, the quality of the final product depends upon the rate of stretching and the simultaneous heating or cooling during that process. So, fluid flow and heat transfer over a stretching surface have a practical significance in many industrial processes. Crane [35] examined the flow due to stretching of a sheet. Sakiadis [36] introduced the concept of boundary layer flow over a moving surface. Tsou et al. [37] conducted the analytical and experimental study to explore the momentum and heat transfer aspects emerging in the stretching surface model. Mass transfer on a moving continuous flat surface via injection/suction on the wall was studied by Erickson et al. [38]. The impacts of chemical reaction and thermal radiation on MHD mixed convection heat and mass transfer in micropolar fluid was discussed by Srinivasacharya and Upendar [39]. Bataller [40] carried out a study to discuss the impacts of a thermal radiation, viscous dissipation and non-uniform heat source on viscoelastic fluid flow and heat transfer past a stretching surface. After that, several authors broadened the notion of a stretching sheet for various fluid models [41–44].

The analysis of MHD flows has been found in several metallurgical, engineering and industrial fields. A magnetohydrodynamics has several significant applications including the biomechanics, petroleum technologies, plasma studies, flow of blood measurements, MHD generators and so forth. Sarpakaya [45] is the pioneer who reported the electrically conducting flow of non-Newtonian fluids.

Anderson and Wendt [46] presented the analytical solutions for magnetohydrodynamics flow of a viscoelastic fluid model over a stretching sheet. They discovered that the MHD rise the skin friction and reduces the boundary layer thickness. Jue [47] investigated the ferrofluid flow by utilizing the semi implicit finite element method to reenact the magnetic gradient and thermal buoyancy induced cavity. Nanjundappa et al. [48] addressed the impact of the magnetic field dependent viscosity on the horizontal layer of ferrofluid. Time dependent electrically conducting mixed convection flow over an exponentially stretching sheet with heat absorption/generation was analyzed by Elbashbeshy et al. [49]. Impact of mass transfer on electrically conducting flow of Casson fluid with suction, thermophoresis, thermal conductivity and variable viscosity is addressed by Animasaun [50]. Turkyilmazoglu [51] inspected the heat transfer of nanofluid flow caused due to a rotating disk. He used a Chebyshev spectral collocation method to produce the numerical solutions of the nonlinear equations. Bahiraei et al. [52] inspected the $Mn - Zn$ ferrite-water ferrofluid through an annulus affected by the non-uniform magnetic field. The influence of electrically conducting convective heat transfer flow of nanofluid inside an enclosure is examined by Sheikholeslami et al. [53]. Nanofluid flow and heat transfer subject to the effect of the magnetic field can also be found in [54–57].

Bioconvection has been explored due to a number of extensive uses in the microbial fuel cell, modeling oil, gas-bearing sedimentary basin, microbial upgraded petroleum recovery biological systems, bioconvection nanotechnological devices and biotechnology [58–60]. Bioconvection takes place whenever microorganisms that are more denser as compared with water and run upward during the flow. As a result of this upward swimming the micro-organisms are inclined to accumulate in the upper part of the fluid layer, hence leading to a higher density stratification that usually gets unstable. The swimming of such self-propelled motile micro-organisms leads to a high density that initiates bioconvection. Khan and Makinde [61] examined a magneto-hydrodynamics nanofluid that contains gyrotactic micro-organisms induced by a stretching

surface. It is noted that both the stretching parameter and bioconvection Lewis number lessen the concentration of motile micro-organisms. Makinde et al. [62] analyzed bioconvection in magneto-hydrodynamics nanofluid flow towards an upper sheet of a paraboloid of revolution by considering chemical reaction and non-linear thermal emission. It was noticed that the local heat transport rate moves up for the decreasing values of temperature and larger values of Prandtl number. Xun et al. [63] evaluated the influence of thermal conductivity as well as temperature dependent viscosity on the bio-convection flow in a rotating system and found that a rise in the thermal conductivity and viscosity lessens the mass, heat transfer and the motile microorganisms flux on the surface. Mosayebidorcheh et al. [64] inspected the effect of nano-bioconvection flow carrying the nanoparticles as well as gyrotactic micro-organisms in a horizontal channel employing modified least square technique and established that the thermophoresis number has an extremely small influence on the distribution of temperature profile while it has a strong impact on concentration and motile micro-organism.

Heat produced due to the dissipation process, is considered an important factor in designing numerous devices. The ability of the velocity to do work against the viscous forces is termed as viscous dissipation whereas the Joule heating is a phenomenon in which heat is generated because of the passage of electric current through a conductor. Viscous dissipation has a pivotal role in connection with various devices which operate at high deceleration or which are subjected to larger rotating speed. It is also crucial in the processes where the gravitational field is strong enough at a large scale, in nuclear engineering related to the cooling of reactors and in the geological processes. Ohmic heating (Joule heating) has gained a deserving attention due to its large range of usage in technological and industrial processes such as electronic cigarette, food processing, electric fuses, electric stoves, electric heaters, thermistor, incandescent light bulb and many others. Ibrahim and Suneetha [65] illustrated the Joule and viscous dissipation effects on a chemically reactive convection flow

of MHD fluid saturated in Darcian medium with Soret and heat source. Shah et al. [66] studied the numerical solution for MHD heat transfer in a UCM fluid flow over a stretching sheet along with thermal radiation and Joule heating. Gopal et al. [67] demonstrated the dissipation effects in Casson fluid flow induced by a chemically reacting stretching surface. Jing et al. [68] evaluated the effects of viscous dissipation and Joule heating on pressure-driven microchannel flow considering surface charge slip. Ferdows et al. [69] discussed the influence of viscous dissipation and Hall current on the boundary layer flow over a stretching surface. Goud and Shekar [70] found the numerical solutions of viscous dissipation effects on magnetohydrodynamic flow over a parabolic vertically inclined plate considering mass diffusion using the finite element technique. Thumma and Misra [71] examined the effects of multi slip boundary conditions on MHD Jeffery nanofluid with dissipation effects. Kumar et al [72] exposed the dissipation analysis of reacting ferro-nanomaterial considering the radiation energy.

Rotating flow and heat transfer problems obtain importance in a vast range of geophysical as well as engineering applications. The rotating flow has more extensive utilization [73] in chemical reactors, rotating machinery, MHD pumps, petroleum refineries, biochemical problem, lubrication and refrigeration system etc. Wang [74] analyzed a rotating flow over a stretching sheet. Nazar et al. [75] studied time dependent rotating flow past a stretching sheet. Rosali et al. [76] interrogated the boundary layer rotating flow due to a shrinking surface by considering suction effect. Sulochana et al. [77] considered the thermal radiation, viscous dissipation and chemical reaction effects on flow past a rotating surface. Seth et al. [78] investigated the boundary layer flow of rotating nanofluid with entropy generation due to a stretching plate. Gireesha et al. [79] studied the effect of nonlinear thermal radiation on unsteady rotating fluid flow of nanotubes using the shooting method technique.

Stratification occurs as a result of differences in temperature, concentration

variations or even the existence of different fluids owning distinct densities. This sort of phenomenon has gained crucial importance as a result of its incorporation in the flows occurring in the rivers, lakes and seas, and water reservoirs etc. Additionally, the effects of solute and thermal stratifications are extremely significant for solar power for the reason that the better stratification refers to better energy productivity. Bearon and Grunbaum [80] illustrated the effect of bioconvection in a stratified environment. They concluded that as a result of a reduction in the gyrotactic parameter, the velocity profile as well as the cell concentration turned up. Kameswaran et al. [81] examined the convective heat transfer in a thermally stratified nanofluid flow over a vertical wavy surface with the main finding that the thermal stratification parameter rises the thermal boundary layer thickness. Madhu and Reddy [82] illustrated the impact of thermal stratification on the magnetohydrodynamics heat transfer flow past an exponentially stretching surface with the conclusion that the temperature gradient is enhanced substantially with a boost in stratification. The references [83–86] incorporate some latest efforts relevant to the variable thermal conductivity.

1.3 Problem Identification

The advancements in the field of nanofluids have potential significance because of its excessive usage in the real life and in the modern heat and mass transport processes. The traditional heat transport fluids cannot meet the rising challenges of contemporary world because of their low thermal conductivity. To overcome these challenges, nanoparticles have been considered for suspension inside the heat transport fluids to boost the heat transport phenomenon tremendously. On the basis of the above-mentioned issues, this analysis has been carried out to explore the impacts of various physical parameters on different MHD nanofluids flowing over a stretching surface. The tangent hyperbolic, Jeffrey and viscous fluids have specially been considered for the present investigation. This study explores how can the presence of nanoparticles affect the velocity, temperature and concentration fields and how can the skin friction, Sherwood number, motile

density rate and Nusselt number be influenced because of the presence of parameters some significant like the magnetic parameter, Deborah number, ratio of relaxation to retardation times, Prandtl number, Brownian motion parameter, thermophoresis parameter and Eckert number.

1.4 Research Objectives

The entire goal of this research is to investigate the characteristics of nanofluid flow, particularly the heat and mass transport for a boundary layer flow past a stretching surface. The major objectives are the following:

- To derive mathematical models with different flow geometries for nanofluids by considering the impact of MHD.
- To apply the methods of finite-difference and Shooting for the numerical solution of the governing mathematical models.
- To develop algorithms of the above mentioned numerical techniques for the solution of the proposed mathematical models .
- To analyze the numerical outcomes of the velocity, temperature, concentration and motile density profiles.
- To work out the dynamics of some important physical quantities like the drag coefficient, heat transfer rate, mass transfer rate and density number for different physical scenarios.

1.5 Scope of Research

This dissertation is restricted to the steady 2D MHD incompressible flows of the tangent hyperbolic, Newtonian viscous and Jeffrey nanofluids past a stretching sheet. In this analysis, Tiwari and Das and Buongiorno models of nanofluid have been utilized. These fluids (Nanofluids) substantially improve the heat and mass transfer rates in many different areas like nuclear reactors, automobiles, micro heat exchangers, electronics, cryopreservation, air-conditioning and nano-drug delivery.

1.6 Significance of Research

The significances of the research work are following:

- The outcomes of the study shall boost the knowledge on the nanofluids flows phenomenon.
- The knowledge gained will provide a better insight on the rheological behavior of viscous fluid, tangent hyperbolic fluid and Jeffrey fluid.
- To provide foresight of the physical behavior of nanoparticles on the fluid flow, heat and mass transport.
- The research will offer as a good tool for heat transfer and mass transfer rates prediction.
- This study provides numerical solutions of complex mathematical models.
- The research can be extended to other generalized cases.

1.7 Thesis Outline

Within this dissertation, we utilize a couple of well-known models specifically the Tiwari and Das model and the Buongiorno's model to investigate a number of interesting boundary layer flow problems that involved nanofluids. Salient features influencing this kind of flows have also been taken into account. Such features include the magnetic field, viscous dissipation, Joule heating, chemical reaction, suction, injection, Brownian motion and thermophoresis diffusion. The transformed differential system is handled numerically through the well-known Keller box method or the shooting technique. The present dissertation comprises of seven chapters that are briefly described as:

Chapter 2 incorporates a comprehensive back-ground of the boundary layer flow due to moving surface. Moreover, the basic fundamental laws governing the flow are discussed in this Chapter. Tensor analysis is performed for the viscous

fluid, Jeffrey fluid and tangent hyperbolic fluid. A brief discussion on the numerical techniques employed in this dissertation is also made part of this chapter.

Chapter 3 analyzes the impact of silver, titanium oxide and alumina nanoparticles on the time independent 2D magnetohydrodynamic boundary layer heat transfer flow of Jeffrey fluid past a stretching surface with Joule heating and viscous dissipation. Numerical study is made by Keller box method. The most important findings of this chapter are published in “**AIP Advances 8, 065316 (2018), DOI: 10.1063/1.5031447**”.

Chapter 4 is devoted to the numerical analysis of tangent hyperbolic nanofluid with chemical reaction, viscous dissipation and Joule heating effects. Nanofluid is comprised of thermophoresis and Brownian motion effects. The system of nonlinear equations are numerically investigated by Keller box technique. Contents of this chapter are published in “**AIP Advances 9, 025007 (2019), DOI: 10.1063/1.5054798**”.

In **Chapter 5**, we analyze the stratified MHD Jeffrey nanofluid flow towards a stretching surface in the presence of gyrotactic micro-organisms. The impacts of a variety of parameters on the fluid motion, heat, mass, density of the motile micro-organisms, local skin friction, local Nusselt number, local Sherwood number and local density number of the motile micro-organisms are examined. This article is submitted for publication in journal.

In **Chapter 6**, we investigate the flow of a nanofluid with water as the base fluid and Cu and Ag as the nanoparticles between two rotating plates. Centripetal and Coriolis forces effects on the rotation of the fluid are also considered. Numerical solution of the system of nonlinear ODEs is obtained through the shooting method. The work presented in this study is published in “**Journal of Nanofluids, Volume 8, Number 2, pages 359-370 (2019), DOI: 10.1166/jon.2019.1578**”.

Chapter 7 summarizes the conclusions drawn from different scenarios presented in chapters 3-6.

Chapter 2

Fundamental Laws and Solution Methodology

2.1 Introduction

A brief review of certain studies relevant to boundary layer flow, basic governing laws of linear momentum, concentration, energy and gyrotatic microorganism has been presented in the present chapter. Mathematical modeling for Jeffrey fluid, tangent hyperbolic fluid and viscous fluid are covered for a better comprehension of forthcoming chapters. The solution methodologies such as Keller box method, an implicit finite difference technique and the shooting method are briefly described in the present chapter.

2.2 Types of Fluid Flow [87, 88]

This section incorporates the various types of fluid flow based on the variation of flow parameters.

2.2.1 Steady and Unsteady Flows

“Steady flow is defined as that type of flow in which the fluid characteristics like velocity, pressure, density etc., at a specific point do not change with time. Let Υ be any fluid property, then the following holds for the steady flow

$$\frac{\partial \Upsilon}{\partial t} = 0,$$

where Υ is any fluid property. Unsteady flow is that type of flow, in which the velocity, pressure or density at a point changes with respect to time. Thus, mathematically, for unsteady flow

$$\frac{\partial \Upsilon}{\partial t} \neq 0.$$

2.2.2 Uniform and Non-uniform Flows

Uniform flow is defined as that type of flow in which the velocity at any given time does not change with respect to space. Mathematically, for uniform flow

$$\left(\frac{\partial \mathbf{V}}{\partial s}\right)_{t=\text{constant}} = 0,$$

where $\partial \mathbf{V}$ = Change of velocity and ∂s = Length of flow in the direction S. Non-uniform flow is that type of flow in which the velocity at any given time changes with respect to space. Thus, mathematically, for non-uniform flow

$$\left(\frac{\partial \mathbf{V}}{\partial s}\right)_{t=\text{constant}} \neq 0.$$

2.2.3 Laminar and Turbulent Flows

Laminar flow is defined as that type of flow in which the fluid particles move along well-defined paths or stream line and all the stream-lines are straight and parallel. Thus the particles move in laminas or layers gliding smoothly over the adjacent

layer. This type of flow is also called stream-line flow or viscous flow. Turbulent flow is that type of flow in which the fluid particles move in a zig-zag way. Due to the movement of fluid particles in a zig-zag way, the eddies formation takes place which are responsible for high energy loss.

2.2.4 One Two and Three Dimensional Flow

One-dimensional flow is that type of flow in which the flow parameter such as velocity is a function of time and one space co-ordinate only. The average flow in a duct can be considered as one-dimensional. Two-dimensional flow is that type of flow in which the velocity is a function of time and two rectangular space co-ordinates. The flow between two parallel plates is an example. Three-dimensional flow is that type of flow in which the velocity is a function of time and three mutually perpendicular directions. When there is no obstruction or channelling, fluid flow can be thought of as three-dimensional flow.

2.2.5 Compressible and Incompressible Flows

Compressible flow is that type of flow in which the density of the fluid changes from point to point or in other words the density (ρ) is not constant for the fluid. Thus, mathematically, for compressible flow $\rho \neq \text{Constant}$. Incompressible flow is that type of flow in which the density is constant for the fluid flow. Liquids are generally incompressible while gases are compressible. Mathematically, for incompressible flow $\rho = \text{Constant}$.

2.2.6 Rotational and Irrotational Flows

Rotational flow is that type of flow in which the fluid particles while flowing along stream-lines, also rotate about their own axis. And if the fluid particles while flowing along stream-lines, do not rotate about their own axis then that type of flow is called irrotational flow".

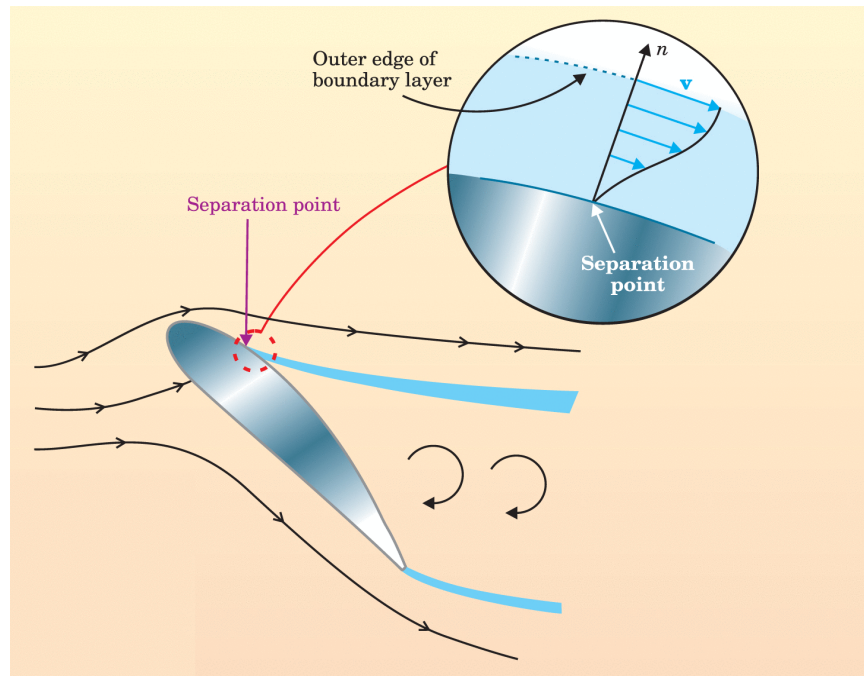


FIG. 2.1: The blowup of the boundary layer shows the flow's velocity profile above the separation point.

2.3 Boundary Layer Theory [89]

“In 1904 a little known physicist revolutionized fluid dynamics with his notion that the effects of friction are experienced only very near an object moving through a fluid. The overall perspective set forth by Prandtl in his 1905 paper was simple and straightforward. In brief, an aerodynamic flow over a body can be divided into two regions, a thin boundary layer near the surface, where friction is dominant, and an inviscid flow external to the boundary layer, where friction is negligible. The outer inviscid flow strongly affects the boundary-layer properties; indeed, the outer flow creates the boundary conditions at the outer edge of the boundary layer and dictates the velocity profile within the layer. On the other hand, the boundary layer is so thin that it has virtually no effect on the outer inviscid flow. The exception to the no-effect rule is if the flow separates; then the outer inviscid flow is greatly modified by the presence of the separation region. Prandtl was referring to the type of flow in which, as sketched in Fig. 2.1, the boundary layer separates from the surface and trails downstream. With the advent of Prandtl's boundary layer concept, it became possible to

quantitatively calculate the aerodynamic drag. Prandtl showed that for the boundary layer, the Navier–Stokes equations can be reduced to a simpler form, applicable only to the boundary layer. The results called the boundary-layer equations are similar to Navier–Stokes in that each system consists of coupled, nonlinear partial differential equations. The major mathematical breakthrough, however, is that the boundary layer equations exhibit a completely different mathematical behavior than the Navier–Stokes equations.

The Navier–Stokes equations have what mathematicians call elliptic behavior. That is to say, the complete flow field must be solved simultaneously, in accord with specific boundary conditions defined along the entire boundary of the flow. In contrast, the boundary-layer equations have parabolic behavior, which affords tremendous analytical and computational simplification. They can be solved step-by-step by marching downstream from where the flow encounters a body, subject to specified inflow conditions at the encounter and specified boundary conditions at the outer edge of the boundary layer. The systematic calculation yields the flow variables in the boundary layer, including the velocity gradient at the wall surface. The shear stress at the wall, hence the skin-friction drag on the surface, is obtained directly from those velocity gradients”.

2.4 Significant Dimensionless Numbers [90–92]

“Dimensionless numbers have high importance in the field of fluid mechanics as they determine behavior of fluid flow in many aspects. These dimensionless forms provides help in computational work in mathematical model by scaling. Dimensionless numbers have extensive use in various practical fields like economics, physics, mathematics, engineering especially in mechanical and chemical engineering. Different dimensionless numbers used for heat transfer and mass transfer. This description of dimensionless numbers in fluid mechanics can help with understanding of all areas of the fluid dynamics including compressible

flow, viscous flow, turbulence, aerodynamics and thermodynamics. Some of the important dimensionless numbers that appear in our thesis are mentioned below:

2.4.1 Reynolds Number

The Reynolds number Re describes the ratio of inertial force to viscous force within the fluid stream. Mathematically, we write

$$Re = \frac{U_0 L}{\nu}, \quad (2.1)$$

where U_0 is the characteristic velocity, L is the reference length and ν is the kinematic viscosity. When the ratio exceeds a certain value, which is different for different geometries, the fluid no longer moves in discrete streamlines. At values of the Reynolds number higher than laminar flow there is a region of mixed boundary layer flow, and then full turbulence.

2.4.2 Prandtl Number

The Prandtl number is a non-dimensional number, its named was given after its innovator, a German architect Ludwig Prandtl. It is defined as

$$Pr = \frac{\nu}{\alpha}, \quad (2.2)$$

where α denotes the thermal diffusivity and ν is the kinematic viscosity of the fluid. We sometimes call the kinematic viscosity term, the molecular diffusivity of momentum, because it is a measure of the rate of momentum transfer between the molecules in the fluid. It is apparent then that the Prandtl number, the ratio of fluid properties, controls the relationship between velocity and temperature distribution. It describes the effects thermo-physical characteristics of fluid on heat transference. It appears in the non-dimensional form of the governing equation of heat transfer.

2.4.3 Lewis Number

The Lewis number is named for Warren Lewis, who introduced the idea of such a number in 1939. It is the relation of the Prandtl and the Schmidt numbers. The Lewis number is important in situations where heat transfer and mass transfer occur simultaneously. It can be expressed as follows

$$Le = \frac{\alpha}{D}, \quad (2.3)$$

where α and D are the thermal and mass diffusivity, respectively.

2.4.4 Eckert Number

The Eckert number is a non-dimensional number, named after Ernst Eckert. This number is proportional to the ratio of the temperature rise of a fluid in an adiabatic compression to the temperature difference between the wall and the fluid at the edge of the boundary layer. It is described mathematically as

$$Ec = \frac{U_0^2}{c_p \Delta T}, \quad (2.4)$$

where U_0 is the reference velocity, c_p represents the specific heat capacity and ΔT shows the difference between wall and fluid ambient temperature.

2.4.5 Skin Friction Coefficient

To study the fluid dynamics, it is suitable to deal with non-dimensional form of governing equations with reduced number of variable and incorporating dimensionless parameters by using some transformation. Skin friction coefficient expresses the dimensionless shear stress at the wall and can be defined as

$$C_f = \frac{2\tau_w}{\rho w_w^2}, \quad (2.5)$$

where ρ the density, u_w the free stream velocity and τ_w represents shear stress at the wall and is given by

$$\tau_w = \mu \left. \frac{\partial u}{\partial y} \right|_{y=0}. \quad (2.6)$$

2.4.6 Nusselt Number

The Nusselt number is the key to finding the heat transfer coefficient, which is usually the unknown variable in most heat transfer problems. It is the ratio convective to conductive heat transfer across (normal) to the surface. It is defined as

$$N_u = \frac{q_w x}{k \Delta T}, \quad (2.7)$$

Where x is the distance of flow from the surface edge, T is the temperature difference between the wall and fluid ambient, q_w is the heat transfer rate at the surface and is given by

$$q_w = -k \left. \frac{\partial T}{\partial y} \right|_{y=0}. \quad (2.8)$$

The Nusselt number was originally expressed by Baptiste Biot, the first person to express the laws of convection in a mathematical form. The relationship was proposed as the Nusselt number in 1933, to commemorate Wilhelm Nusselt, the German engineer who later derived the number in 1905.

2.4.7 Sherwood Number

The Sherwood number is similar to the Nusselt number for heat transfer, but is used to describe mass transfer. It signifies the ratio of rate of mass transfer to the rate of mass diffusivity. Mathematically it can be represented as

$$S_h = \frac{HL}{D}, \quad (2.9)$$

Here L represents characteristic length, D is mass diffusivity and H signifies mass transfer coefficient”.

2.4.8 Weissenberg Number [93]

“The Weissenberg number is a dimensionless number used in the study of viscoelastic flows. It is named after Karl Weissenberg. The dimensionless number compares the elastic forces to the viscous forces. It can be variously defined, but it is usually given by the relation of stress relaxation time of the fluid and a specific process time. For instance, in simple steady shear, the Weissenberg number, often abbreviated as We , is defined as the shear rate $\dot{\gamma}$ times the relaxation time λ .

$$We = \dot{\gamma}\lambda \quad (2.10)$$

The Weissenberg number indicates the degree of anisotropy or orientation generated by the deformation, and is appropriate to describe flows with a constant stretch history, such as simple shear.

2.4.9 Deborah Number

Formally, the Deborah number is defined as the ratio of the relaxation time characterizing the time it takes for a material to adjust to applied stresses or deformations, and the characteristic time scale of an experiment (or a computer simulation) probing the response of the material

$$\beta = \frac{\text{time of relaxation}}{\text{time of observation}} \quad (2.11)$$

At lower Deborah numbers, the material behaves in a more fluidlike manner, with an associated Newtonian viscous flow. At higher Deborah numbers, the material behavior enters the non-Newtonian regime, increasingly dominated by elasticity and demonstrating solid like behavior”.

2.5 Heat Transfer [94]

“Heat transfer is the science that seeks to predict the energy transfer that may take place between material bodies as a result of a temperature difference. Thermodynamics teaches that this energy transfer is defined as heat. The

science of heat transfer seeks not merely to explain how heat energy may be transferred, but also to predict the rate at which the exchange will take place under certain specified conditions. The fact that a heat-transfer rate is the desired objective of an analysis points out the difference between heat transfer and thermodynamics. Heat transfer supplements the first and second principles of thermodynamics by providing additional experimental rules that may be used to establish energy-transfer rates. There are three modes of heat transfer: conduction, convection and radiation.

2.5.1 Convection

It is well known that a hot plate of metal will cool faster when placed in front of a fan than when exposed to still air. We say that the heat is convected away, and we call the process convection heat transfer. Convection heat depends on viscosity, thermal conductivity, specific heat and density of the fluid. The application of heat transfer has become more intense in modern technology in areas such as energy production, heat exchangers.

2.5.2 Conduction

When a temperature gradient exists in a body, experience has shown that there is an energy transfer from the high-temperature region to the low-temperature region. We say that the energy is transferred by conduction and that the heat-transfer rate per unit area is proportional to the normal temperature gradient. Such types of heat transfer occurs in the solid.

2.5.3 Radiation

In contrast to the mechanisms of conduction and convection, where energy transfer through a material medium is involved, heat may also be transferred through regions where a perfect vacuum exists. The mechanism in this case is

electromagnetic radiation. An example of radiation would be atmosphere, the atmosphere is heated by the radiation of the sun”.

2.6 Mass Transfer [94]

“When a mixture of gases or liquids is contained such that there exists a concentration gradient of one or more of the constituents across the system, there will be a mass transfer on a microscopic level as the result of diffusion from regions of high concentration to regions of low concentration. One must remember that the general subject of mass transfer encompasses both mass diffusion on a molecular scale and the bulk mass transport that may result from a convection process. There is a mass transfer associated with convection in that mass is transported from one place to another in the flow system. This type of mass transfer occurs on a macroscopic level and is usually treated in the subject of fluid mechanics. In many technical applications, heat transfer processes occur simultaneously with mass transfer processes. Mass transfer occurs in many processes, such as absorption, evaporation, drying, precipitation, membrane filtration, and distillation”.

2.7 Classification of Fluids [95]

2.7.1 Ideal Fluid

“A fluid can be defined as a material that deforms continually under the application of an external force. In other words, a fluid can flow and has no rigid three-dimensional structure. An ideal fluid may be defined as one in which there is no friction. Thus the forces acting on any internal section of the fluid are purely pressure forces, even during motion. Ideal fluid do not actually exist in nature, but sometimes used for fluid flow problems. All the fluids in actual practice are real fluids.

2.7.2 Real Fluid

The fluid containing some viscosity effect is said to be a real or viscous fluid. In a real fluid, shearing (tangential) and extensional forces always come into play whenever motion takes place, thus given rise to fluid friction, because these forces oppose the movement of one particle relative to another. These friction forces are due to a property of the fluid called viscosity. The friction forces in fluid flow result from the cohesion and momentum interchange between the molecules in the fluid.

2.7.3 Newtonian Fluid

An important parameter that characterizes the behaviour of fluids is viscosity because it relates the local stresses in a moving fluid to the rate of deformation of the fluid element. When a fluid is sheared, it begins to move at a rate of deformation inversely proportional to viscosity. A fluid for which the constant of proportionality (i.e., the viscosity) does not change with rate of deformation is said to be a Newtonian fluid and can be represented by a straight line in Fig. 2.2.

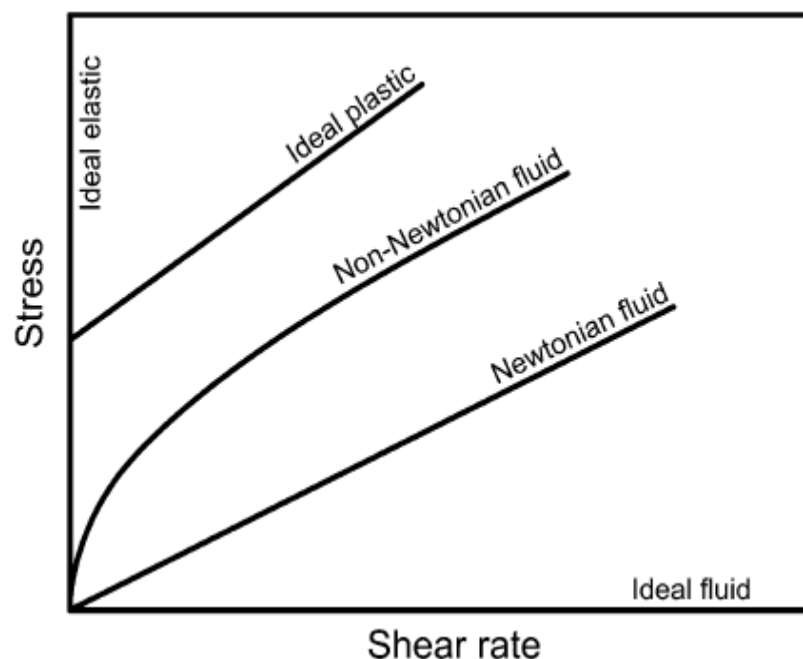


FIG. 2.2: Rheological behaviour of materials.

The slope of this line is determined by the viscosity. The ideal fluid, with no viscosity, is represented by the horizontal axis, while the true elastic solid is represented by the vertical axis. A plastic body which sustains a certain amount of stress before suffering a plastic flow can be shown by a straight line intersecting the vertical axis at the yield stress.

2.7.4 Non-Newtonian Fluid

There is a certain class of fluids, called non-Newtonian fluids, in which the viscosity varies with the shear rate. A particular feature of many non-Newtonian fluids is the retention of a fading memory of their flow history which is termed elasticity. Typical representatives of non-Newtonian fluids are liquids which are formed either partly or wholly of macromolecules (polymers), or two phase materials, like, for example, high concentration suspensions of solid particles in a liquid carrier solution.

There are various types of non-Newtonian fluids. Pseudoplastic fluids are those fluids for which viscosity decreases with increasing shear rate and hence are often referred to as shear-thinning fluids. These fluids are found in many real fluids, such as polymer melts and solutions or glass melt. When the viscosity increases with shear rate the fluids are referred to as dilatant or shear-thickening fluids. These fluids are less common than with pseudoplastic fluids. Dilatant fluids have been found to closely approximate the behaviour of some real fluids, such as starch in water and an appropriate mixture of sand and water. Some fluids do not flow unless the stress applied exceeds a certain value referred to as the yield stress. These fluids are termed fluids with yield stress or viscoplastic fluids. The variation of the shear stress with shear rate for pseudoplastic and dilatant fluids with and without yield stress is shown in Fig. 2.3.

Viscoelastic fluids are those fluids that possess the added feature of elasticity apart from viscosity. These fluids have a certain amount of energy stored inside

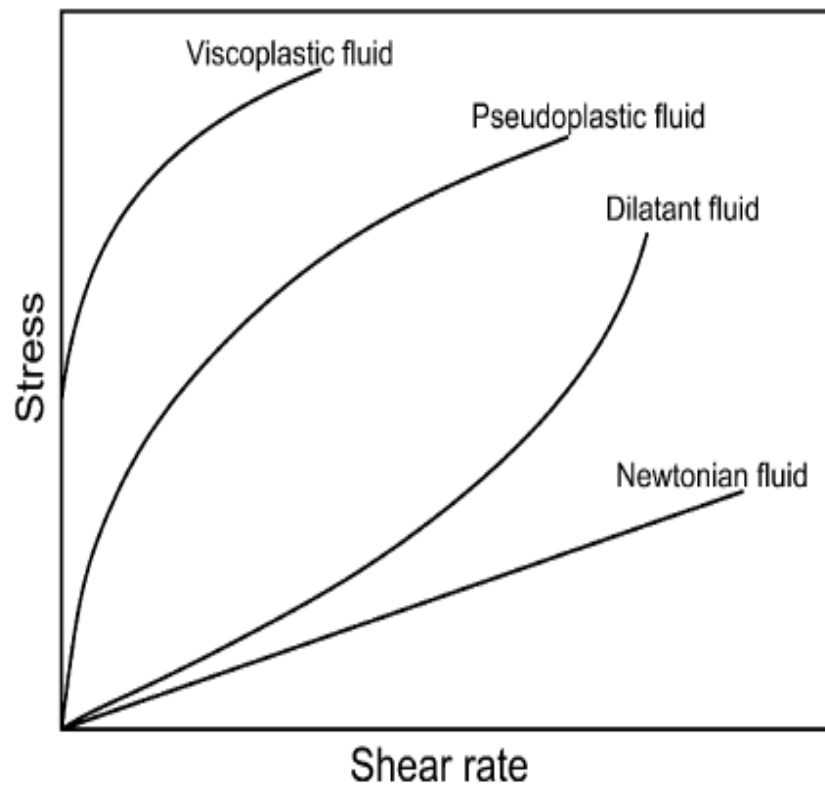


FIG. 2.3: Rheological behaviour of non-Newtonian fluids.

them as strain energy thereby showing a partial elastic recovery upon the removal of a deforming stress. In the case of thixotropic fluids, the shear stress decreases with time at a constant shear rate. An example of a thixotropic material is non-drip paint, which becomes thin after being stirred for a time, but does not run on the wall when it is brushed on. By contrast, when the shear stress increases with time at a constant shear rate the fluids are referred to as rheopectic fluids. Some clay suspensions exhibit rheopectic behaviour. Viscoelastic fluids have some additional features. When a viscoelastic fluid is suddenly strained and then the strain is maintained constant afterward, the corresponding stresses induced in the fluid decrease with time. This phenomenon is called stress relaxation. If the fluid is suddenly stressed and then the stress is maintained constant afterward, the fluid continues to deform, and the phenomenon is called creep. If the fluid is subjected to a cycling loading, the stress-strain relationship in the loading process is usually somewhat different from that in the unloading process, and the phenomenon is called hysteresis ”.

2.8 Nanofluids [96]

“ Nanofluids are colloidal suspensions of nanosized solid particles in a liquid. Recently conducted experiments have indicated that nanofluids tend to have substantially higher thermal conductivity than the base fluids. Among the many advantages of nanofluids over conventional solid–liquid suspensions, the following are worth mentioning: higher specific surface area, higher stability of the colloidal suspension, lower pumping power required to achieve the equivalent heat transfer, reduced particle clogging compared to conventional colloids, and higher level of control of the thermodynamics and transport properties by varying the particle material, concentration, size, and shape. The nanoparticles used in nanofluids are typically made of metals, oxides, carbides, or carbon nanotubes. In analysis such as computational fluid dynamics, nanofluids can be assumed to be single phase fluids.

There is a large number of engineering applications that can benefit from a better understanding of the thermal conductivity enhancement of nanofluids. One example is ionic liquids, which are salts that are liquid at room temperature. However, ionic liquids do not have a very high thermal conductivity compared to (say) water, and if this could be improved by the addition of nanoparticles, the liquid would be better suited for heat transfer applications such as in absorption refrigeration or cooling circuits. Liquid cooling with high thermal conductivity fluids would also address many other heat dissipation problems. For instance, microelectro-mechanical systems generate large quantities of heat during operation and require high-performance coolants to mitigate the large heat flux. Such a system requires precise temperature control, and a higher conductive fluid would allow for more efficient heat transfer control. There are also many everyday applications in which nanofluids could be suitable for, such as in the automotive industry. The high thermal conductivity enhancement observed in ethylene glycol based nanofluids suggests that this common antifreeze could have better performance simply with a nanoparticle suspension”.

2.9 Brownian Motion

“Nanoparticles move through the molecules of the base fluid and sometimes collide with each other by means of Brownian motion. Particularly, when two particles collide, the solid–solid heat transfer mode could increase the overall thermal conductivity of the nanofluid. The effect of Brownian motion is a diffusive process. As we note, the higher the temperature, the higher the diffusivity, and thus the higher the thermal conductivity.

2.10 Thermophoresis

Particle thermophoresis is a nonequilibrium cross-flow effect between mass and heat transport, quite similar to thermal diffusion (the Soret effect) in simple fluid mixtures. When a colloidal suspension is placed in a temperature gradient, the dispersed particles display, on top of Brownian motion, a steady drift velocity, where the thermophoretic mobility is usually dubbed the thermal diffusion coefficient. Then, depending on the sign, the particles focus either at the cold or the hot side, leading to the steady-state concentration gradient given, for low particle concentration ”.

2.11 Viscous Dissipation [97]

“Viscous dissipation effects are typically only significant for high viscous flows or in presence of high gradient in velocity distribution. In macroscale, such high gradients occur in high velocity flows. In microscale devices, however, because of small dimensions, such high gradients may occur even for low velocity flows. So, for microchannels the viscous dissipation should be taken into consideration. Viscous dissipation features as a source term in the fluid flow due to the conversion of the kinetic motion of the fluid to the thermal energy and causes variation in temperature distribution”.

2.12 Joule Heating [98]

“Joule heating is named for James Prescott Joule, the first to articulate what is now Joule’s law. Joule heating (also referred to as resistive or ohmic heating) describes the process where the energy of an electric current is converted into heat as it flows through a resistance. In particular, when the electric current flows through a solid or liquid with finite conductivity, electric energy is converted to heat through resistive losses in the material. The heat is generated on the microscale when the conduction electrons transfer energy to the conductor’s atoms by way of collisions”.

2.13 Magnetohydrodynamics [99, 100]

MHD is a branch of mechanics that is associated with the mutual interaction of fluid flow and magnetic field such as salt water, plasmas and electrolytes. Additionally, whenever the magnetic field exists, the following four additional laws are taken into account

$$\nabla \cdot \mathbf{B} = 0 \quad (\text{Gauss's Law for magnetic field}), \quad (2.12)$$

$$\nabla \cdot \mathbf{E} = \frac{\rho_e}{\varepsilon_0} \quad (\text{Gauss's Law}), \quad (2.13)$$

$$\nabla \times \mathbf{B} = \mu_0 \mathbf{j} + \mu_0 \varepsilon_0 \frac{\partial \mathbf{E}}{\partial t} \quad (\text{Ampere's Law}), \quad (2.14)$$

$$\nabla \times \mathbf{E} = -\frac{\partial \mathbf{B}}{\partial t} \quad (\text{Faraday's Law}), \quad (2.15)$$

in which

$$\mathbf{j} = \sigma(\mathbf{E} + \mathbf{V} \times \mathbf{B}). \quad (2.16)$$

In the above description, \mathbf{j} is the current density, μ_0 is the magnetic permeability, \mathbf{E} is the electric field, ρ_e is the charge density, \mathbf{B} is the magnetic field, ε_0 is the permittivity of free space and σ is the fluid electrical conductivity. In equation of

motion, electromagnetic force \mathbf{F} is expressed as

$$\mathbf{F} = j \times \mathbf{B} = \sigma(\mathbf{E} \times \mathbf{B}) \times \mathbf{B}. \quad (2.17)$$

2.14 Basic Laws

2.14.1 Conservation of Mass [101]

The mathematical equation that results from employing the law of conservation of mass to a flow is named as the continuity equation and mathematically written as

$$\frac{\partial \rho}{\partial t} + \nabla \cdot (\rho \mathbf{V}) = 0. \quad (2.18)$$

A fluid flow in which ρ remains constant is referred to as an incompressible flow i.e.

$$\nabla \cdot \mathbf{V} = 0. \quad (2.19)$$

In the Cartesian coordinates Eq. (2.19) can be written as

$$\frac{\partial u}{\partial x} + \frac{\partial v}{\partial y} = 0. \quad (2.20)$$

2.14.2 Momentum Equation

The conservation of linear momentum states that the total linear momentum of a system stays constant. Mathematically

$$\rho \frac{D\mathbf{V}}{Dt} = \nabla \cdot \boldsymbol{\tau}_{ij} + \rho \mathbf{B}. \quad (2.21)$$

The stress tensor $\boldsymbol{\tau}_{ij}$ is given as

$$\boldsymbol{\tau}_{ij} = -p\mathbf{I} + \mathbf{S}. \quad (2.22)$$

So, Eq. (2.21) can be written in the form

$$\rho \frac{D\mathbf{V}}{Dt} = \nabla \cdot (-p\mathbf{I} + \mathbf{S}) + \rho\mathbf{B}, \quad (2.23)$$

where, $\mathbf{V} = [u(t, x, y, z), v(t, x, y, z), w(t, x, y, z)]$ is the velocity field, p the pressure, \mathbf{B} the body force and \mathbf{S} the extra stress tensor.

$$\tau_{ij} = \begin{bmatrix} \tau_{xx} & \tau_{xy} & \tau_{xz} \\ \tau_{yx} & \tau_{yy} & \tau_{yz} \\ \tau_{zx} & \tau_{zy} & \tau_{zz} \end{bmatrix} \quad (2.24)$$

where $i, j = x, y, z$, $\tau_{xy}, \tau_{xz}, \tau_{yx}, \tau_{yz}, \tau_{zx}, \tau_{zy}$ are shear stresses and $\tau_{xx}, \tau_{yy}, \tau_{zz}$ are normal stresses. A general version of Eq. (2.23) in the scalar form is

$$\left. \begin{aligned} \rho \left(\frac{\partial u}{\partial t} + u \frac{\partial u}{\partial x} + v \frac{\partial u}{\partial y} + w \frac{\partial u}{\partial z} \right) &= \frac{\partial(\tau_{xx})}{\partial x} + \frac{\partial(\tau_{xy})}{\partial y} + \frac{\partial(\tau_{xz})}{\partial z} + \rho B_x, \\ \rho \left(\frac{\partial v}{\partial t} + u \frac{\partial v}{\partial x} + v \frac{\partial v}{\partial y} + w \frac{\partial v}{\partial z} \right) &= \frac{\partial(\tau_{yx})}{\partial x} + \frac{\partial(\tau_{yy})}{\partial y} + \frac{\partial(\tau_{yz})}{\partial z} + \rho B_y, \\ \rho \left(\frac{\partial w}{\partial t} + u \frac{\partial w}{\partial x} + v \frac{\partial w}{\partial y} + w \frac{\partial w}{\partial z} \right) &= \frac{\partial(\tau_{zx})}{\partial x} + \frac{\partial(\tau_{zy})}{\partial y} + \frac{\partial(\tau_{zz})}{\partial z} + \rho B_z. \end{aligned} \right\} \quad (2.25)$$

In the two dimensional case, the above equations can be expressed as

$$\left. \begin{aligned} \rho \left(\frac{\partial u}{\partial t} + u \frac{\partial u}{\partial x} + v \frac{\partial u}{\partial y} \right) &= \frac{\partial(\tau_{xx})}{\partial x} + \frac{\partial(\tau_{xy})}{\partial y} + \rho B_x, \\ \rho \left(\frac{\partial v}{\partial t} + u \frac{\partial v}{\partial x} + v \frac{\partial v}{\partial y} \right) &= \frac{\partial(\tau_{yx})}{\partial x} + \frac{\partial(\tau_{yy})}{\partial y} + \rho B_y. \end{aligned} \right\} \quad (2.26)$$

2.14.3 Energy Conservation

The heat transfer equation for incompressible flows has the form

$$\rho c_p \left(\frac{\partial T}{\partial t} + (\mathbf{V} \cdot \nabla) T \right) = \tau_{ij} \cdot \mathbf{L} + k \nabla^2 T + \rho r_h, \quad (2.27)$$

in which T denotes the temperature, $\tau_{ij} \cdot \mathbf{L}$ represents the viscous dissipation, k the thermal conductivity and r_h the radiative heating. In the case of absence of

radiative heating, i.e. when $r_h = 0$, the resulting equation is

$$\rho c_p \left(\frac{\partial T}{\partial t} + (\mathbf{V} \cdot \nabla) T \right) = \tau_{ij} \cdot \mathbf{L} + k \nabla^2 T. \quad (2.28)$$

2.14.4 Conservation Law of Concentration

It states that the total species concentration of the system under consideration is always constant. The mass flux based on the thermophoretic diffusion as well as the Brownian motion is provided by

$$\mathbf{j} = \mathbf{j}_T + \mathbf{j}_B = -\rho D_B \nabla C - \rho D_T \frac{\nabla T}{T_\infty}. \quad (2.29)$$

The equation for mass transfer in the absence of chemical reaction is generally presented as below

$$\frac{dC}{dt} = -\frac{1}{\rho} \nabla \cdot \mathbf{j}. \quad (2.30)$$

Therefore equation of mass transport turns into

$$\frac{\partial C}{\partial t} + \mathbf{V} \cdot \nabla C = \nabla \cdot \left(D_B \nabla C + D_T \frac{\nabla T}{T_\infty} \right). \quad (2.31)$$

2.14.5 Microorganism Transport Equation

There exist three major mechanisms of microorganism transfer that is macroscopic convection, random motion of micro-organisms and self propelled swimming. The flux \mathbf{j}_1 of microorganisms is defined as

$$\mathbf{j}_1 = n \mathbf{V} + n \mathbf{W}_c \hat{p} - D_m \nabla n, \quad (2.32)$$

where $n \mathbf{V}$ is the flux due to advection, $\mathbf{W}_c \hat{p}$ is the average relative swimming velocity and D_m is the diffusivity of microorganisms. The governing microorganism equation is expressed as follows

$$\frac{\partial n}{\partial t} = -\nabla \cdot \mathbf{j}_1, \quad (2.33)$$

in which \mathbf{j}_1 is the flux of microorganisms.

2.15 Mathematical Description of some Fluid Models [101, 102]

2.15.1 Viscous Fluid

Those fluid models which offer flow resistance are named as viscous fluid models. Viscous fluid can be described by two characteristics: (1) shearing stresses occur if the fluid particles are deformed, (2) whenever a viscous fluid flows alongside the surface it will stick to the surface, i.e., the fluid layer in close contact with the surface does not have any velocity relative to it. For viscous fluids, the rate of deformation as well as the shear stress are directly proportional to each other. In the case of viscous fluids, extra stress tensor is expressed by

$$\mathbf{S} = \mu \mathbf{A}_1, \quad (2.34)$$

where mathematical expression for \mathbf{A}_1 is $\mathbf{A}_1 = \nabla \mathbf{V} + (\nabla \mathbf{V})^t$.

2.15.2 Jeffrey Fluid [103]

A rate type fluid model which depicts the characteristics of both the relaxation as well as retardation times is called the Jeffrey fluid. The Jeffrey model is known as a generalisation of the commonly used Newtonian fluid model owing to the fact that its stress tensor can be simplified as a special case to that of the Newtonian model. The equation that manifests the rheological characteristics of Jeffrey fluid model is represented by

$$\mathbf{S} = \frac{\mu}{1 + \lambda_1} \left(\mathbf{A}_1 + \lambda_2 \frac{d\mathbf{A}_1}{dt} \right), \quad (2.35)$$

where mathematical expression for \mathbf{A}_1 is $\mathbf{A}_1 = \nabla \mathbf{V} + (\nabla \mathbf{V})^t$. Eq. (2.35) in the component form is generally expressed as

$$S_{xx} = \frac{\mu}{1 + \lambda_1} \left[2 \frac{\partial u}{\partial x} + 2\lambda_2 \left(u \frac{\partial}{\partial x} + v \frac{\partial}{\partial y} + w \frac{\partial}{\partial z} \right) \frac{\partial u}{\partial x} \right], \quad (2.36)$$

$$S_{yy} = \frac{\mu}{1 + \lambda_1} \left[2 \frac{\partial v}{\partial y} + 2\lambda_2 \left(u \frac{\partial}{\partial x} + v \frac{\partial}{\partial y} + w \frac{\partial}{\partial z} \right) \frac{\partial v}{\partial y} \right], \quad (2.37)$$

$$S_{zz} = \frac{\mu}{1 + \lambda_1} \left[2 \frac{\partial w}{\partial z} + 2\lambda_2 \left(u \frac{\partial}{\partial x} + v \frac{\partial}{\partial y} + w \frac{\partial}{\partial z} \right) \frac{\partial w}{\partial z} \right], \quad (2.38)$$

$$S_{xy} = S_{yx} = \frac{\mu}{1 + \lambda_1} \left[\left(\frac{\partial u}{\partial y} + \frac{\partial v}{\partial x} \right) + \lambda_2 \left(u \frac{\partial}{\partial x} + v \frac{\partial}{\partial y} + w \frac{\partial}{\partial z} \right) \left(\frac{\partial u}{\partial y} + \frac{\partial v}{\partial x} \right) \right], \quad (2.39)$$

$$S_{yz} = S_{zy} = \frac{\mu}{1 + \lambda_1} \left[\left(\frac{\partial v}{\partial z} + \frac{\partial w}{\partial y} \right) + \lambda_2 \left(u \frac{\partial}{\partial x} + v \frac{\partial}{\partial y} + w \frac{\partial}{\partial z} \right) \left(\frac{\partial v}{\partial z} + \frac{\partial w}{\partial y} \right) \right], \quad (2.40)$$

$$S_{zx} = S_{xz} = \frac{\mu}{1 + \lambda_1} \left[\left(\frac{\partial u}{\partial z} + \frac{\partial w}{\partial x} \right) + \lambda_2 \left(u \frac{\partial}{\partial x} + v \frac{\partial}{\partial y} + w \frac{\partial}{\partial z} \right) \left(\frac{\partial u}{\partial z} + \frac{\partial w}{\partial x} \right) \right]. \quad (2.41)$$

2.15.3 Tangent Hyperbolic Fluid [104]

The extra stress tensor \mathbf{S} for the tangent hyperbolic fluid can be presented as

$$\mathbf{S} = \mu_\infty \bar{\dot{\gamma}} + (\mu_0 + \mu_\infty) \bar{\dot{\gamma}} \tanh(\Gamma \bar{\dot{\gamma}})^n, \quad (2.42)$$

in which μ_∞ , μ_0 , n and Γ represent the infinite shear rate viscosity, the zero shear rate viscosity, the power-law index, the time dependent material constant respectively and also $\bar{\dot{\gamma}}$ is described as

$$\bar{\dot{\gamma}} = \left(\frac{1}{2} \sum_i \sum_j \bar{\dot{\gamma}}_{ij} \bar{\dot{\gamma}}_{ji} \right)^{\frac{1}{2}} = \left(\frac{1}{2} \mathbf{\Pi} \right)^{\frac{1}{2}}, \quad (2.43)$$

in which $\mathbf{\Pi} = \frac{1}{2} \text{tr}(\nabla \mathbf{V} + (\nabla \mathbf{V})^t)^2$. In case of $\mu_\infty = 0$ and $\Gamma \bar{\dot{\gamma}} < 1$, it is allowed to write Eq. (2.42) as follows

$$\mathbf{S} = \mu_0 \bar{\dot{\gamma}} (\Gamma \bar{\dot{\gamma}})^n = \mu_0 \bar{\dot{\gamma}} \left((1 + \Gamma \bar{\dot{\gamma}} - 1)^n \right) = \mu_0 \bar{\dot{\gamma}} (1 + n(\Gamma \bar{\dot{\gamma}} - 1)). \quad (2.44)$$

2.16 Solution Methodologies

In this section, an introductory material on the numerical techniques opted for the present work has been included.

2.16.1 Keller Box Method [105–107]

“The finite-difference method of solving two-point boundary value problems converts the set of differential equations into a finite set of algebraic or transcendental equations. The solution of the set of algebraic or transcendental equations yields approximations to the solution of the original differential equations at discrete points. If the original ordinary differential equations are linear, the finite difference equations will be linear algebraic equations. If the ordinary differential equations are nonlinear, the resulting finite difference equations will be nonlinear algebraic or transcendental equations. There are two ways to linearize the problem. One is by linearizing the differential equations before they are written in finite-difference form by methods such as quasi linearization. Another is first to write the differential equation in finite difference form and then to linearize the resulting nonlinear algebraic or transcendental equations. Finite-difference methods have been proved to be a very useful technique for solving numerically sensitive two-point boundary value problems. This is due to the fact that the finite difference equations incorporate both specified initial and terminal conditions in the final set of equations, and thus the resulting solutions of these equations are constrained to satisfy these boundary conditions. Another difference is that the solution is produced simultaneously at all points, whereas in a shooting method the solutions at different points are generated in sequence. The linearized algebraic equations exhibit banded matrix structure. The factorization scheme developed by Keller, as outlined in this chapter, is the most efficient way to solve such equations. Its value extends far beyond the solution of boundary value problems of ordinary differential equations. Keller box technique is an extremely efficient, numerical implicit finite

difference procedure. Its stability is reported in the literature as its main feature". The numerical codes are developed using MATLAB software. The algorithmic form of the Keller box method has been explained through a flow chart in Fig. 2.4: Its complete procedure has been explained with the help of

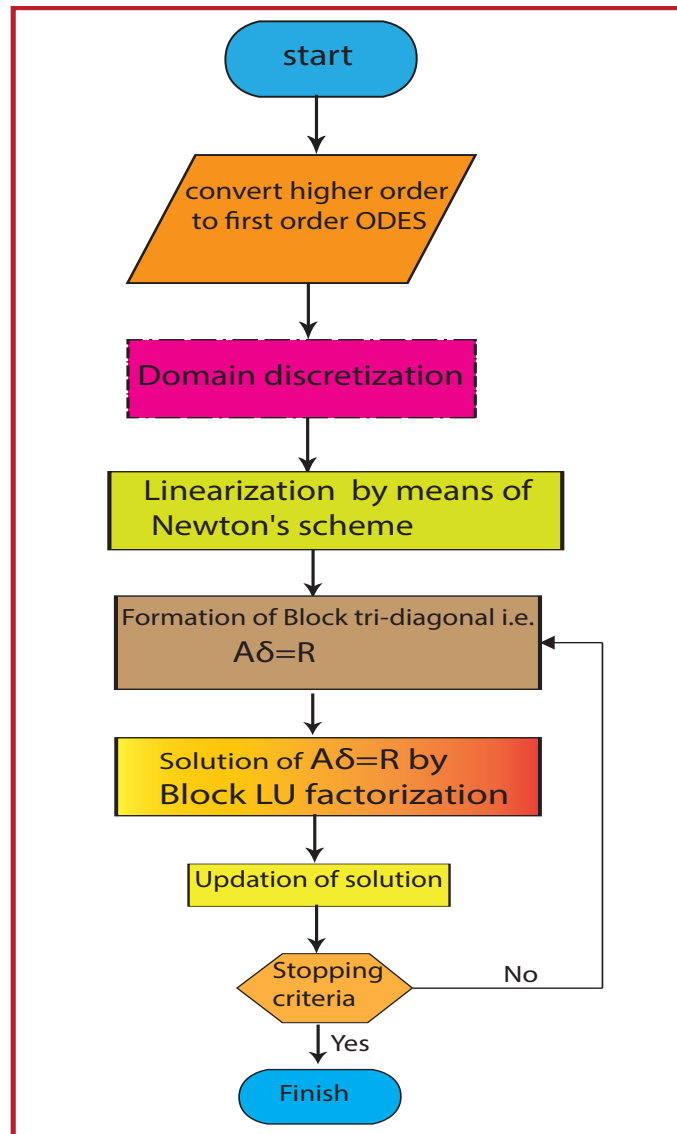


FIG. 2.4: Flow diagram of the present technique.

following example.

Example Consider the set of following equations

$$\left. \begin{aligned} f'''(\eta) + 3f(\eta)f''(\eta) - 2\left(f'(\eta)\right)^2 + g &= 0, \\ g''(\eta) + 3f(\eta)g'(\eta) &= 0. \end{aligned} \right\} \quad (2.45)$$

with the boundary conditions:

$$\left. \begin{aligned} f(0) = 0, \quad f'(0) = 0, \quad g(0) = 1 \quad \text{at} \quad \eta = 0, \\ f'(\eta) \rightarrow 0, \quad g(\eta) \rightarrow 0 \quad \text{as} \quad \eta \rightarrow \infty. \end{aligned} \right\} \quad (2.46)$$

We now replace the system of Eqs. (2.45) and (2.46) by a system of first-order equations, namely

$$\left. \begin{aligned} f' = p_1, \quad p_1' = p_2, \quad g' = p_3, \\ p_2' + 3fp_2 - 2p_1^2 + g = 0, \\ p_3' + 3fp_3 = 0. \end{aligned} \right\} \quad (2.47)$$

The end point conditions are

$$\left. \begin{aligned} f(0) = 0, \quad p_1(0) = 0, \quad g(0) = 1 \quad \text{at} \quad \eta = 0, \\ p_1(\eta) \rightarrow 0, \quad g(\eta) \rightarrow 0 \quad \text{as} \quad \eta \rightarrow \infty. \end{aligned} \right\} \quad (2.48)$$

Next, the derivatives have been approximated by using the central difference at midpoint and the domain has been discretized by using the following nodes:

$\eta_0 = 0, \quad \eta_j = \eta_{j-1} + h_j, \quad \eta_J = \eta_\infty$ where $j = 1, 2, 3, \dots, J$ and h_j is the mesh-size which can be taken uniform. Typical grid structure for difference approximations is shown in the Fig. 2.5. The system of Eqs. (2.47) then becomes

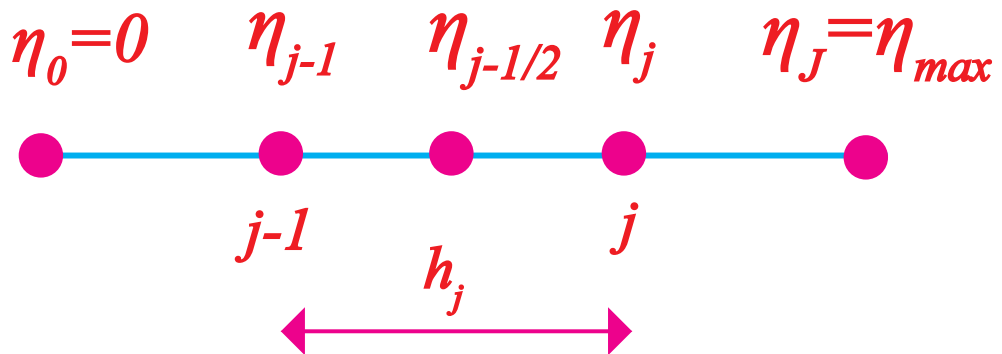


FIG. 2.5: Grid structure for difference approximations.

$$\left. \begin{aligned}
 \frac{f_j - f_{j-1}}{h_j} - \frac{(p_1)_j + (p_1)_{j-1}}{2} &= 0, \\
 \frac{(p_1)_j - (p_1)_{j-1}}{h_j} - \frac{(p_2)_j + (p_2)_{j-1}}{2} &= 0, \\
 \frac{g_j - g_{j-1}}{h_j} - \frac{(p_3)_j + (p_3)_{j-1}}{2} &= 0, \\
 \left(\frac{(p_2)_j - (p_2)_{j-1}}{h_j} \right) + 3 \left(\frac{f_j + f_{j-1}}{2} \right) \left(\frac{(p_2)_j + (p_2)_{j-1}}{2} \right) \\
 - 2 \left(\frac{(p_1)_j + (p_1)_{j-1}}{2} \right)^2 + \left(\frac{g_j + g_{j-1}}{2} \right) &= 0, \\
 \left(\frac{(p_3)_j - (p_3)_{j-1}}{h_j} \right) + 3 \left(\frac{f_j + f_{j-1}}{2} \right) \left(\frac{(p_3)_j + (p_3)_{j-1}}{2} \right) &= 0.
 \end{aligned} \right\} \quad (2.49)$$

The system of Eqs. (2.49) is nonlinear algebraic equations and thus need to be linearized prior to the factorization scheme can be used. The system of nonlinear Eqs. (2.49) is linearized by considering the following Newton iterates

$$\left. \begin{aligned}
 f_j^{n+1} &= f_j^n + \delta f_j^n, \quad (p_1)_j^{n+1} = (p_1)_j^n + \delta(p_1)_j^n, \\
 (p_2)_j^{n+1} &= (p_2)_j^n + \delta(p_2)_j^n, \quad (p_3)_j^{n+1} = (p_3)_j^n + \delta(p_3)_j^n, \\
 g_j^{n+1} &= g_j^n + \delta g_j^n,
 \end{aligned} \right\} \quad (2.50)$$

for all dependent variables. By utilizing the above expressions into the system of Eqs. (2.49) and then neglecting the quadratic as well as the higher-order terms in $\delta f_j^n, (\delta p_1)_j^n, (\delta p_2)_j^n, (\delta p_3)_j^n$ and δg_j^n , the subsequent linearized system is achieved

$$\delta f_j - \delta f_{j-1} - \frac{h_j}{2} \left((\delta p_1)_j + (\delta p_1)_{j-1} \right) = (r_1)_j, \quad (2.51)$$

$$(\delta p_1)_j - (\delta p_1)_{j-1} - \frac{h_j}{2} \left((\delta p_2)_j + (\delta p_2)_{j-1} \right) = (r_2)_j, \quad (2.52)$$

$$\delta g_j - \delta g_{j-1} - \frac{h_j}{2} \left((\delta p_3)_j + (\delta p_3)_{j-1} \right) = (r_3)_j, \quad (2.53)$$

$$\begin{aligned}
 (\xi_1)_j (\delta p_2)_j + (\xi_2)_j (\delta p_2)_{j-1} + (\xi_3)_j \delta g_j + (\xi_4)_j \delta g_{j-1} + (\xi_5)_j (\delta p_1)_j \\
 + (\xi_6)_j (\delta p_1)_{j-1} + (\xi_7)_j \delta f_j + (\xi_8)_j f_{j-1} = (r_5)_j,
 \end{aligned} \quad (2.54)$$

$$\begin{aligned}
 (\gamma_1)_j (\delta p_3)_j + (\gamma_2)_j (\delta p_3)_{j-1} + (\gamma_3)_j \delta f_j + (\gamma_4)_j \delta f_{j-1} + (\gamma_5)_j \delta g_j \\
 + (\xi_6)_j g_{j-1} + (\gamma_7)_j \delta (\delta p_1)_j + (\gamma_8)_j (\delta p_1)_{j-1} = (r_6)_j,
 \end{aligned} \quad (2.55)$$

subject to the boundary conditions

$$\delta f_0 = 0, (\delta p_1)_0 = 0, (\delta p_1)_J = 0, \delta g_0 = 0, \delta g_J = 0, \quad (2.56)$$

in which

$$\left. \begin{aligned} (\xi_1)_j &= 1 + \frac{3}{4}h_j(f_j + f_{j-1}), & (\xi_2)_j &= (\xi_1)_j - 2, \\ (\xi_3)_j &= \frac{1}{2}h_j, & (\xi_4)_j &= (\xi_3)_j, \\ (\xi_5)_j &= -2h_j \frac{((\delta p_1)_j + (\delta p_1)_{j-1})}{2} = (\xi_6)_j, \\ (\xi_7)_j &= \frac{3}{2}h_j \frac{((\delta p_2)_j + (\delta p_2)_{j-1})}{2} = (\xi_8)_j, \end{aligned} \right\} \quad (2.57)$$

$$\left. \begin{aligned} (\gamma_1)_j &= 1 + \frac{3}{4}h_j(f_j + f_{j-1}), & (\gamma_2)_j &= (\gamma_1)_j - 2, \\ (\gamma_3)_j &= \frac{3}{2}h_j \frac{((\delta p_3)_j + (\delta p_3)_{j-1})}{2} = (\gamma_4)_j, \\ (\gamma_5)_j &= 0 = (\gamma_6)_j, & (\gamma_7)_j &= 0 = (\gamma_8)_j, \end{aligned} \right\} \quad (2.58)$$

$$\left. \begin{aligned} (r_1)_j &= (f_j - f_{j-1}) + h_j \frac{((\delta p_1)_j + (\delta p_1)_{j-1})}{2}, \\ (r_2)_j &= ((\delta p_1)_j - (\delta p_1)_{j-1}) + h_j \frac{((\delta p_2)_j + (\delta p_2)_{j-1})}{2}, \\ (r_3)_j &= (g_j - g_{j-1}) + h_j \frac{((\delta p_3)_j + (\delta p_3)_{j-1})}{2}, \\ (r_4)_j &= ((\delta p_2)_j - (\delta p_2)_{j-1}) - h_j \frac{(g_j + g_{j-1})}{2} \\ &\quad - 3h_j \frac{(f_j + f_{j-1})}{2} \frac{((\delta p_2)_j + (\delta p_2)_{j-1})}{2} + 2h_j \frac{((\delta p_1)_j + (\delta p_1)_{j-1})^2}{4}, \\ (r_5)_j &= ((\delta p_3)_j - (\delta p_3)_{j-1}) - 3h_j \frac{(f_j + f_{j-1})}{2} \frac{((\delta p_3)_j + (\delta p_2)_{j-1})}{2}. \end{aligned} \right\} \quad (2.59)$$

We have a block-tridiagonal structure after linearization that can be represented

in the block matrix form as

$$A\delta = R, \tag{2.60}$$

in which

$$\begin{bmatrix} [A_1] [C_1] \\ [B_2] [A_2] [C_2] \\ \vdots \\ \vdots \\ \vdots \\ [B_{J-1}] [A_{J-1}] [C_{J-1}] \\ [B_J] [A_J] \end{bmatrix} \begin{bmatrix} [\delta_1] \\ [\delta_2] \\ \vdots \\ \vdots \\ \vdots \\ [\delta_{J-1}] \\ [\delta_J] \end{bmatrix} = \begin{bmatrix} [R_1] \\ [R_2] \\ \vdots \\ \vdots \\ \vdots \\ [R_{J-1}] \\ [R_J] \end{bmatrix}.$$

The entries of the matrices are

$$[A_1] = \begin{bmatrix} 0 & 0 & 1 & 0 & 0 \\ -0.5h_1 & 0 & 0 & -0.5h_1 & 0 \\ 0 & -0.5h_1 & 0 & 0 & -0.5h_1 \\ (\xi_2)_1 & 0 & (\xi_3)_1 & (\xi_1)_1 & 0 \\ 0 & (\gamma_2)_1 & (\gamma_3)_1 & 0 & (\gamma_1)_1 \end{bmatrix},$$

$$[A_j] = \begin{bmatrix} -0.5h_j & 0 & 1 & 0 & 0 \\ -1 & 0 & 0 & -0.5h_j & 0 \\ 0 & -1 & 0 & 0 & -0.5h_j \\ (\xi_6)_j & (\xi_8)_j & (\xi_3)_j & (\xi_1)_j & 0 \\ (\gamma_8)_j & (\gamma_6)_j & (\gamma_3)_j & 0 & (\gamma_1)_j \end{bmatrix}, \quad 2 < j < J$$

$$[B_j] = \begin{bmatrix} 0 & 0 & -1 & 0 & 0 \\ 0 & 0 & 0 & -0.5h_j & 0 \\ 0 & 0 & 0 & 0 & -0.5h_j \\ 0 & 0 & (\xi_4)_j & (\xi_2)_j & 0 \\ 0 & 0 & (\gamma_4)_j & 0 & (\gamma_2)_j \end{bmatrix}, \quad 2 < j < J$$

$$[C_j] = \begin{bmatrix} -0.5h_j & 0 & 0 & 0 & 0 \\ 1 & 0 & 0 & 0 & 0 \\ 0 & 1 & 0 & 0 & 0 \\ (\xi_5)_j & (\xi_7)_j & 0 & 0 & 0 \\ (\gamma_7)_j & (\gamma_5)_j & 0 & 0 & 0 \end{bmatrix}, \quad 1 < j < J - 1$$

$$[\delta_1] = \begin{bmatrix} (\delta p_2)_0 \\ (\delta p_3)_0 \\ \delta f_0 \\ (\delta p_2)_1 \\ (\delta p_3)_1 \end{bmatrix}, \quad [\delta_j] = \begin{bmatrix} (\delta p_1)_{j-1} \\ \delta g_{j-1} \\ \delta f_{j-1} \\ (\delta p_2)_j \\ (\delta p_3)_j \end{bmatrix}, \quad 2 < j < J$$

$$[r_j] = \begin{bmatrix} (r_1)_{j-\frac{1}{2}} \\ (r_2)_{j-\frac{1}{2}} \\ (r_3)_{j-\frac{1}{2}} \\ (r_4)_{j-\frac{1}{2}} \\ (r_5)_{j-\frac{1}{2}} \end{bmatrix}, \quad 2 < j < J.$$

Now we factorize A as

$$A = LU, \tag{2.61}$$

where

$$L = \begin{bmatrix} [a_1] \\ [B_2] [a_2] \\ \ddots \\ \ddots [a_{J-1}] \\ [B_J] [a_J] \end{bmatrix}, \quad U = \begin{bmatrix} [I] [\kappa_1] \\ [I] [\kappa_2] \\ \ddots \ddots \\ [I] [\kappa_{J-1}] \\ [I] \end{bmatrix},$$

In which $[a_i]$ and $[\kappa_i]$ are 5×5 matrices and $[I]$ is an identity matrix of order 5 whose elements are calculated by the subsequent equations:

$$\left. \begin{aligned} [a_1] &= [A_1], \quad [A_1][\kappa_1] = [C_1], \\ [a_j] &= [A_j] - [B_j][\kappa_{j-1}], \quad j = 2, 3, \dots, J \\ [a_j][\kappa_j] &= [C_j], \quad j = 2, 3, \dots, J \end{aligned} \right\} \tag{2.62}$$

From Eqs. (2.60) and (2.61) we have

$$[L][U][\delta] = [R]. \tag{2.63}$$

Equation (2.63) turns into

$$[L][W] = [R]. \tag{2.64}$$

By defining

$$[U][\delta] = [W], \tag{2.65}$$

in which

$$[W] = \begin{bmatrix} [W_1] \\ [W_2] \\ [W_3] \\ [W_4] \\ [W_5] \end{bmatrix},$$

and $[W_j]$ are column matrices of order 5×1 . The elements $[W]$ can be solved from Eq. (2.65):

$$\left. \begin{aligned} [a_1][W_1] &= [R_1], \\ [a_j][W_j] &= [r_j] - [B_j][W_{j-1}], \quad j = 2, 3, \dots, J. \end{aligned} \right\} \tag{2.66}$$

After that, the elements δ is determined by the subsequent relations

$$\left. \begin{aligned} [\delta_J] &= [W_J], \\ [\delta_j] &= [W_j] - [\kappa_j][\delta_{j+1}], \quad j = 2, 3, \dots, J. \end{aligned} \right\} \tag{2.67}$$

These computations are continued till some convergence criterion is fulfilled.

2.16.2 Shooting Method [108]

“ In a shooting method, the missing (unspecified) initial condition at the initial point of the interval is assumed, and the differential equation is then integrated numerically as an initial value problem to the terminal point. The accuracy of the assumed missing initial condition is then checked by comparing the calculated value of the dependent variable at the terminal point with its given value there. If a difference exists, another value of the missing initial condition must be assumed and the process is repeated. This process

is continued until the agreement between the calculated and the given condition at the terminal point is within the specified degree of accuracy. Newton's method is used for the purpose of the updation of the initial guess. In this method, the differential equation is kept in its nonlinear form and the missing slope is found systematically by Newton's method. This method provides quadratic convergence of the iteration and is far better than the usual cut-and-try methods. Due to the sensitivity of the initial guesses in the Newton's method, some time this method diverges due to the singular Jacobian matrix. There is no general hard and fast rule for the successful choice of initial guesses". The whole computation procedure is implemented using MATLAB software. "To understand the functioning of the shooting technique, choose the following 2nd order non-linear BVP

$$y''(x) = f(x, y, y'(x)) \quad (2.68)$$

subject to the boundary conditions

$$y(0) = 0, \quad y(L) = A. \quad (2.69)$$

Setting $y = y_1$ and $y' = y_2$, Eq. (2.68) subject to boundary conditions (2.69) is presented as the following first-order system

$$\left. \begin{aligned} y_1' &= y_2, & y_2' &= f(x, y_1, y_2), \\ y_1(0) &= 0, & y_1(L) &= A. \end{aligned} \right\} \quad (2.70)$$

Denote the missing initial condition $y_2(0)$ by s , to have

$$\left. \begin{aligned} y_1' &= y_2, & y_2' &= f(x, y_1, y_2), \\ y_1(0) &= 0, & y_2(0) &= s. \end{aligned} \right\} \quad (2.71)$$

Now the problem is to find s such that the solution of the IVP (2.71) satisfies the boundary condition $y(L) = A$. In other words, if the solutions of the initial value problem (2.71) are denoted by $y_1(x, s)$ and $y_2(x, s)$, one should search for that value of s which is an approximate root of the equation

$$y_1(L, s) - A = \phi(s) = 0. \quad (2.72)$$

For Newton's method, the iteration formula for s is given by

$$s_{n+1} = s_n - \frac{\phi(s_n)}{\frac{d\phi(s_n)}{ds}} \quad (2.73)$$

or

$$s_{n+1} = s_n - \frac{y_1(L, s_n) - A}{\frac{dy_1(L, s_n)}{ds}}. \quad (2.74)$$

To find the derivative of y_1 with respect of s , differentiate the IVP (2.71) with respect to s . For simplification, use the following notations

$$\frac{dy_1}{ds} = y_3, \quad \frac{dy_2}{ds} = y_4. \quad (2.75)$$

This process results in the following IVP

$$\left. \begin{aligned} y_3' &= y_4, \quad y_4' = \frac{\partial f}{\partial y_1} y_3 + \frac{\partial f}{\partial y_2} y_4, \\ \text{with } y_3(0) &= 0, \quad y_4(0) = 1. \end{aligned} \right\} \quad (2.76)$$

Now, solving the IVP (2.76), the value of y_3 at L can be computed. This value is actually the derivative of y_1 with respect of s computed at L . Setting the value of $y_3(L, s)$ in Eq. (2.74), the modified value of s can be achieved. This new value of s is used to solve the IVP (2.71) and the process is repeated until the value of s is within a described degree of accuracy".

Chapter 3

Numerical Simulation of MHD Jeffrey Nanofluid Flow and Heat Transfer over a Stretching Sheet

3.1 Introduction

The purpose of this chapter is to numerically examine the impact of silver, titanium oxide and alumina nanoparticles on the steady 2D magnetohydrodynamic boundary layer flow and heat transfer of Jeffrey fluid over a stretching sheet with Joule heating and viscous dissipation. The governing non-linear partial differential equations (PDEs) are reduced to the non-linear ordinary differential equations (ODEs) by using some appropriate dimensionless variables and then solved numerically by using the Keller-box technique. The impacts of nanoparticle volume fraction, magnetic parameter, Deborah number, Prandtl number and Eckert number on the velocity and temperature profiles, local Nusselt number and skin friction are investigated through graphs and tables. The results indicate that the silver-ethylene glycol nanofluid has comparatively less velocity, skin friction and local Nusselt number than those of the base fluid. However the temperature is enhanced due to the inclusion of the

nanoparticles. Furthermore, it is concluded that both the skin friction and the Nusselt number are increased by increasing the Deborah number whereas these are decreased by increasing the magnetic parameter.

3.2 Mathematical Formulation

We investigate the steady, two-dimensional, laminar and electrically conducting flow of an incompressible Jeffrey nanofluid fluid due to a stretching sheet coinciding with the plane $y = 0$. The fluid is magnetohydrodynamic in the presence of time independent magnetic field B_0 applied in the y -direction, restricted in $y > 0$ (see Fig. 3.1). In this case, x -axis is considered parallel to the stretching surface. The flow is produced because of the linear stretch of the surface away from the leading edge with the velocity $U_w = ax$, $a > 0$. The plate is taken into account to own a temperature T_w in the quadratic form at the surface $y = 0$ i.e. $T_w = A(\frac{x}{L})^2 + T_\infty$. The induced magnetic field is neglected as we consider the small magnetic Reynolds number. The subjected model

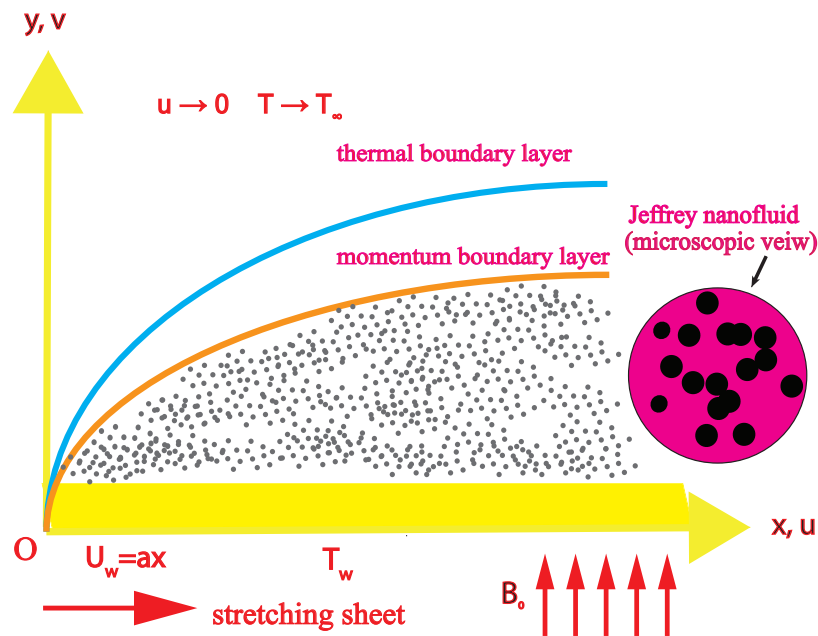


FIG. 3.1: Geometry of the problem.

is governed by the following boundary layer equations[109] of continuity, momentum and energy.

$$\frac{\partial u}{\partial x} + \frac{\partial v}{\partial y} = 0, \tag{3.1}$$

$$u \frac{\partial u}{\partial x} + v \frac{\partial u}{\partial y} = \frac{\nu_{nf}}{(1 + \lambda_1)} \left(\lambda_2 \left(u \frac{\partial^3 u}{\partial x \partial^2 y} - \frac{\partial u}{\partial x} \frac{\partial^2 u}{\partial y^2} \right) + \frac{\partial u}{\partial y} \frac{\partial^2 u}{\partial x \partial y} + v \frac{\partial^3 u}{\partial y^3} \right) + \frac{\partial^2 u}{\partial y^2} - \frac{\sigma_{nf}}{\rho_{nf}} B_0^2 u, \quad (3.2)$$

$$u \frac{\partial T}{\partial x} + v \frac{\partial T}{\partial y} = \frac{\mu_{nf}}{(\rho c_p)_{nf}(1 + \lambda_1)} \left(\lambda_2 \left(u \frac{\partial u}{\partial y} \frac{\partial^2 u}{\partial x \partial y} + v \frac{\partial u}{\partial y} \frac{\partial^2 u}{\partial y^2} \right) + \left(\frac{\partial u}{\partial y} \right)^2 \right) + \frac{k_{nf}}{(\rho c_p)_{nf}} \frac{\partial^2 T}{\partial y^2} + \frac{\sigma_{nf}}{(\rho c_p)_{nf}} B_0^2 u^2. \quad (3.3)$$

The boundary conditions are

$$\left. \begin{aligned} u = u_w, \quad v = 0, \quad T = T_w \quad \text{at} \quad y = 0, \\ u \rightarrow 0, \quad \frac{\partial u}{\partial y} \rightarrow 0, \quad T \rightarrow T_\infty \quad \text{as} \quad y \rightarrow \infty, \end{aligned} \right\} \quad (3.4)$$

where $\nu_{nf} = \frac{\mu_{nf}}{\rho_{nf}}$ is the kinematic viscosity and u and v are the x and y components of velocity. The ratio of the relaxation to the retardation time and the retardation time are represented by λ_1 and λ_2 respectively and T is the nanofluid temperature. Thermophysical properties of the base fluid and different nanoparticles are shown in Table 3.1.

Nanofluid effective density [8] is given by

$$\rho_{nf} = (1 - \phi)\rho_f + \phi\rho_s. \quad (3.5)$$

The effective heat capacity $(\rho c_p)_{nf}$ and the effective dynamic viscosity μ_{nf} of the nanofluid [110] are given as

$$(\rho c_p)_{nf} = (1 - \phi)(\rho c_p)_f + \phi(\rho c_p)_s, \quad \mu_{nf} = \frac{\mu_f}{(1 - \phi)^{2.5}}. \quad (3.6)$$

We consider the Maxwell Garnett model [111] for the effective thermal conductivity k_{nf} of the nanofluids

$$\frac{k_{nf}}{k_f} = \frac{(k_s + 2k_f) - 2\phi(k_f - k_s)}{(k_s + 2k_f) + (k_f - k_s)\phi}. \quad (3.7)$$

Moreover, the electrical conductivity σ_{nf} of nanofluids [112] is as follows

$$\frac{\sigma_{nf}}{\sigma_f} = 1 + \frac{3(\sigma_s - \sigma_f)\phi}{(\sigma_s + 2\sigma_f) - (\sigma_s - \sigma_f)\phi}. \quad (3.8)$$

TABLE 3.1: Thermophysical properties of the base fluid and different nanoparticles[113].

Physical properties	Base fluid	Nanoparticles		
	$C_2H_6O_2$	Ag	Al_2O_3	TiO_2
ρ (kg/m^3)	1115	10500	3970	4250
k (W/mK)	0.259	429	40	8.953
c_p (J/kgK)	2386	235	765	686.2
σ_f (S/m)	1.07×10^{-8}	62.1×10^6	35×10^6	2.6×10^6

Introduce the following similarity transformation for conversion of Eqs. (3.1)–(3.3) into the ordinary differential equations,

$$\eta = \sqrt{\frac{a}{\nu}}y, \quad \psi = -\sqrt{a\nu}xf(\eta), \quad \theta = \frac{T - T_\infty}{T_w - T_\infty}, \tag{3.9}$$

where f is the dimensionless stream function, θ is the dimensionless temperature, η is the similarity variable and ψ is the stream function satisfying $u = \frac{\partial\psi}{\partial y}$ and $v = -\frac{\partial\psi}{\partial x}$. Thus, we have

$$u = axf'(\eta), \quad v = -\sqrt{a\nu}f(\eta). \tag{3.10}$$

Invoking Eqs. (3.9) and (3.10), Eq. (3.1) is automatically satisfied and Eqs. (3.2) and (3.3) are reduced to

$$f''' - \frac{A_2}{A_1}(1 + \lambda_1)[(f')^2 - ff''] + \beta[(f'')^2 - ff'''] - (1 + \lambda_1)\frac{A_3}{A_1}Mf' = 0, \tag{3.11}$$

$$\begin{aligned} \theta'' + \frac{A_4}{A_5}Pr(f\theta' - 2\theta f') + \frac{A_1}{A_5}PrEc\left((f'')^2 + \lambda_2 f''(f'f'' - ff''')\right) \\ + \frac{A_3}{A_5}EcPrM(f')^2 = 0, \end{aligned} \tag{3.12}$$

having the subsequent dimensionless end-point conditions:

$$\left. \begin{aligned} f(0) = 0, \quad f'(0) = 1, \quad \theta(0) = 1 \quad \text{at } \eta = 0, \\ f' \rightarrow 0, \quad f'' \rightarrow 0, \quad \theta \rightarrow 0 \quad \text{as } \eta \rightarrow \infty. \end{aligned} \right\} \tag{3.13}$$

Parameters involved in the non-dimensional equations are given by

$$\beta = a\lambda_2 \quad (\text{Deborah number}), \quad M = \frac{\sigma_f B_0^2}{a\rho_f} \quad (\text{magnetic parameter}), \quad (3.14)$$

$$Pr = \frac{\mu_f(c_p)_f}{k_f} \quad (\text{Prandtl number}), \quad Ec = \frac{a^2 l^2}{A(c_p)_f} \quad (\text{Eckert number}), \quad (3.15)$$

$$A_1 = \frac{1}{(1-\phi)^{2.5}}, \quad A_2 = \left[(1-\phi) + \phi \frac{\rho_s}{\rho_f} \right], \quad (3.16)$$

$$A_3 = 1 + \frac{3\left(\frac{\rho_s}{\rho_f} - 1\right)\phi}{\left(\frac{\rho_s}{\rho_f} + 2\right) - \left(\frac{\rho_s}{\rho_f} - 1\right)\phi}, \quad A_4 = \left[(1-\phi) + \phi \frac{(\rho c_p)_s}{(\rho c_p)_f} \right], \quad (3.17)$$

$$A_5 = \frac{(k_s + 2k_f) - 2\phi(k_f - k_s)}{(k_s + 2k_f) + (k_f - k_s)}, \quad (\text{thermal conductivities ratio}). \quad (3.18)$$

The important physical parameters, skin-friction coefficient C_f and local Nusselt number Nu_x , are specified as

$$C_f = \frac{2\tau_w}{\rho_f u_w^2}, \quad Nu_x = \frac{xq_w}{k_f(T_w - T_\infty)}, \quad (3.19)$$

where $\tau_w = \mu_{nf}\left(\frac{\partial u}{\partial y}\right)$ is the wall shear-stress and $q_w = -k_{nf}\left(\frac{\partial T}{\partial y}\right)$ is the heat flux at wall. Using the similarity transformation presented above, Eq. (3.19) can be reduced as:

$$C_f Re_x^{1/2} = (1-\phi)^{-2.5} f''(0), \quad Re_x^{-1/2} Nu_x = -\frac{k_{nf}}{k_f} \theta'(0), \quad (3.20)$$

where the local Reynolds number is given by $Re_x = \frac{U_x}{\nu}$.

3.3 Solution Methodology

The resulting system of nonlinear ODEs (3.11) - (3.12) subject to the end-point conditions (3.13) has been attempted numerically through the Keller-box method [114, 115] for different values of the governing parameters. The subsequent steps are involved to obtain the numerical solution:

1. Transformation of the coupled non-linear momentum as well as heat equations in the form of a system of first order differential equations.

2. Utilization of the central difference approximations for getting the difference equations.
3. Linearization of the nonlinear system by the Newton's method.
4. Iterative solution of the linear system by the block tri-diagonal elimination scheme.

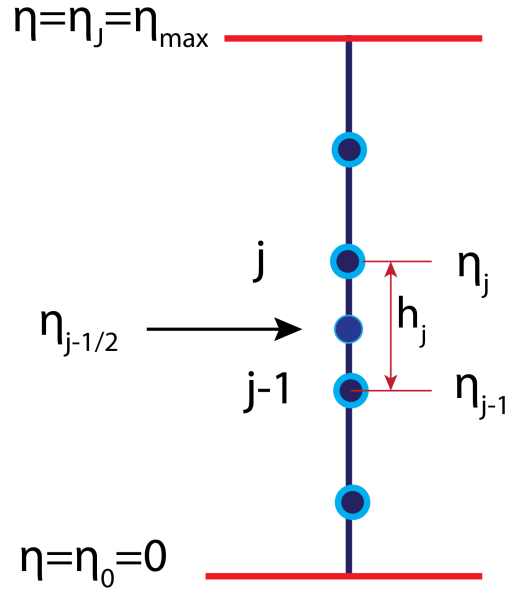


FIG. 3.2: Typical grid structure for difference approximations.

Typical grid structure for difference approximations[105] is shown in the Fig. 3.2. The domain has been discretized by using the following nodes:

$$\eta_0 = 0, \quad \eta_j = \eta_{j-1} + h_j, \quad j = 1, 2, 3, \dots, J, \quad \eta_J = \eta_\infty \quad \text{where, } h_j \text{ is the step-size.}$$

We bring in the dependent variables \tilde{u} , \tilde{v} , \tilde{w} and \tilde{t} such that

$$\frac{df}{d\eta} = \tilde{u}, \quad \frac{d\tilde{u}}{d\eta} = \tilde{v}, \quad \frac{d\tilde{v}}{d\eta} = \tilde{w}, \quad \frac{d\theta}{d\eta} = \tilde{t}. \quad (3.21)$$

So Eqs. (3.11) and (3.12) can be presented as

$$-\beta f \frac{d\tilde{w}}{d\eta} + \tilde{w} - \frac{A_2}{A_1}(1 + \lambda_1)[\tilde{u}^2 - f\tilde{v}] + \beta \tilde{v}^2 - \frac{A_3}{A_1}(1 + \lambda_1)M\tilde{u} = 0 \quad (3.22)$$

$$\frac{d\tilde{t}}{d\eta} + \frac{A_4}{A_5}Pr(f\tilde{t} - 2\tilde{u}\theta) + \frac{A_1}{A_5}PrEc\left((\tilde{v})^2 + \lambda_2\tilde{v}(\tilde{u}\tilde{v} - f\tilde{w})\right) + \frac{A_3}{A_5}MPrEc\tilde{u}^2 = 0. \quad (3.23)$$

The transformed boundary conditions for the problem are

$$\left. \begin{aligned} f(0) = 0, \tilde{u}(0) = 1, \theta(0) = 1, \\ \tilde{u} \rightarrow 0, \tilde{v} \rightarrow 0, \theta \rightarrow 0 \quad \text{as } \eta \rightarrow \infty. \end{aligned} \right\} \quad (3.24)$$

Eqs. (3.21) - (3.23) have been approximated by using the central difference at midpoint $\eta_{j-1/2}$, as follows

$$\frac{f_j - f_{j-1}}{h_j} = \tilde{u}_{j-\frac{1}{2}}, \quad \frac{\tilde{u}_j - \tilde{u}_{j-1}}{h_j} = \tilde{v}_{j-\frac{1}{2}}, \quad (3.25)$$

$$\frac{\tilde{v}_j - \tilde{v}_{j-1}}{h_j} = \tilde{w}_{j-\frac{1}{2}}, \quad \frac{\theta_j - \theta_{j-1}}{h_j} = \tilde{t}_{j-\frac{1}{2}}, \quad (3.26)$$

$$\begin{aligned} \tilde{w}_{j-\frac{1}{2}} - \frac{A_2}{A_1}(1 + \lambda_1) \left[\left(\tilde{u}_{j-\frac{1}{2}} \right)^2 - \left(f_{j-\frac{1}{2}} \right) \left(\tilde{v}_{j-\frac{1}{2}} \right) \right] + \\ \beta \left[\left(\tilde{v}_{j-\frac{1}{2}} \right)^2 - \left(f_{j-\frac{1}{2}} \right) \left(\frac{\tilde{w}_j - \tilde{w}_{j-1}}{h_j} \right) \right] - \frac{A_3}{A_1} M(1 + \lambda_1) \left(\tilde{u}_{j-\frac{1}{2}} \right) = 0 \end{aligned} \quad (3.27)$$

$$\begin{aligned} \frac{\tilde{t}_j - \tilde{t}_{j-1}}{h_j} + \frac{A_4}{A_5} Pr \left(f_{j-\frac{1}{2}} \right) \left(\tilde{t}_{j-\frac{1}{2}} \right) - 2 \frac{A_4}{A_5} Pr \left(\tilde{u}_{j-\frac{1}{2}} \right) \left(\theta_{j-\frac{1}{2}} \right) + \frac{A_1}{A_5} Pr Ec \\ \left(\left(\tilde{v}_{j-\frac{1}{2}} \right)^2 + \lambda_2 \tilde{v}_{j-\frac{1}{2}} \left(\tilde{u}_{j-\frac{1}{2}} \tilde{v}_{j-\frac{1}{2}} - f_{j-\frac{1}{2}} \tilde{w}_{j-\frac{1}{2}} \right) \right) + \frac{A_3}{A_5} M Pr Ec \left(\tilde{u}_{j-\frac{1}{2}} \right)^2 = 0 \end{aligned} \quad (3.28)$$

in which $\tilde{u}_{j-\frac{1}{2}} = \frac{\tilde{u}_j + \tilde{u}_{j-1}}{2}$ etc. To linearize the system of nonlinear Eqs. (3.25) - (3.28) by Newton's method, the following substitution has been introduced:

$$\left. \begin{aligned} f_j^{n+1} = f_j^n + \delta f_j^n, \quad \tilde{u}_j^{n+1} = \tilde{u}_j^n + \delta \tilde{u}_j^n, \quad \tilde{v}_j^{n+1} = \tilde{v}_j^n + \delta \tilde{v}_j^n, \\ \tilde{w}_j^{n+1} = \tilde{w}_j^n + \delta \tilde{w}_j^n, \quad \tilde{t}_j^{n+1} = \tilde{t}_j^n + \delta \tilde{t}_j^n, \quad \theta_j^{n+1} = \theta_j^n + \delta \theta_j^n. \end{aligned} \right\} \quad (3.29)$$

Putting these expressions in Eqs. (3.25) - (3.28) and dropping the higher-order terms in δ , the following system is obtained:

$$\delta f_j - \delta f_{j-1} - \frac{h_j}{2} (\delta \tilde{u}_j + \delta \tilde{u}_{j-1}) = (r_1)_j, \quad (3.30)$$

$$\delta \tilde{u}_j - \delta \tilde{u}_{j-1} - \frac{h_j}{2} (\delta \tilde{v}_j + \delta \tilde{v}_{j-1}) = (r_2)_j, \quad (3.31)$$

$$\delta \tilde{v}_j - \delta \tilde{v}_{j-1} - \frac{h_j}{2} (\delta \tilde{w}_j + \delta \tilde{w}_{j-1}) = (r_3)_j, \quad (3.32)$$

$$\delta \theta_j - \delta \theta_{j-1} - \frac{h_j}{2} (\delta \tilde{t}_j + \delta \tilde{t}_{j-1}) = (r_4)_j, \quad (3.33)$$

$$\begin{aligned} (\xi_1)_j \delta \tilde{w}_j + (\xi_2)_j \delta \tilde{w}_{j-1} + (\xi_3)_j \delta f_j + (\xi_4)_j \delta f_{j-1} + (\xi_5)_j \delta \tilde{v}_j \\ + (\xi_6)_j \delta \tilde{v}_{j-1} + (\xi_7)_j \delta \tilde{u}_j + (\xi_8)_j \delta \tilde{u}_{j-1} = (r_5)_j, \end{aligned} \quad (3.34)$$

$$\begin{aligned} (\gamma_1)_j \delta \tilde{t}_j + (\gamma_2)_j \delta \tilde{t}_{j-1} + (\gamma_3)_j \delta f_j + (\gamma_4)_j \delta f_{j-1} + (\gamma_5)_j \delta \tilde{u}_j + (\xi_6)_j \delta \tilde{u}_{j-1} \\ + (\gamma_7)_j \delta \theta_j + (\gamma_8)_j \delta \theta_{j-1} + (\gamma_9)_j \delta \tilde{v}_j + (\gamma_{10})_j \delta \tilde{v}_{j-1} = (r_6)_j, \end{aligned} \quad (3.35)$$

where the elements defined in Eq. (3.38) are

$$\begin{aligned}
 [A_1] &= \begin{bmatrix} 0 & 0 & 0 & 1 & 0 & 0 \\ -0.5h_1 & 0 & 0 & 0 & 0 & 0 \\ -1 & -0.5h_1 & 0 & 0 & -0.5h_1 & 0 \\ 0 & 0 & -0.5h_1 & 0 & 0 & -0.5h_1 \\ (\xi_6)_1 & (\xi_2)_1 & 0 & (\xi_3)_1 & (\xi_1)_1 & 0 \\ (\gamma_{10})_1 & 0 & (\gamma_2)_1 & (\gamma_3)_1 & 0 & (\gamma_1)_1 \end{bmatrix}, \\
 [A_j] &= \begin{bmatrix} -0.5h_j & 0 & 0 & 1 & 0 & 0 \\ -1 & -0.5h_j & 0 & 0 & 0 & 0 \\ 0 & -1 & 0 & 0 & -0.5h_j & 0 \\ 0 & 0 & -1 & 0 & 0 & -0.5h_j \\ (\xi_8)_j & (\xi_6)_j & 0 & (\xi_3)_j & (\xi_1)_j & 0 \\ (\gamma_6)_j & (\gamma_{10})_j & (\gamma_8)_j & (\gamma_3)_j & 0 & (\gamma_1)_j \end{bmatrix}, 2 \leq j \leq J \\
 [B_j] &= \begin{bmatrix} 0 & 0 & 0 & -1 & 0 & 0 \\ 0 & 0 & 0 & 0 & 0 & 0 \\ 0 & 0 & 0 & 0 & -0.5h_j & 0 \\ 0 & 0 & 0 & 0 & 0 & -0.5h_j \\ 0 & 0 & 0 & (\xi_4)_j & (\xi_2)_j & 0 \\ 0 & 0 & 0 & (\gamma_4)_j & 0 & (\gamma_2)_j \end{bmatrix}, 2 \leq j \leq J \\
 [C_j] &= \begin{bmatrix} -0.5h_j & 0 & 0 & 0 & 0 & 0 \\ 1 & -0.5h_j & 0 & 0 & 0 & 0 \\ 0 & 1 & 0 & 0 & 0 & 0 \\ 0 & 0 & 1 & 0 & 0 & 0 \\ (\xi_7)_j & (\xi_5)_j & 0 & 0 & 0 & 0 \\ (\gamma_5)_j & (\gamma_9)_j & (\gamma_7)_j & 0 & 0 & 0 \end{bmatrix}, 1 \leq j \leq J - 1.
 \end{aligned}$$

Now we factorize A as

$$A = LU, \tag{3.39}$$

where

$$L = \begin{bmatrix} [\alpha_1] & & & & & \\ [B_2] [\alpha_2] & & & & & \\ & \ddots & & & & \\ & & \ddots & & & \\ & & & [\alpha_{J-1}] & & \\ & & & & [B_J] [\alpha_J] & \end{bmatrix}, U = \begin{bmatrix} [I] [\Gamma_1] & & & & & \\ & [I] [\Gamma_2] & & & & \\ & & \ddots & \ddots & & \\ & & & & [I] [\Gamma_{J-1}] & \\ & & & & & [I] \end{bmatrix},$$

where $[I]$ is the identity matrix of order 6, $[\alpha_i]$, $[B_i]$ and $[\Gamma_i]$ are 6×6 matrices. Eq. (3.38) is solved by the LU factorization for the solution of δ . Since the physical domain of the problem is unbounded, we use far field boundary at $\eta_{max} = 14$ due to the observation that the variations in the solution after $\eta = 14$ are ignorable. For mathematical calculations, a grid size of $\eta_j = 0.01$ is appear to be adequate, and the solutions are attained having an error tolerance of 10^{-5} . In order to validate the accuracy of the numerical procedure, we have assimilated our outcomes with the ones reported by Ishak et al. [116] and Pal et al. [117] for $\theta'(0)$ in the case of $\beta = \phi = Ec = M = 0$ and found an outstanding agreement as revealed in Table 3.2. In the absence of the nanoparticle volume fraction i.e., $\phi = 0$, the problem reduces to that of Ahmad et al. [118].

TABLE 3.2: Comparison of $-f''(0)$ with various values of M .

Pr	Ishak et al. [116]	Pal et al. [117]	Present study
1.0	1.3333	1.333333	1.337050
3.0	2.5097	2.509715	2.500405
10	4.7969	4.796871	4.798532

3.4 Results and Discussions

The MHD flow of Jeffrey nanofluid over a stretching surface is investigated numerically by using the Keller box technique. Silver (Ag), alumina (Al_2O_3) and titanium oxide (TiO_2) nanoparticles are suspended in ethylene glycol. The values of the local drag coefficient as well as the local heat transfer rate for various values of ϕ , β , M , Pr and Ec are displayed in Table 3.3. The flow and heat profiles are examined with the presence and absence of the magnetic field. From Table 3.3, it is noted that an increment in ϕ and M tends to decrease the skin friction at surface whereas it increases for the raising

values of β . An increment in the nanoparticle volume fraction ϕ , Deborah number β and Prandtl number Pr tends to enhance the Nusselt number whereas the same decreases for the raising values of M , and Ec .

TABLE 3.3: Numerical values of $C_f Re_x^{1/2}$ and $Nu_x Re_x^{-1/2}$ for various values of parameters.

ϕ	β	M	Pr	Ec	$C_f Re_x^{1/2}$	$Nu_x Re_x^{-1/2}$
0.0	0.5	0.5	10	0.3	-1.000029	4.010241
0.05					-1.063858	4.155549
0.1					-1.101554	4.293515
0.05	0.0	0.2	10	0.3	-0.923876	5.303468
	0.5				-0.791391	6.241483
	1				-0.685693	6.937440
0.05	0.2	0.0	10	0.3	-0.829830	6.512465
		0.5			-0.979298	3.954082
		1			-1.119629	1.456768
0.05	0.5	0.5	7	0.3	-0.875963	4.081095
			9		-0.875963	4.488608
			11		-0.875963	4.830241
0.05	2	0.5	10	0.5	-0.619606	3.619765
				1	-0.619606	-2.898086
				1.5	-0.619606	-9.415937

Figs 3.3-3.20 are drawn to observe the variations in the fluid flow and heat transfer behavior for various values of ϕ , β , M , Pr and Ec . Fig. 3.3 displays the impact of various nanoparticles i.e. Ag , Al_2O_3 and TiO_2 on the velocity profile with $C_2H_6O_2$ as the base liquid. It is noted that the velocity field for Al_2O_3 -ethylene glycol Jeffrey nanofluid is higher compared with Ag -ethylene glycol and TiO_2 -ethylene glycol Jeffrey nanofluids. The results indicate that the thermal conductivity and viscosity of the Al_2O_3 nanofluid is greater as compared to the Ag -ethylene glycol and TiO_2 -ethylene glycol nanofluids. Fig. 3.4 portrays the behaviour of the temperature field for Ag , Al_2O_3 and TiO_2 suspended in the ethylene glycol. It is observed that Ag -ethylene glycol Jeffrey nanofluid has a higher temperature profile when compared with Al_2O_3 -ethylene glycol and TiO_2 -ethylene glycol based Jeffrey nanofluids.

It is seen from Fig. 3.5 that an increment in ϕ decreases the velocity field. Actually, due to addition of solid particles in the base liquid, the density of the whole mixture increases substantially. Hence, the velocity of the nanofluid gets slower compared to

that of the base liquid. Fig. 3.6 illustrates the impact of ϕ on the thermal profile. An increment in ϕ produces an augmentation in the thermal profile and so the thickness of thermal boundary layer. Physically, enhancing ϕ causes a rise in the conduction of heat inside the mixture, which then increases the thickness of boundary layer and an augmentation in the thermal profile.

Fig. 3.7 illustrates the influence of the β on the flow profile. It might be seen that a boost in β enhances the flow velocity and so the thickness of boundary layer. As β depends upon the stretching rate a , so an increment in β triggers an increment in the fluid movement near the boundary adjacent to the sheet. As a result, it enhances the velocity as well as thickness of the boundary layer. The impact of M can also be observed from this figure and it is concluded that a rise in M reduces the thickness of boundary layer and the velocity profile. The reason behind is that the magnetic field produces the electromagnetic force that gives opposition to the motion of fluid and hence reduces the fluid velocity. Fig. 3.8 reveals the effect of β on the thermal field $\theta(\eta)$. It is evident that a diminishing behavior in the thermal profile appears for the escalating values of β . A rise in the temperature is revealed in Fig. 3.8 due to the resistance offered to the flow and retardation of the fluid flow.

In Fig. 3.9, the velocity field is plotted for different values of the Deborah number β . It is clear that there is a growth in the velocity profile with an increment in β , because the Deborah number β is directly related to the stretching rate a of sheet. An augmentation in β leads to accelerate the nanofluid motion in the momentum boundary layer. Additionally, an increment in the nanofluid motion leads to rise in the boundary layer thickness and the nanofluid velocity. Fig. 3.10 shows the impact of Pr on the temperature fields for $\beta=0$ (viscous nanofluid) and $\beta=1$ (Jeffrey nanofluid). An increment in Pr quickly decreases θ as well as the thickness of boundary layer. The viscosity of the mixture increases due to the Prandtl number which results in lessening the temperature profile. It can also be observed that the introduction of β reduces the surface temperature of the sheet.

In Fig. 3.11, the impact of Ec on the thermal profile is exhibited for both the viscous nanofluid and the Jeffrey nanofluid. It might be viewed from Fig. 3.11 that an

increment in Ec has boosted the thermal profile θ because the heat is accumulated in the nanofluid caused by the frictional heating. It is identified that near the surface, the thermal profile overshoots for the larger values of Ec . The behavior of $-\theta'(0)$ against Ec for various values of β is plotted in Fig. 3.12. It is noted that an increment in β boost $-\theta'(0)$ and the heat transfer rate is found to be low for the larger values of Ec . Fig. 3.13 reflects that $-\theta'(0)$ increases as β increases which as a result increases the heat transfer in the boundary layer. It is noticed that the heat transfer rate is reduced when the magnetic parameter M is raised. The drag coefficient $f''(0)$ on the surface versus Deborah number β for distinct values of M is plotted in Fig. 3.14. It is found that for increasing values of β , the drag coefficient is increased. Fig. 3.14 reveals that the enhancing values of M decrease the drag coefficient.

It can be observed from Fig. 3.15 that $-\theta'(0)$ is a steadily increasing function of ϕ . On the other hand, Figs. 3.16 and 3.17-3.18 show that $-\theta'(0)$ is declined for the increasing values of ϕ . It is determined from the Figs. 3.15-3.18 that $-\theta'(0)$ is decreased for the rising values of M and Ec whereas it is increased for the increasing values of β and Pr . Physically, for a higher Prandtl number Pr , the nanofluid thermal conductivity is lowered down, due to which their heat conduction potential diminishes. Thus the thickness of thermal boundary layer gets decreased. As a result, the heat transport rate is improved at the wall. The raising magnetic parameter also raises the thickness of boundary layer and consequently the heat transport rate diminishes due to an improvement in the magnetic parameter.

The drag coefficient $f''(0)$ on the surface versus the nanoparticle volume fraction ϕ for a variety of values of the magnetic parameter is plotted in Fig. 3.19. In this case, we found that the skin friction coefficient is decreased whenever we enhance the values of ϕ . Fig. 3.19 reveals that the increasing values of the magnetic parameter M decrease the drag coefficient. The behavior of the the drag coefficient $f''(0)$ against the nanoparticle volume fraction ϕ for various values of β is plotted in Fig. 3.20. It is found that the drag coefficient is decreased when ever we boost the values of ϕ . Fig. 3.20 reveals the influence of β on the drag coefficient. It is evident that a rise in β enhances the skin friction coefficient. The magnitude of the drag coefficient is decreased by enlarging the nanoparticle volume fraction ϕ .

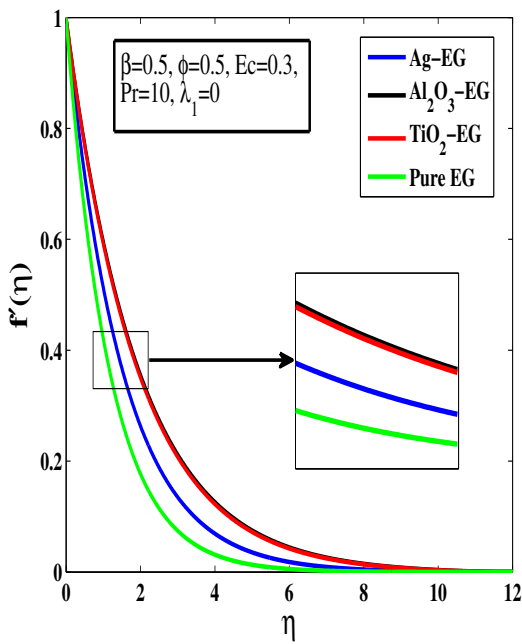


FIG. 3.3: Velocity field for various types of nanofluids.

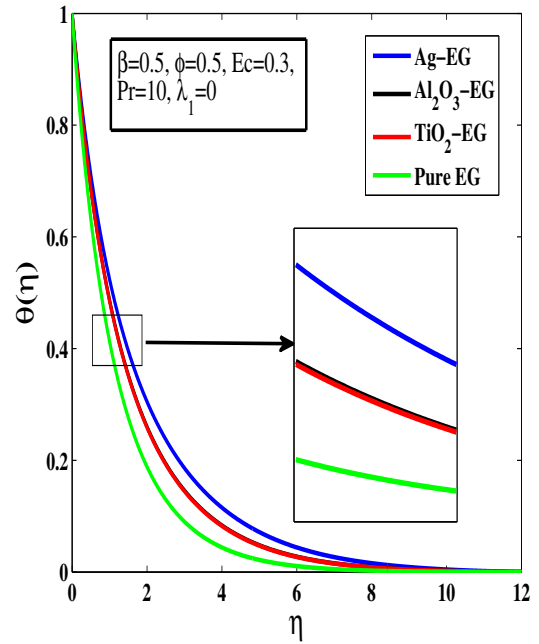


FIG. 3.4: Temperature field for various types of nanofluids.

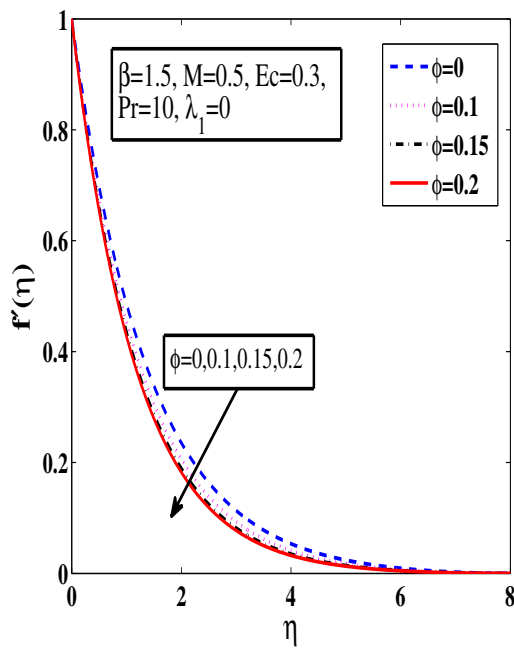


FIG. 3.5: Velocity field corresponding to various values of ϕ .

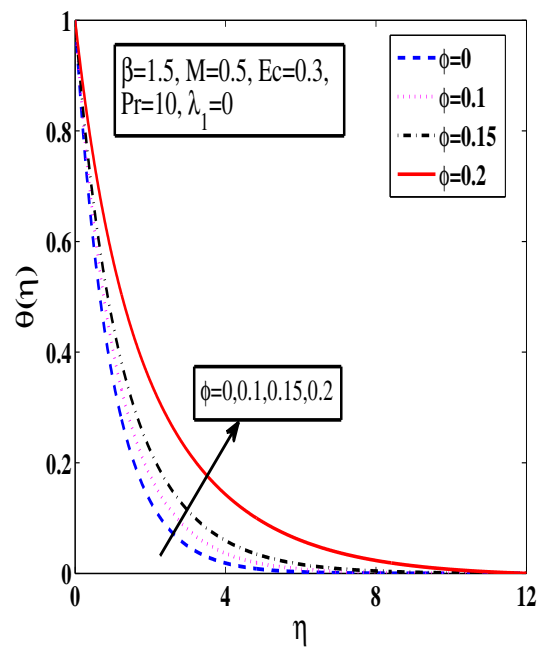


FIG. 3.6: Temperature field corresponding to various values of ϕ .

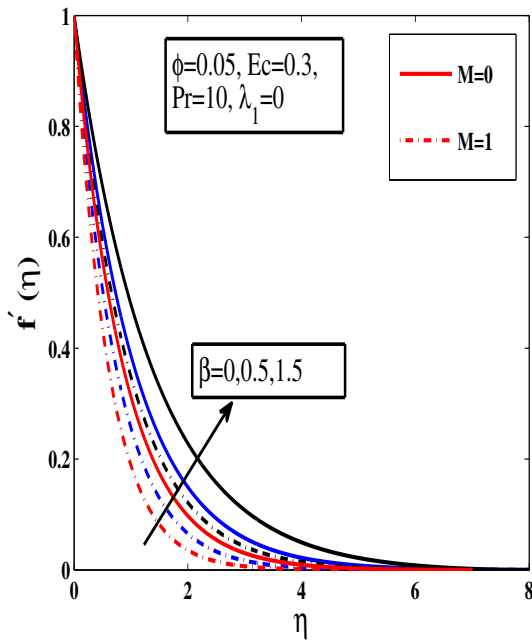


FIG. 3.7: Velocity profile corresponding to various values of Deborah number β .

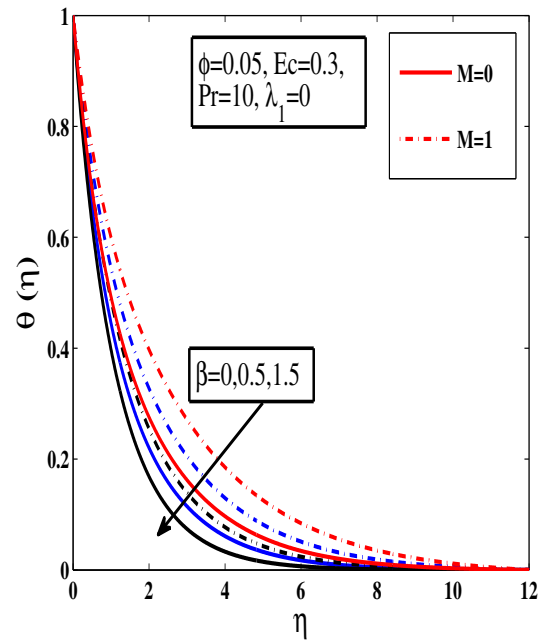


FIG. 3.8: Temperature profile corresponding to various values of Deborah number β .

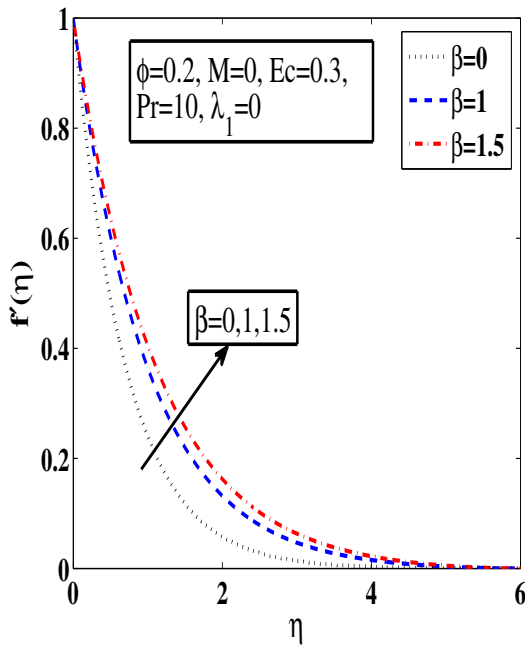


FIG. 3.9: The velocity profile $f''(0)$ for various values of β .

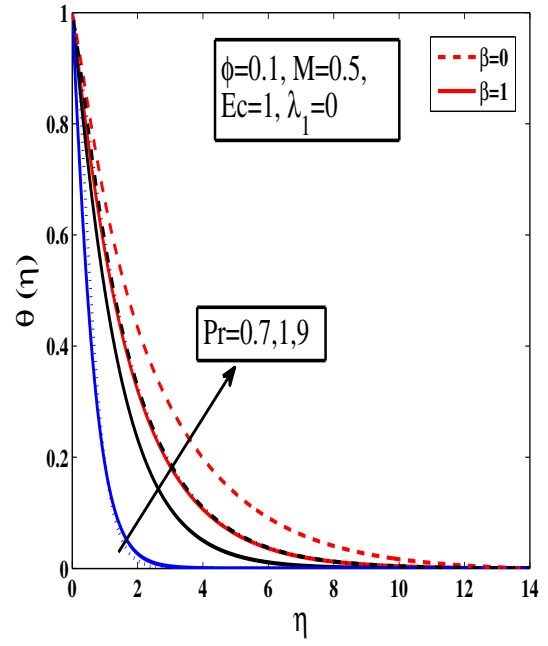


FIG. 3.10: The temperature profile θ for different values of Pr and β .

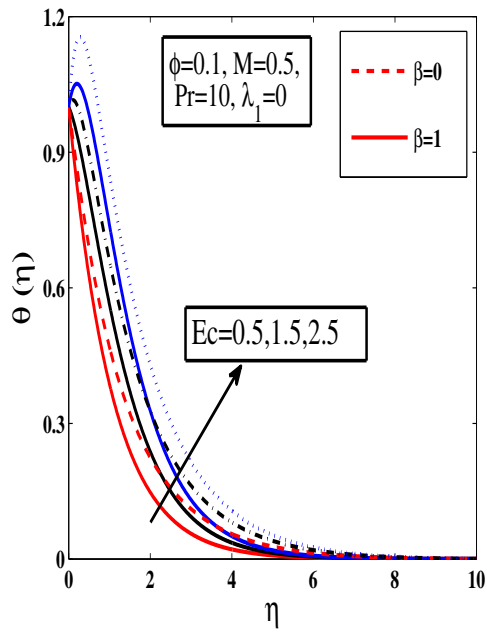


FIG. 3.11: Temperature distribution for different values of Ec and β .

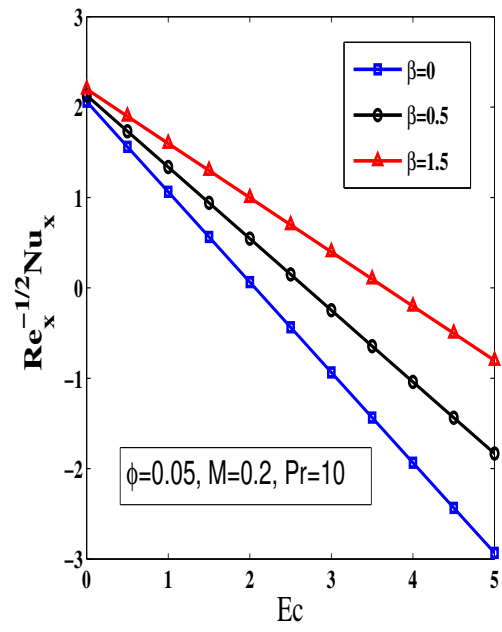


FIG. 3.12: variation of the local Nusselt number against Ec for various values of β .

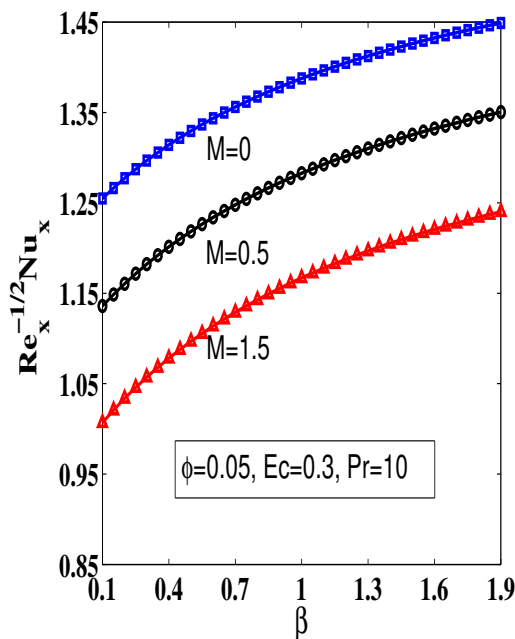


FIG. 3.13: Variation of Nusselt number against β for various values of M .

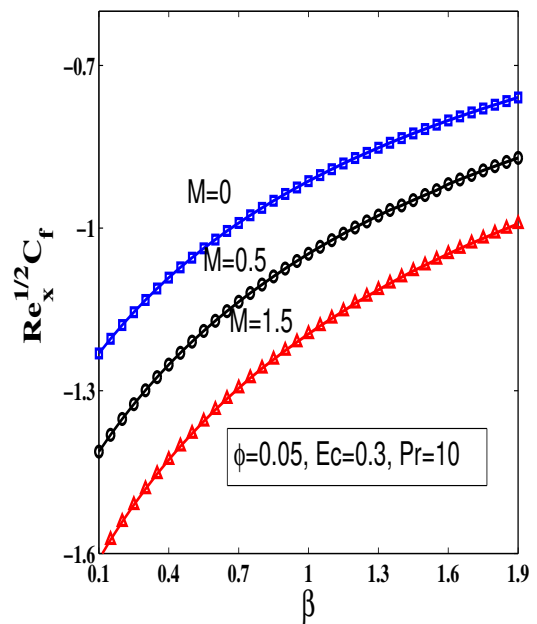


FIG. 3.14: Variation of skin friction coefficient against β for various values of M .

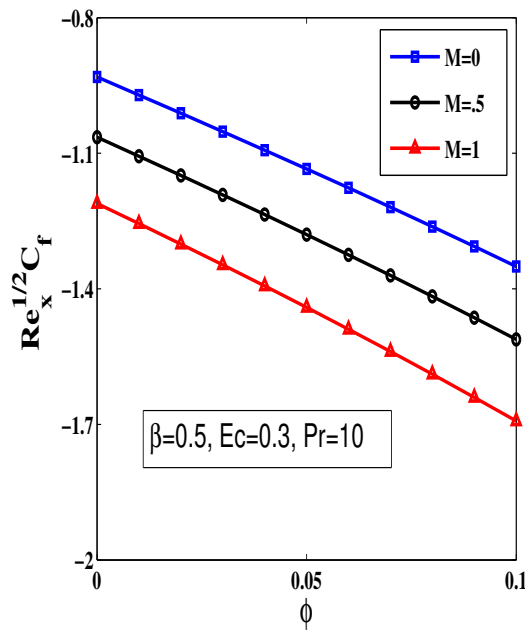


FIG. 3.15: Variation of skin friction coefficient against ϕ for various values of M .

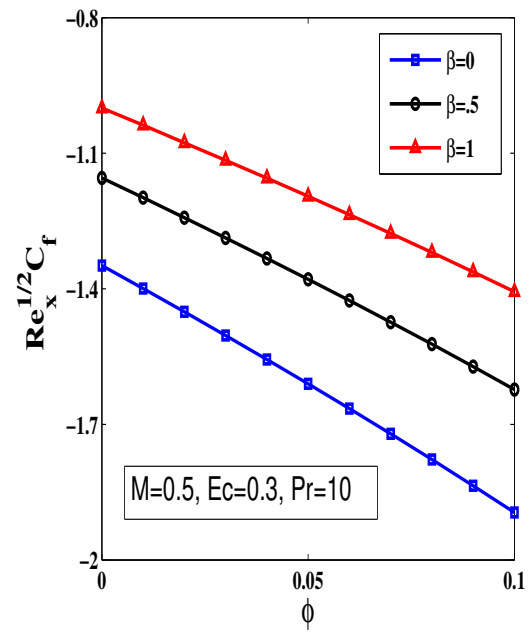


FIG. 3.16: Variation of skin friction coefficient against ϕ for various values of β .

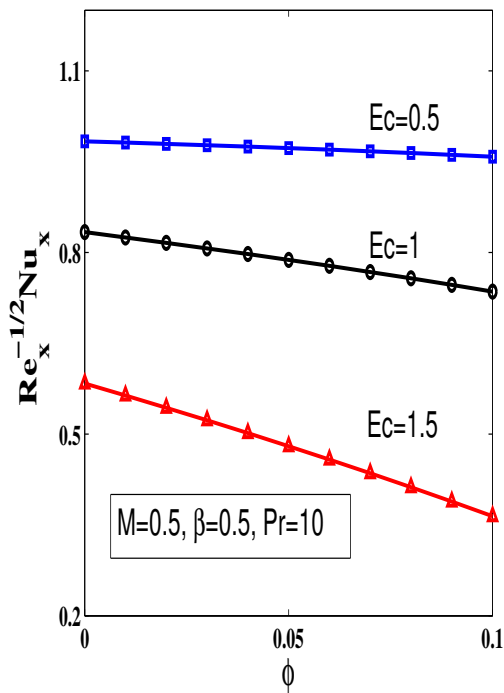


FIG. 3.17: Variation of Nusselt number against ϕ for various values of Ec .

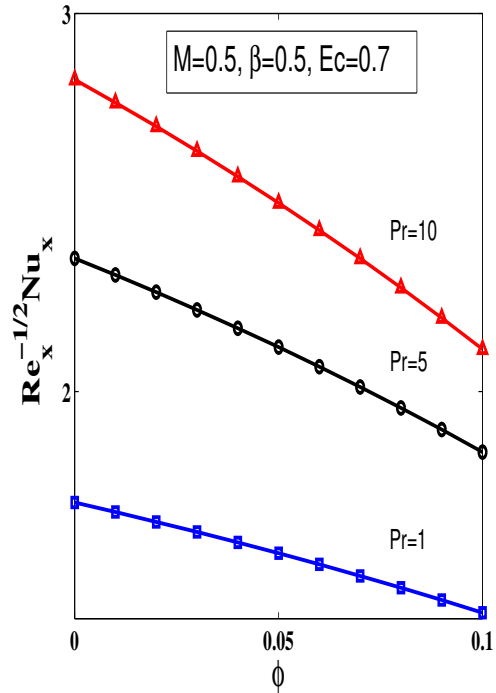


FIG. 3.18: Variation of Nusselt number against ϕ for various values of Pr .

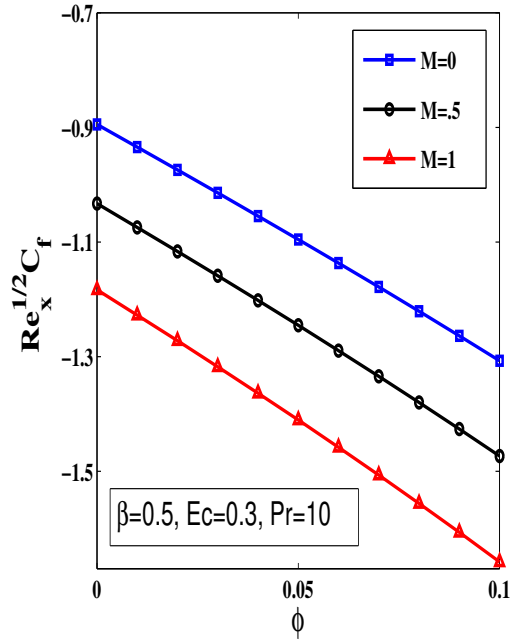


FIG. 3.19: Variation of skin friction coefficient against ϕ for various values of M .

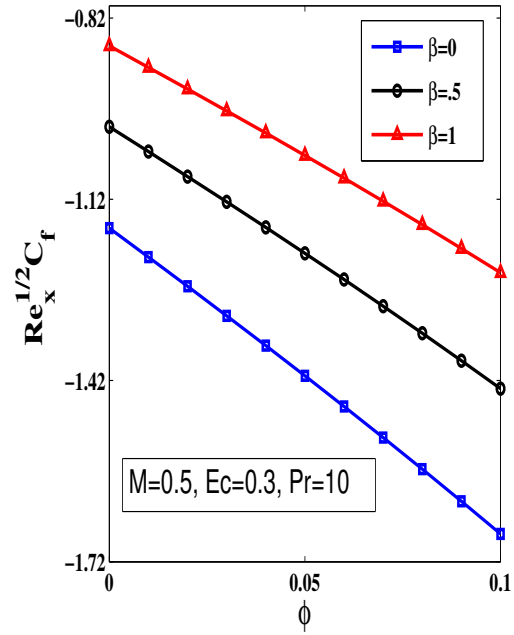


FIG. 3.20: Variation of skin friction coefficient against ϕ for various values of β .

3.5 Concluding Remarks

This article presents the magnetohydrodynamics boundary layer flow and heat transfer of the Jeffrey nanofluid over a stretching sheet in the presence of viscous dissipation and Joule heating. The main outcomes of this work are summarized as follows:

- The velocity of the silver-ethylene glycol Jeffrey nanofluid is lower than that of the base fluid while there is an opposite finding regarding the temperature.
- Increasing the Deborah number leads to increase the velocity profile while the magnetic parameter makes it to decrease.
- The thermal field is a growing function of the nanoparticle volume fraction ϕ , magnetic parameter M , Deborah number β , Prandtl number Pr and Eckert number Ec .
- The silver-ethylene glycol Jeffrey nanofluid gives less resistance to the fluid flow as compared with the base fluid. So silver-ethylene glycol Jeffrey nanofluid has small skin friction coefficient as compared with the base fluid but the same fluid

has higher Nusselt number against the solid volume fraction as compared with the base fluid.

- The drag increases with an enhancement in β but decreases by increasing the solid volume fraction ϕ and the magnetic number M .
- The Nusselt number increases with an increment in the Deborah number β and Prandtl number Pr but decreases by increasing the Eckert number Ec , the magnetic parameter M and the solid volume fraction ϕ .
- The thermal profile of Ag-ethylene glycol Jeffrey nanofluid is higher than those of $Al_2O_3 - C_2H_6O_2$ and $TiO_2 - C_2H_6O_2$ nanofluids.
- The silver-ethylene glycol Jeffrey nanofluid has lesser velocity than the $Al_2O_3 - C_2H_6O_2$ and $TiO_2 - C_2H_6O_2$ nanofluids.

Chapter 4

MHD Tangent Hyperbolic Nanofluid with Chemical Reaction, Viscous Dissipation and Joule Heating Effects

4.1 Introduction

In this chapter, the motion of a non-Newtonian tangent hyperbolic nanofluid due to a stretching sheet is analyzed. Nanofluid is comprised of thermophoresis and Brownian motion effects. Magnetic field is implemented in vertical direction under the assumption of low magnetic Reynolds number. The phenomenon of heat transfer has been examined subject to the viscous dissipation and Joule heating whereas the mass transfer has been analyzed under the effect of chemical reaction. The PDEs governing the flow, heat and mass transport are re-framed in the form ODEs by means of the similarity solutions. A numerical procedure known as the Keller-box method has been implemented to obtain the solutions for the accomplished ODEs. The effects of the variations of different involved parameters on fluid temperature, velocity and concentration distributions are disclosed through graphs and analyzed in detail. The features of skin friction, heat and mass transfer coefficient are tabulated and graphed in order to perceive the flow, heat

and mass transport phenomena. It is noticed that an increment in the Weissenberg number leads to a reduction in the velocity profile.

4.2 Mathematical Formulation

A time independent, laminar, two dimensional and magnetohydrodynamics transport of a constant density tangent hyperbolic fluid past a continuous surface, in the region $y > 0$ has been explored. The flow is conducted as a result of the linear stretching at $y = 0$. A uniform magnetic field of intensity B_0 is employed perpendicular to the sheet, so that the magnetic Reynolds number is chosen smaller. Consequently the induced magnetic field is neglected for small magnetic Reynolds number. The important features of such type of a flow are displayed in Fig. 4.1. Under these specific aspects and the nanofluid model

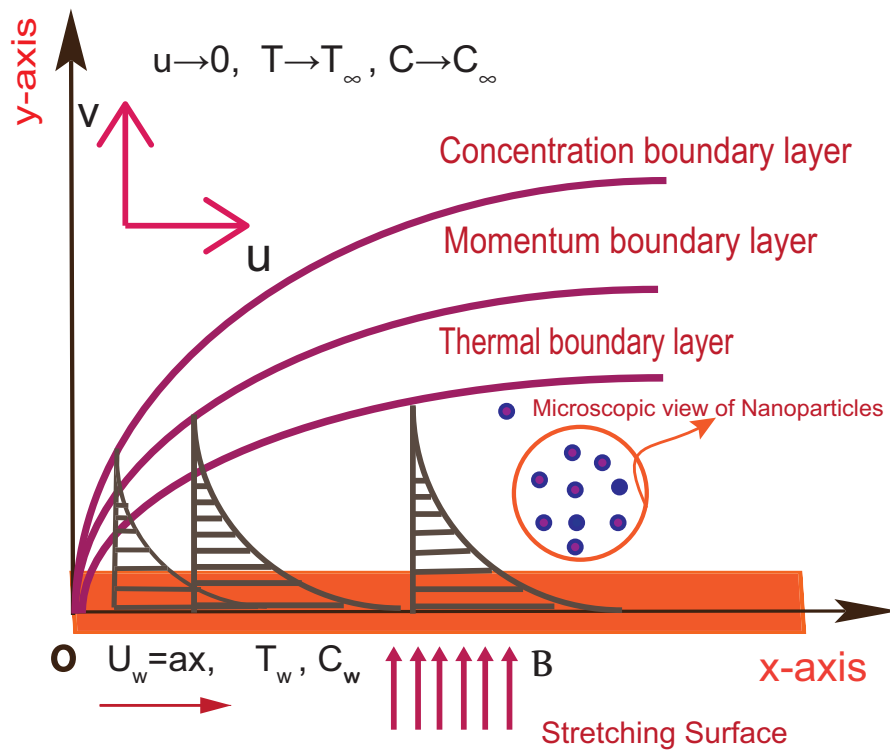


FIG. 4.1: Geometry of the problem.

of Buongiorno, boundary layer equations of momentum, temperature and concentration are provided below [119, 120]:

$$u \frac{\partial u}{\partial x} + v \frac{\partial u}{\partial y} = \nu (1 - n) \frac{\partial^2 u}{\partial y^2} + \sqrt{2} \Gamma n \frac{\partial u}{\partial x} \frac{\partial^2 u}{\partial y^2} - \frac{\sigma_f B_0^2}{\rho} u, \quad (4.1)$$

$$u \frac{\partial T}{\partial x} + v \frac{\partial T}{\partial y} = \alpha \frac{\partial^2 T}{\partial y^2} + \tau \left(D_B \left(\frac{\partial C}{\partial y} \right) \left(\frac{\partial T}{\partial y} \right) + \frac{D_T}{T_\infty} \left(\frac{\partial T}{\partial y} \right)^2 \right) + \frac{\sigma_f B_0^2 u^2}{\rho c_p} + \frac{\nu}{c_p} \left[(1-n) + \frac{n\Gamma}{\sqrt{2}} \frac{\partial u}{\partial y} \right] \left(\frac{\partial u}{\partial y} \right)^2, \quad (4.2)$$

$$u \frac{\partial C}{\partial x} + v \frac{\partial C}{\partial y} = D_B \frac{\partial^2 C}{\partial y^2} + \frac{D_T}{T_\infty} \left(\frac{\partial^2 T}{\partial y^2} \right) - k_1 (C - C_\infty). \quad (4.3)$$

The end-point conditions are considered to be

$$\left. \begin{aligned} u = u_w(x) = ax, \quad v = 0, \quad T = T_w, \quad C = C_w, \quad \text{at } y = 0, \\ u \rightarrow 0, \quad T \rightarrow T_\infty, \quad C \rightarrow C_\infty, \quad \text{as } y \rightarrow \infty. \end{aligned} \right\} \quad (4.4)$$

Eqs. (4.1)-(4.4) are turned into the dimensionless form by introducing the subsequent appropriate dimensionless variables [121]

$$\eta = \sqrt{\frac{a}{\nu}} y, \quad \psi = -\sqrt{a\nu} x f(\eta), \quad \theta = \frac{T - T_\infty}{T_w - T_\infty}, \quad \phi = \frac{C - C_\infty}{C_w - C_\infty}, \quad (4.5)$$

in which ψ is the stream function expressed as $u = \frac{\partial \psi}{\partial y}$ and $v = -\frac{\partial \psi}{\partial x}$. As a result, we get the same expressions of u and v as in Eq.(3.10). The equations of motion, energy and concentration in the non-dimensional form after making use of Eqs. (3.10) and (4.5) turn into

$$((1-n) + nWe f'') f''' - (f')^2 + f f'' - M^2 f' = 0, \quad (4.6)$$

$$\theta'' + Pr (f \theta' + Nb \theta' \phi') + Nt (\theta')^2 + (1-n) Pr Ec (f'')^2 + \frac{1}{2} n Pr Ec We (f'')^3 + Pr Ec M (f')^2 = 0, \quad (4.7)$$

$$\phi'' + Pr Le f \phi' + \frac{Nt}{Nb} \theta'' - Le \gamma \phi = 0, \quad (4.8)$$

with the following dimensionless end-point conditions:

$$\left. \begin{aligned} f(0) = 0, \quad f'(0) = 1, \quad \theta(0) = 1, \quad \phi(0) = 1, \quad \text{at } \eta = 0, \\ f'(\eta) \rightarrow 0, \quad \theta(\eta) \rightarrow 0, \quad \phi(\eta) \rightarrow 0, \quad \text{as } \eta \rightarrow \infty. \end{aligned} \right\} \quad (4.9)$$

The non-dimensional parameters utilized in Eqs. (4.6)-(4.8) are described as

$$\left. \begin{aligned}
 We &= \Gamma x \sqrt{\frac{2a^3}{\nu}} \quad (\text{Weissenberg number}), \\
 M &= \frac{\sigma_f B_0^2}{a\rho} \quad (\text{Magnetic parameter}), \\
 Pr &= \frac{\nu}{\alpha} \quad (\text{Prandtl number}), \\
 Le &= \frac{\nu}{D_B} \quad (\text{Lewis number}), \\
 Nt &= \frac{(\rho c)_p D_B (T_w - T_\infty)}{T_\infty \nu (\rho c)_f} \quad (\text{Thermophoresis parameter}), \\
 Nb &= \frac{(\rho c)_p D_B (\phi_w - \phi_\infty)}{\nu (\rho c)_f} \quad (\text{Brownian motion parameter}), \\
 Ec &= \frac{U_m^2}{c_p (T_w - T_\infty)} \quad (\text{Eckert number}), \\
 \gamma &= \frac{k_1}{a}, \quad (\text{Chemical reaction parameter}).
 \end{aligned} \right\} \quad (4.10)$$

The important physical parameters, skin-friction coefficient C_f , local Nusselt number Nu_x and local Sherwood Sh_x number are described as

$$C_f = \frac{2\tau_w}{\rho u_w^2}, \quad Nu_x = \frac{xq_w}{k(T_w - T_\infty)}, \quad Sh_x = \frac{xq_m}{D_B(\phi_w - \phi_\infty)}, \quad (4.11)$$

where $\tau_w = \mu(1-n)(\frac{\partial u}{\partial y})_{y=y_0} + \frac{n\Gamma}{\sqrt{2}}(\frac{\partial u}{\partial y})_{y=y_0}^2$ is the wall shear-stress, $q_w = -k(\frac{\partial T}{\partial y})_{y=y_0}$ is the heat flux and $q_m = -D_B(\frac{\partial \phi}{\partial y})_{y=y_0}$ is the mass flux at wall. Employing the similarity transform introduced above, (4.11) can further be described as:

$$\left. \begin{aligned}
 \frac{1}{2}C_f Re^{1/2} &= (1-n)f''(0) + \frac{1}{2}nWe(f''(0))^2, \\
 Nu_x Re_x^{-1/2} &= -\theta'(0), \quad Sh_x Re_x^{-1/2} = -\phi'(0),
 \end{aligned} \right\} \quad (4.12)$$

in which $Re_x = \frac{xU_w}{\nu}$ refers to the local Reynolds number.

4.3 Numerical Procedure

The above non-linear coupled ordinary differential Eqs. (4.6)-(4.8) alongside the end-point conditions (4.9) have been attempted numerically through the implicit finite difference technique (Keller-box scheme) [122, 123] for various values of the concerned parameters. This technique is found to be the very adaptable of the typical techniques and in spite of latest advancements in various numerical techniques, it is still a highly

effective and extremely accurate strategy for parabolic type of boundary layer problems. Additionally, it is flexible to solve problems of any order as well as unconditionally stable [114, 124].

By introducing the following new variables p_1 , p_2 , p_3 and p_4 ,

$$f'(\eta) = p_1, \quad p_1'(\eta) = p_2, \quad \theta'(\eta) = p_3, \quad \phi'(\eta) = p_4, \quad (4.13)$$

Eqs. (4.6)-(4.8) can be expressed as:

$$((1-n) + nWe p_2)p_2' - (p_1)^2 + fp_2 - M^2 p_1 = 0, \quad (4.14)$$

$$p_3' + Pr(f p_3 + Nb p_3 p_4) + Nt(p_3)^2 + PrEc(p_2)^2 + \frac{1}{2}nPrEcWe(p_2)^3 + PrEcM(p_1)^2 = 0, \quad (4.15)$$

$$p_4' + PrLe f p_4 + \frac{Nt}{Nb} p_3' - Le\gamma\phi = 0. \quad (4.16)$$

The transformed end point conditions are:

$$\left. \begin{aligned} f(0) = 0, \quad p_1(0) = 1, \quad \theta(0) = 1, \quad \phi(0) = 1, \quad \text{at } \eta = 0, \\ p_1(\eta) \rightarrow 0, \quad \theta(\eta) \rightarrow 0, \quad \phi(\eta) \rightarrow 0, \quad \text{as } \eta \rightarrow \infty. \end{aligned} \right\} \quad (4.17)$$

The net points have been set as

$\eta_j = \eta_{j-1} + h_j$, $\eta_0 = 0$, $\eta_J = \eta_\infty$, where $j = 1, 2, 3, \dots, J$ and h_j is the uniform mesh-size. Eqs. (4.13)-(4.16) are approximated through the utilization of the central difference at midpoint $\eta_{j-1/2}$, depicted below

$$\frac{f_j - f_{j-1}}{h_j} = (p_1)_{j-\frac{1}{2}}, \quad (4.18)$$

$$\frac{(p_1)_j - (p_1)_{j-1}}{h_j} = (p_2)_{j-\frac{1}{2}}, \quad (4.19)$$

$$\frac{\theta_j - \theta_{j-1}}{h_j} = (p_3)_{j-\frac{1}{2}}, \quad (4.20)$$

$$\frac{\phi_j - \phi_{j-1}}{h_j} = (p_4)_{j-\frac{1}{2}}, \quad (4.21)$$

$$\begin{aligned} & \left[(1-n) + nWe (p_2)_{j-\frac{1}{2}} \right] \left(\frac{(p_2)_j - (p_2)_{j-1}}{h_j} \right) - ((p_1)_{j-\frac{1}{2}})^2 \\ & + (f_{j-\frac{1}{2}})((p_2)_{j-\frac{1}{2}}) - M^2 ((p_1)_{j-\frac{1}{2}}) = 0, \end{aligned} \quad (4.22)$$

$$\begin{aligned}
& \left(\frac{(p_3)_j - (p_3)_{j-1}}{h_j} \right) + Pr \left[(f_{j-\frac{1}{2}}) ((p_3)_{j-\frac{1}{2}}) + Nb ((p_3)_{j-\frac{1}{2}}) ((p_4)_{j-\frac{1}{2}}) \right] \\
& + Nt ((p_3)_{j-\frac{1}{2}})^2 + PrEc ((p_2)_{j-\frac{1}{2}})^2 + \frac{1}{2} n PrEcWe ((p_2)_{j-\frac{1}{2}})^3 \\
& + PrEcM ((p_1)_{j-\frac{1}{2}})^2 = 0,
\end{aligned} \tag{4.23}$$

$$\begin{aligned}
& \left(\frac{(p_4)_j - (p_4)_{j-1}}{h_j} \right) + PrLe (f_{j-\frac{1}{2}}) ((p_4)_{j-\frac{1}{2}}) + \frac{Nt}{Nb} \left(\frac{(p_3)_j - (p_3)_{j-1}}{h_j} \right) \\
& - Le\gamma ((p_4)_{j-\frac{1}{2}}) = 0,
\end{aligned} \tag{4.24}$$

in which $f_{j-\frac{1}{2}} = \frac{f_j + f_{j-1}}{2}$ etc. In order to, linearized the above non-linear system of Eqs. (4.18)-(4.24) by Newton's technique, the subsequent substitution have been inserted.

$$\left. \begin{aligned}
f_j^{n+1} &= f_j^n + \delta f_j^n, (p_1)_j^{n+1} = (p_1)_j^n + \delta (p_1)_j^n, (p_2)_j^{n+1} = (p_2)_j^n + \delta (p_2)_j^n, \\
(p_3)_j^{n+1} &= (p_3)_j^n + \delta (p_3)_j^n, (p_4)_j^{n+1} = (p_4)_j^n + \delta (p_4)_j^n, \theta_j^{n+1} = \theta_j^n + \delta \theta_j^n, \\
\phi_j^{n+1} &= \phi_j^n + \delta \phi_j^n.
\end{aligned} \right\} \tag{4.25}$$

Putting these expressions in Eqs. (4.18)-(4.24) and getting rid of the higher-order terms in δ , the following system is obtained:

$$(\delta f_j - \delta f_{j-1}) - \frac{h_j}{2} (\delta (p_1)_j + \delta (p_1)_{j-1}) = (r_1)_j, \tag{4.26}$$

$$(\delta (p_1)_j - \delta (p_1)_{j-1}) - \frac{h_j}{2} (\delta (p_1)_j + \delta (p_1)_{j-1}) = (r_2)_j, \tag{4.27}$$

$$(\delta \theta_j - \delta \theta_{j-1}) - \frac{h_j}{2} (\delta (p_3)_j + \delta (p_3)_{j-1}) = (r_2)_j, \tag{4.28}$$

$$(\delta \phi_j - \delta \phi_{j-1}) - \frac{h_j}{2} (\delta (p_4)_j + \delta (p_4)_{j-1}) = (r_4)_j, \tag{4.29}$$

$$\begin{aligned}
& (\xi_1)_j \delta f_j + (\xi_2)_j \delta f_{j-1} + (\xi_3)_j \delta (p_1)_j + (\xi_4)_j \delta (p_1)_{j-1} + (\xi_5)_j \delta (p_2)_j \\
& + (\xi_6)_j \delta (p_2)_{j-1} = (r_5)_j,
\end{aligned} \tag{4.30}$$

$$\begin{aligned}
& (\beta_1)_j \delta (p_3)_j + (\beta_2)_j \delta (p_3)_{j-1} + (\beta_3)_j \delta f_j + (\beta_4)_j \delta f_{j-1} + (\beta_5)_j \delta (p_4)_j + (\beta_6)_j \delta (p_4)_{j-1} \\
& + (\beta_7)_j \delta (p_1)_j + (\beta_8)_j \delta (p_1)_{j-1} + (\beta_9)_j \delta (p_2)_j + (\beta_{10})_j \delta (p_2)_{j-1} = (r_6)_j,
\end{aligned} \tag{4.31}$$

$$\begin{aligned}
& (\gamma_1)_j \delta (p_4)_j + (\gamma_2)_j \delta (p_4)_{j-1} + (\gamma_3)_j \delta f_j + (\gamma_4)_j \delta f_{j-1} + (\gamma_5)_j \delta (p_3)_j + (\gamma_6)_j \delta (p_3)_{j-1} \\
& = (r_7)_j,
\end{aligned} \tag{4.32}$$

where

$$\left. \begin{aligned} (\xi_1)_j &= \frac{h_j}{4} \left((p_2)_j + (p_2)_{j-1} \right) = (\xi_2)_j, \\ (\xi_3)_j &= -\frac{h_j}{2} M^2 - \frac{h_j}{2} \left((p_1)_j + (p_1)_{j-1} \right) = (\xi_4)_j, \\ (\xi_5)_j &= \left(1 - n + \frac{h_j}{4} + (f_j + f_{j-1}) + nWe(p_2)_j \right), \\ (\xi_6)_j &= \left(-1 + n + \frac{h_j}{4} + (f_j + f_{j-1}) - nWe(p_2)_{j-1} \right), \\ (r_5)_j &= \frac{1}{2} h_j M^2 (p_1)_{j-\frac{1}{2}} + (p_1)_{j-\frac{1}{2}}^2 - f_{j-\frac{1}{2}} (p_2)_{j-\frac{1}{2}} + \frac{n}{2} We \left((p_2)_{j-1}^2 + (p_2)_j^2 \right), \end{aligned} \right\} \quad (4.33)$$

$$\left. \begin{aligned} (\beta_1)_j &= 1 + \frac{h_j N_b Pr}{4} \left((p_4)_j + (p_4)_{j-1} \right) + \frac{h_j Pr}{4} (f_j + f_{j-1}) \\ &\quad + \frac{h_j N_t Pr}{2} \left((p_3)_j + (p_3)_{j-1} \right), \quad (\beta_2)_j = (\beta_1)_j - 2, \\ (\beta_3)_j &= \frac{h_j Pr}{4} \left((p_3)_j + (p_3)_{j-1} \right) = (\beta_4)_j, \\ (\beta_5)_j &= \frac{h_j N_b Pr}{4} \left((p_3)_j + (p_3)_{j-1} \right) = (\beta_6)_j, \\ (\beta_7)_j &= \frac{h_j Pr M^2 Ec}{2} \left((p_1)_j + (p_1)_{j-1} \right) = (\beta_8)_j, \\ (\beta_9)_j &= \frac{h_j Pr Ec}{2} \left((p_2)_j + (p_2)_{j-1} \right) = (\beta_{10})_j, \\ (r_6)_j &= \left((p_3)_{j-1} - (p_3)_j \right) - h_j N_b Pr (p_3)_{j-\frac{1}{2}} (p_4)_{j-\frac{1}{2}} \\ &\quad - h_j Pr (p_3)_{j-\frac{1}{2}} f_{j-\frac{1}{2}} - \frac{h_j N_t Pr}{4} (p_3)_{j-\frac{1}{2}}^2 \\ &\quad - \frac{h_j M^2 Pr Ec}{4} (p_1)_{j-\frac{1}{2}}^2 - \frac{h_j Pr Ec}{4} (p_2)_{j-\frac{1}{2}}^2, \end{aligned} \right\} \quad (4.34)$$

$$\left. \begin{aligned} (\gamma_1)_j &= 1 - \frac{h_j \gamma Le}{2} \left((p_4)_j + (p_4)_{j-1} \right) + \frac{h_j Le Pr}{4} (f_j + f_{j-1}), \\ (\gamma_2)_j &= -1 - \frac{h_j \gamma Le}{2} \left((p_4)_j + (p_4)_{j-1} \right) + \frac{h_j Le Pr}{4} (f_j + f_{j-1}), \\ (\gamma_3)_j &= \frac{h_j Le Pr}{4} \left((p_4)_j + (p_4)_{j-1} \right) = (\gamma_4)_j, \\ (\gamma_5)_j &= \frac{N_t}{N_b} = -(\gamma_6)_j, \\ (r_7)_j &= \left((p_4)_{j-1} - (p_4)_j \right) - h_j Le Pr (p_4)_{j-\frac{1}{2}} f_{j-\frac{1}{2}} + \frac{N_t}{N_b} \left((p_3)_{j-1} - (p_3)_j \right) \\ &\quad + h_j \gamma Le \left((p_3)_j + (p_3)_{j-1} \right)^2. \end{aligned} \right\} \quad (4.35)$$

After the linearization procedure we get the subsequent block-tridiagonal structure

$$\begin{bmatrix} [A_1] [B_1] \\ [C_2] [A_2] [B_2] \\ \vdots \\ \vdots \\ \vdots \\ [C_{J-1}] [A_{J-1}] [B_{J-1}] \\ [C_J] [A_J] \end{bmatrix} = \begin{bmatrix} [\delta_1] \\ [\delta_2] \\ \vdots \\ \vdots \\ \vdots \\ [\delta_{J-1}] \\ [\delta_J] \end{bmatrix} \begin{bmatrix} [g_1] \\ [g_2] \\ \vdots \\ \vdots \\ \vdots \\ [g_{J-1}] \\ [g_J] \end{bmatrix}$$

or

$$[A][\delta] = [g]. \quad (4.36)$$

where the elements defined in Eq. (4.36) are

$$[A_1] = \begin{bmatrix} 0 & 0 & 0 & 1 & 0 & 0 & 0 \\ -0.5h_1 & 0 & 0 & 0 & -0.5h_1 & 0 & 0 \\ 0 & -0.5h_1 & 0 & 0 & 0 & -0.5h_1 & 0 \\ 0 & 0 & -0.5h_1 & 0 & 0 & 0 & -0.5h_1 \\ (\xi_6)_1 & 0 & 0 & (\xi_1)_1 & (\xi_5)_1 & 0 & 0 \\ (\beta_{10})_1 & (\beta_2)_1 & (\beta_6)_1 & (\beta_3)_1 & (\beta_9)_1 & (\beta_1)_1 & (\beta_5)_1 \\ 0 & (\gamma_6)_1 & (\gamma_2)_1 & (\gamma_3)_1 & 0 & (\gamma_5)_1 & (\gamma_1)_1 \end{bmatrix},$$

$$[A_j] = \begin{bmatrix} -0.5h_j & 0 & 0 & 1 & 0 & 0 & 0 \\ -1 & 0 & 0 & 0 & -0.5h_j & 0 & 0 \\ 0 & -1 & 0 & 0 & 0 & -0.5h_j & 0 \\ 0 & 0 & -1 & 0 & 0 & 0 & -0.5h_j \\ (\xi_4)_j & 0 & 0 & (\xi_1)_j & (\xi_5)_j & 0 & 0 \\ (\beta_8)_j & 0 & 0 & (\beta_3)_j & (\beta_9)_j & (\beta_1)_j & (\beta_5)_j \\ 0 & 0 & 0 & (\gamma_3)_j & 0 & (\gamma_5)_j & (\gamma_1)_j \end{bmatrix}, 2 \leq j \leq J$$

$$[B_j] = \begin{bmatrix} 0 & 0 & 0 & -1 & 0 & 0 & 0 \\ 0 & 0 & 0 & 0 & -0.5h_j & 0 & 0 \\ 0 & 0 & 0 & 0 & 0 & -0.5h_j & 0 \\ 0 & 0 & 0 & 0 & 0 & 0 & -0.5h_j \\ 0 & 0 & 0 & (\xi_2)_j & (\xi_6)_j & 0 & 0 \\ 0 & 0 & 0 & (\beta_4)_j & (\beta_{10})_j & (\beta_2)_j & (\beta_6)_j \\ 0 & 0 & 0 & (\gamma_4)_j & 0 & (\gamma_6)_j & (\gamma_2)_j \end{bmatrix}, 2 \leq j \leq J$$

$$[C_j] = \begin{bmatrix} -0.5h_j & 0 & 0 & 0 & 0 & 0 & 0 \\ 1 & 0 & 0 & 0 & 0 & 0 & 0 \\ 0 & 1 & 0 & 0 & 0 & 0 & 0 \\ 0 & 0 & 1 & 0 & 0 & 0 & 0 \\ (\xi_3)_j & 0 & 0 & 0 & 0 & 0 & 0 \\ (\beta_7)_j & 0 & 0 & 0 & 0 & 0 & 0 \\ 0 & 0 & 0 & 0 & 0 & 0 & 0 \end{bmatrix}, 1 \leq j \leq J-1.$$

In order to solve Eq. (4.36), we assume A as a non-singular matrix that can be factorized as

$$A = LU, \quad (4.37)$$

in which

$$L = \begin{bmatrix} [\alpha_1] \\ [\beta_2] [\alpha_2] \\ \ddots \\ \ddots [\alpha_{J-1}] \\ [\beta_J] [\alpha_J] \end{bmatrix},$$

$$U = \begin{bmatrix} [I] [\xi_1] & & & & & & \\ & [I] [\xi_2] & & & & & \\ & & \ddots & \ddots & & & \\ & & & & [I] [\xi_{J-1}] & & \\ & & & & & & [I] \end{bmatrix}.$$

where, $[I]$ is an identity matrix of order 7, and $[\alpha_i]$ and $[\xi_i]$ are 7×7 matrices. This block tridiagonal matrix presented in Eq. (4.36) is solved by LU factorization for the solution δ . In numerical computation, the appropriate step size h_j as well as boundary layer thickness η_∞ must be provided. For numerical calculations, we consider the step size $h_j = 0.001$ and we operate the simulation until $\eta_{max} = 12$. The results are achieved with an error tolerance of 10^{-5} . To be able to validate the correctness of the numerical method, a comparison of the found outcomes of $-f''(0)$ with the ones reported by Ibrahim [125] and Ali et al. [126] for $We = n = 0$ has been presented in Table 4.1.

TABLE 4.1: Comparison of $-f''(0)$ with various values of M .

M	Ibrahim[125]	Ali et al. [126]	Present study
0.0	1.0000	1.00000	1.000000
1	1.4142	1.41421	1.414211
5	2.4495	2.44948	2.449501

4.4 Results and Discussions

In this section, the significant aspects of flow, energy and mass transport phenomena for various emerging parameters have been demonstrated graphically and tabulated numerically. The impact of M on the velocity profile is highlighted in Fig. 4.2. As expected, due to an augmentation in M , the thickness of momentum boundary layer as well as the velocity profile decrease. In fact, it happens because of a high intensity of external electric field which generates a wall-parallel resistive force, called the Lorentz

force. Fig. 4.3 illustrates the velocity distribution for wide range of values of the power law index n . It is observed that an increment in n causes a reduction in the velocity profile. In fact, amplitude of the shear thinning phenomenon is decreased by the increasing power law index, which consequently results in a decay in the fluid velocity. The dynamics of the horizontal velocity due to the Weissenberg number We is exhibited in Fig. 4.4. It can be observed that the velocity field is reduced by enhancing the Weissenberg number We . Physically, the dominant values of We cause an enhancement in the relaxation time which resists the fluid motion due to weak cohesive forces between the fluid particles. The thickness of boundary layer corresponding to the velocity field exhibits a reducing trend with an intensity in Weissenberg number We . Fig. 4.5 captures the influence of the magnetic parameter M on the temperature field. It is noted that with an increment in M , the fluid temperature is increased throughout the boundary layer regime. Further boundary layer thickness is also increases. As the magnetic parameter M strengthens the Lorentz force which enhances the frictional effects, more heat is generated.

The effects of Pr on the temperature field are displayed in Fig. 4.6. It is evident that an increment in Pr leads to a reduction in the temperature field as well as in the thickness of thermal boundary layer. As the Prandtl number Pr dilates, the thermal diffusivity suffers a decay which causes a low heat transfer rate from plate to the fluid and therefore the fluid temperature is reduced. The temperature distribution is graphed against the Eckert number Ec in Fig. 4.7. This figure indicates an increasing trend in the temperature field for the dominating values of Ec . Due to the dominant Eckert number Ec , more heat generation in the fluid occurs because of the strong frictional force between the fluid particles, resulting in the temperature augmentation. Variation in the thermal field corresponding to the thermophoresis parameter Nt , is presented in Fig. 4.8. The temperature profile is observed to increase with growing thermophoresis parameter Nt . The associated boundary layer thickness is also increased. In fact, a rise in the thermophoresis force between fluid particles provides more heat transfer to the working fluid. Hence the temperature distribution is enhanced. Fig. 4.9 displays the impact of the Brownian motion parameter Nb on the temperature field. It is depicted that a higher Nb strengthens the fluid temperature due to more collisions between the fluid particles. Fig. 4.10 discloses the effects of Nb

on the concentration distribution. It is noticed that the fluid concentration is declined by the dominating Nb . In fact, larger values of Nb cause a boost in the collision between the fluid particles due to which less mass is transferred and consequently a decline in the concentration field is observed.

Fig. 4.11 describes the impact of Nt on the concentration distribution. It is depicted that the concentration distribution and the corresponding thickness of the solutal boundary layer show an increasing behavior for the growing Nt . Physically, larger values of the thermophoresis parameter Nt correspond to more thermophoresis force which leads to strengthen the diffusive effects. Fig. 4.12 highlights how the Lewis number Le affects the concentration distribution. As expected, the concentration field faces a decay due to the dominating values of Le . Physically, higher values of Lewis number Le reduces the mass transfer rate due to a decrement in the mass diffusivity due to which, a abatement in ϕ is noticed. Further, for lower Lewis number Le , dominant thickness of solutal boundary layer is observed. Fig. 4.13 is plotted for the concentration profile against destructive chemical reaction parameter ($\gamma > 0$). Generally, it is noticed that the concentration distribution is a reducing function of $\gamma > 0$. In fact, the heat generation is enhanced for the increasing positive values of γ resulting in a down-fall in the concentration profile. Fig. 4.14 is portrayed to reveal the impact of constructive chemical reaction ($\gamma < 0$) on ϕ . It is revealed from Fig. 4.14 that the intensity of the concentration distribution and the associated thickness of the solutal boundary layer boost up for the chemical reaction parameter $\gamma < 0$.

Fig. 4.15 is plotted to highlight the effects of Weissenberg number We and the magnetic parameter M on skin friction coefficient. It shows a decaying trend for We and M . The variation in the skin friction coefficient corresponding to the power law index n and the magnetic parameter M is discussed in Fig. 4.16. The skin friction coefficient shows an increasing behavior for n , while it shows a decaying trend for M . Fig. 4.17 depicts the result of the local Nusselt number for various values of Nb and Pr . It is noted that the Nusselt number is decreased with an increment in Brownian motion parameter Nb while the Prandtl number Pr has an opposite effect on it. The effects of Nt and Pr on the Nusselt number are illustrated in Fig. 4.18. It is revealed that the Nusselt number is reduced with an enhancement in Nt although Pr offers an

opposite impact on it. Fig. 4.19 is plotted to predict the behavior of Le and Nt on Sherwood number. It is viewed that the parameters Le and Nt significantly enhance the Sherwood number. Fig. 4.20 illustrates the impact of Le and Nb on the Sherwood number. It is identified that the parameters Le and Nb considerably boost the Sherwood number. Moreover, Table 4.2 exhibits the dynamics of the skin friction coefficient, the Nusselt number and the Sherwood number under the influence of various emerging physical parameters. The tabular numerical values reflect the same trend as observed already in the discussed graphical results.

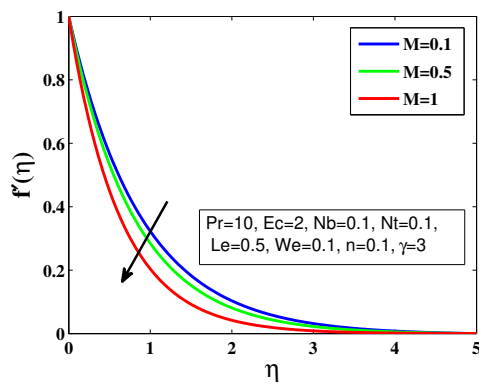


FIG. 4.2: Velocity plot $f'(\eta)$ for assorted values of magnetic parameter M .

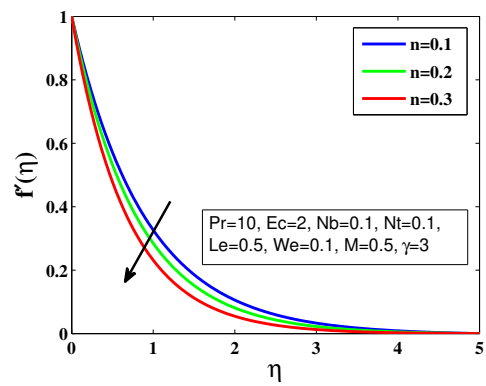


FIG. 4.3: Velocity plot $f'(\eta)$ for assorted values of power-law index n .

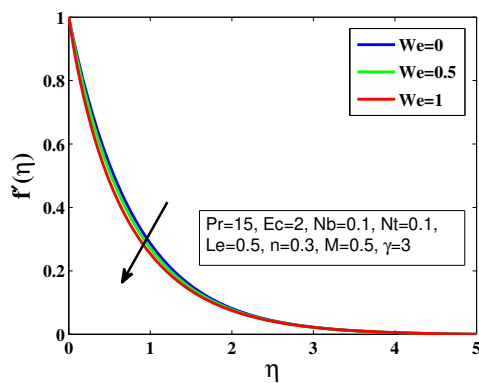


FIG. 4.4: Velocity plot $f'(\eta)$ for assorted values of Weissenberg number We .

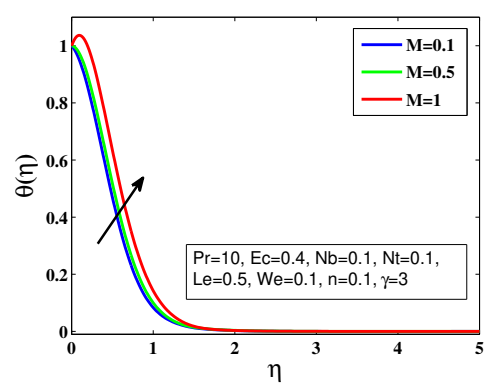


FIG. 4.5: Temperature plot $\theta(\eta)$ for assorted values of magnetic parameter M .

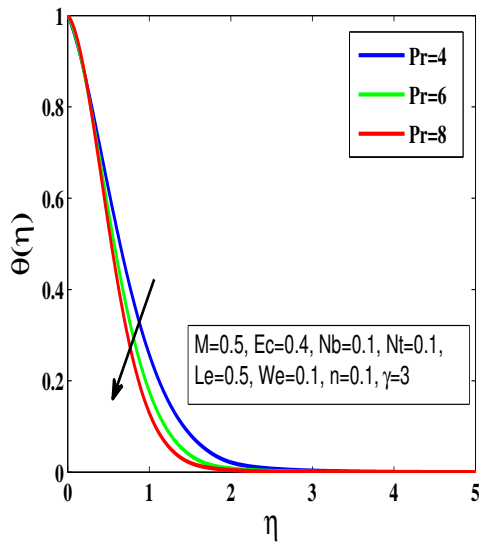


FIG. 4.6: Temperature plot $\theta(\eta)$ for assorted values of Prandtle Pr .

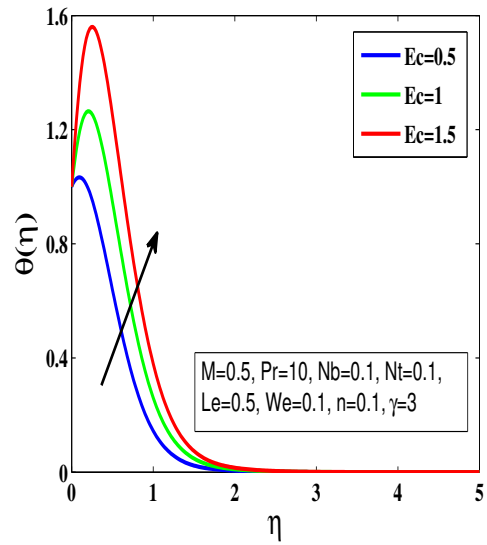


FIG. 4.7: Temperature plot $\theta(\eta)$ for assorted values of Eckert Ec .

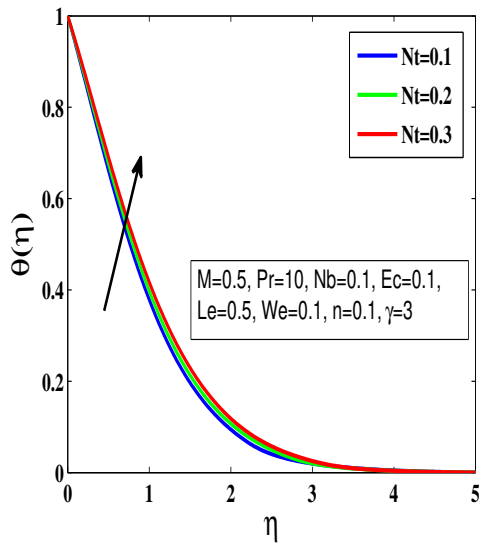


FIG. 4.8: Temperature plot $\theta(\eta)$ for assorted values of Nt .

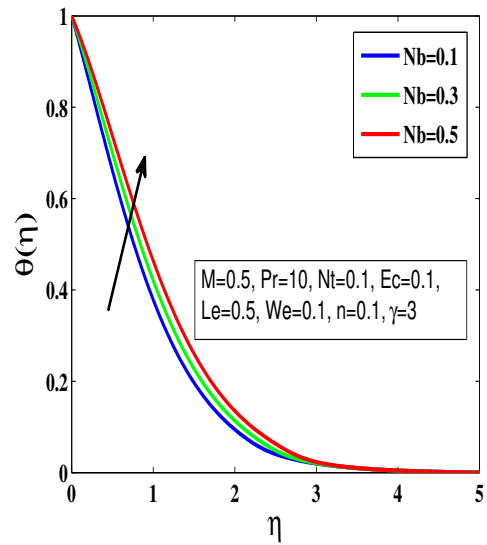


FIG. 4.9: Temperature plot $\theta(\eta)$ for assorted values of Nb .

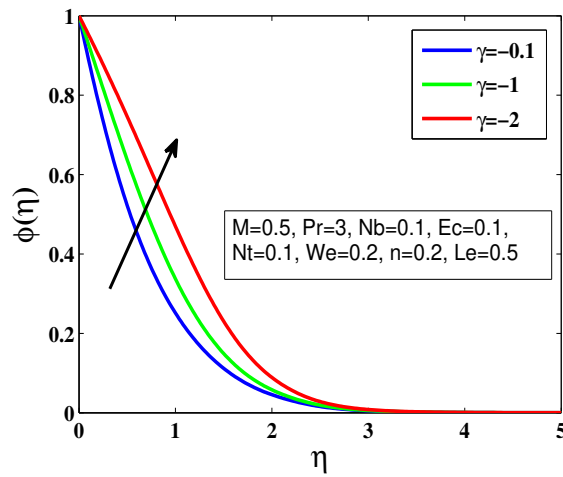
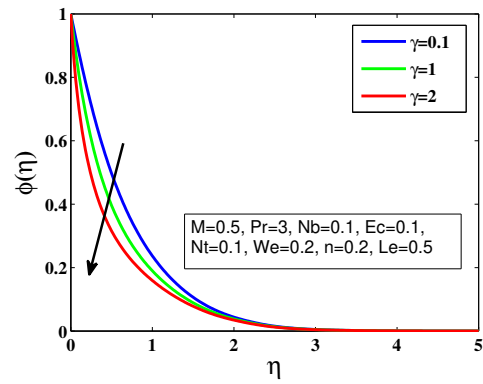
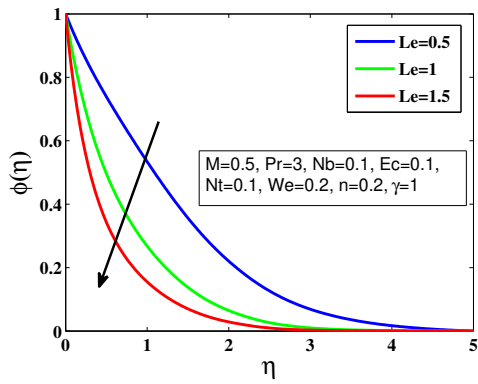
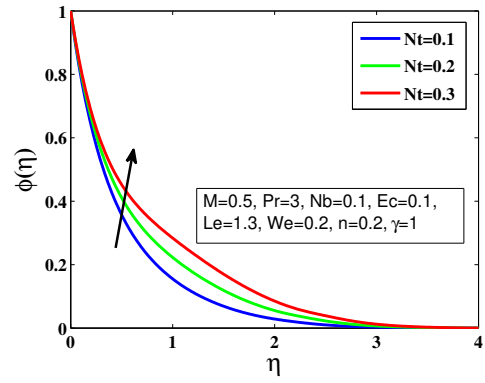
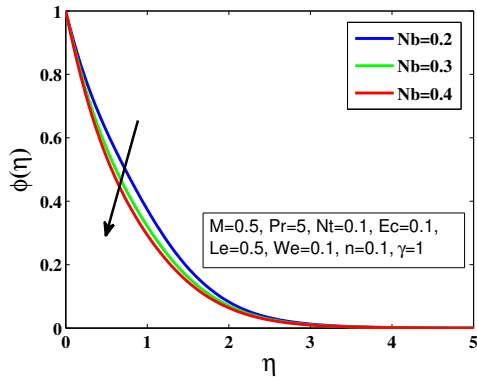


FIG. 4.14: Concentration plot $\phi(\eta)$ for assorted values of $\gamma < 0$.

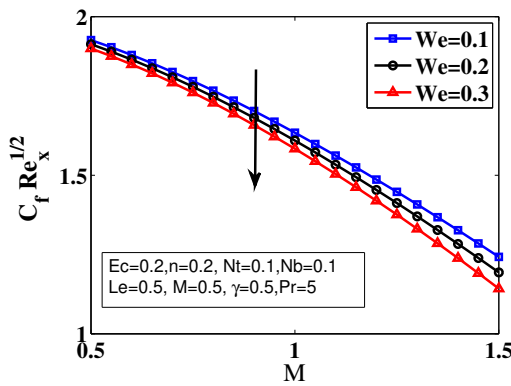


FIG. 4.15: Influence of M and We on drag coefficient.

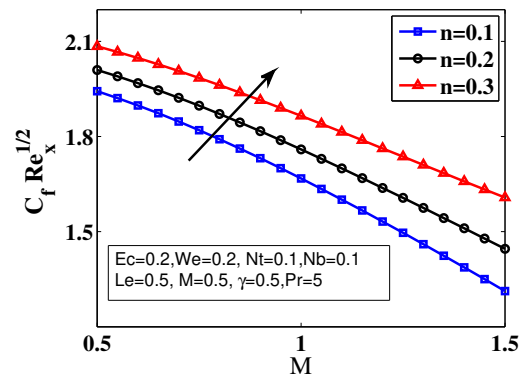


FIG. 4.16: Influence of M and n on drag coefficient.

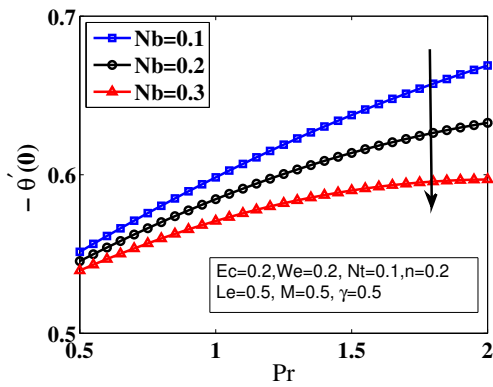


FIG. 4.17: Influence of Nb and Pr on local Nusselt number $-\theta'(0)$.

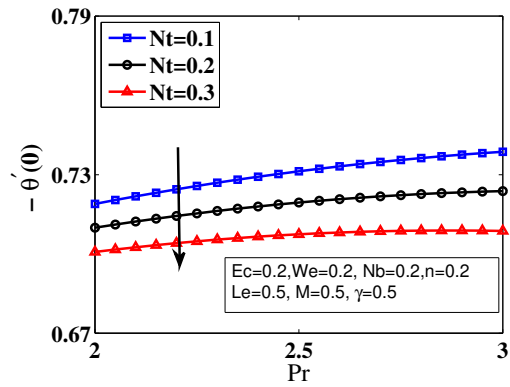


FIG. 4.18: Influence of Nt and Pr on local Nusselt number $-\theta'(0)$.

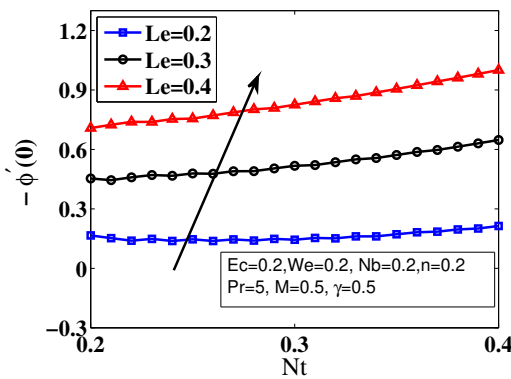


FIG. 4.19: Influence of Nt and Le on local Sherwood number $-\phi'(0)$.

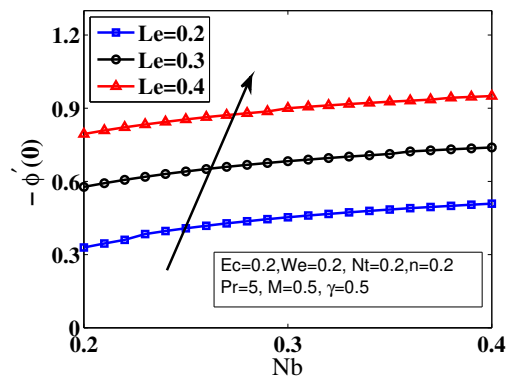


FIG. 4.20: Influence of Nb and Le on local Sherwood number $-\phi'(0)$.

TABLE 4.2: Values of $C_f Re_x^{1/2}$, $Nu_x^{-1/2}$ and $Sh_x^{-1/2}$ for various sorts of parameters in flow.

M	Nt	Nb	We	n	Pr	Ec	Le	γ	$C_f Re_x^{1/2}$	$Nu_x^{-1/2}$	$Sh_x^{-1/2}$
0.5	0.1	0.1	0.3	0.2	10	1	1	1	-0.97968	0.73829	1.56511
									-1.21401	0.45359	1.67699
									-1.48865	0.04808	1.87323
		0.2							-0.97968	0.50639	1.69953
		0.3							-0.97968	0.33289	2.12136
		0.4							-0.97968	0.20446	2.70793
			0.1						-0.97968	0.73829	1.56511
			0.2						-0.97968	0.34822	1.91879
			0.3						-0.97968	0.11105	2.00051
				0.1					-0.99030	0.74279	1.56490
				0.2					-0.97968	0.73829	1.56511
				0.3					-0.96821	0.73357	1.56541
					1				-0.97968	0.43430	0.16987
					5				-0.97968	0.83718	0.66990
					10				-0.97968	0.73829	1.56511
						0.2			-0.97968	0.37901	1.89984
						0.4			-0.97968	-0.35680	2.62318
						0.6			-0.97968	-1.11098	3.42282
							0.5		-0.97968	0.73829	1.56511
							1		-0.97968	0.57721	3.41850
							1.5		-0.97968	0.51119	5.84310
								0.5	-0.97968	0.75298	1.42393
								1	-0.97968	0.73829	1.56511
								1.5	-0.97968	0.72444	1.72399

4.5 Concluding Remarks

A study of the simultaneous impacts of the magnetic field and non-Newtonian rheology on nanofluid flow along a stretching surface in the presence of Joule heating, viscous dissipation and chemical reaction is conducted. The Keller-box iterative scheme is utilized for the numerical solutions of the transformed non-linear dimensionless governing differential equations illustrating the flow regime. The innovative results for the involved key parameters are exhibited through graphs. The core findings are listed below:

- The velocity field is reduced for the escalating values of the magnetic parameter.

- Weissenberg number reduces the velocity distribution.
- Brownian motion parameter as well as the thermophoresis parameter cause a rise in the temperature profile.
- The concentration is decreasing function of Brownian motion parameter while it behaves the other way round for the thermophoresis parameter.
- The temperature profile is enhanced with an increment in the magnetic parameter as well as the Eckert number.
- The concentration distribution shows an opposite trend with chemical reaction parameter for both destructive reaction ($\gamma > 0$) and constructive reaction ($\gamma < 0$) case.

Chapter 5

Stratified MHD Jeffrey Nanofluid Flow with Gyrotactic Microorganisms past a Stretching Surface

5.1 Introduction

In this chapter, an elaborated evaluation has been presented for the stratified MHD Jeffrey nanofluid flow towards a stretching surface in the presence of gyrotactic micro-organisms. The governing nonlinear system of PDEs, administering the flow, are turned to a group of the nonlinear ODEs via using an appropriate similarity transformation and later solved numerically by implementing the Keller-box approach. The impacts of a range of parameters on the fluid motion, heat, mass, density of the motile micro-organisms, local skin friction, local Nusselt number, local Sherwood number and local density number of the motile micro-organisms are examined with the aid of graphs as well as tables. The results suggest that the motile micro-organisms density is a decreasing function of the bioconvection Lewis number, bioconvection Peckel number and microorganisms concentration difference. The

Sherwood number and density rate of motile micro-organisms are higher in the case of magnetic parameter and Lewis number. It is identified that temperature, density of nanoparticles and motile micro-organisms density stratification parameters lead to decrease the temperature, density of nanoparticles and motile micro-organisms density profiles.

5.2 Mathematical Formulation

A steady, two-dimensional and laminar flow of an incompressible Jeffery nanofluid fluid due to a stretching surface coinciding with the plane $y = 0$ has been investigated. Furthermore, magnetohydrodynamics as well as nanoparticles effects are considered along with the gyrotactic microorganisms. The thermophoresis and Brownian motion impacts have also been taken into consideration. The uniform magnetic field B_0 is employed parallel to y -direction and fluid is confined in region $y > 0$ (see Fig. 5.1). Here, x -axis has been taken along the stretching sheet and the flow is assumed to be produced by stretching the sheet with linear velocity $U_w = ax$ away from the leading edge such that a is a positive constant. The temperature, concentration and motile micro-organisms transfer rate have been analyzed under the stratification effects. The induced magnetic field is neglected, because it is quite small in comparison to the magnetic Reynolds number. By the use of boundary layer approximation, the

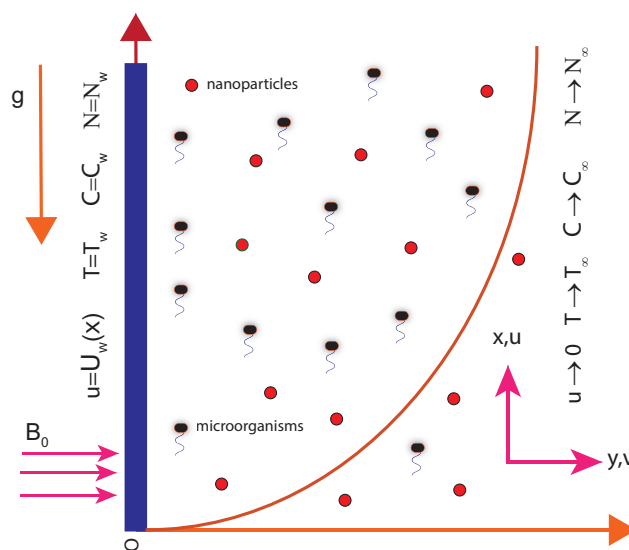


FIG. 5.1: Physical model of the flow.

momentum, energy, concentration and microorganisms[127] equations are:

$$\left(u \frac{\partial u}{\partial x} + v \frac{\partial u}{\partial y} \right) = \frac{\nu}{(1 + \lambda_1)} \left[\frac{\partial^2 u}{\partial y^2} + \lambda_2 \left(u \frac{\partial^3 u}{\partial x \partial y^2} - \frac{\partial u}{\partial x} \frac{\partial^2 u}{\partial y^2} \right) \right] - \frac{\sigma_f}{\rho_f} B_0^2 u$$

$$+ \frac{g}{\rho_f} [(1 - C_\infty)\rho_f\beta^*(T - T_\infty) - (\rho_p - \rho_f)(C - C_\infty) - (N - N_\infty)\gamma^*(\rho_m - \rho_f)], \quad (5.1)$$

$$u \frac{\partial T}{\partial x} + v \frac{\partial T}{\partial y} = \alpha \frac{\partial^2 T}{\partial y^2} + \tau \left(D_B \left(\frac{\partial C}{\partial y} \right) \left(\frac{\partial T}{\partial y} \right) + \frac{D_T}{T_\infty} \left(\frac{\partial T}{\partial y} \right)^2 \right) + \frac{\sigma_f}{(\rho c_p)_f} B_0^2 u^2$$

$$+ \frac{\mu}{(\rho c_p)_f (1 + \lambda_1)} \left(\lambda_2 \left(u \frac{\partial u}{\partial y} \frac{\partial^2 u}{\partial x \partial y} + v \frac{\partial u}{\partial y} \frac{\partial^2 u}{\partial y^2} \right) + \left(\frac{\partial u}{\partial y} \right)^2 \right), \quad (5.2)$$

$$u \frac{\partial C}{\partial x} + v \frac{\partial C}{\partial y} = D_B \frac{\partial^2 C}{\partial y^2} + \frac{D_T}{T_\infty} \left(\frac{\partial^2 T}{\partial y^2} \right), \quad (5.3)$$

$$u \frac{\partial N}{\partial x} + v \frac{\partial N}{\partial y} + \frac{bW_c}{(C_w - C_0)} \frac{\partial}{\partial y} \left(N \frac{\partial C}{\partial y} \right) = D_m \frac{\partial^2 N}{\partial y^2}. \quad (5.4)$$

The set of associated boundary conditions has been taken as:

$$\left. \begin{aligned} u = u_w(x) = ax, \quad v = 0, \quad T = T_w = T_o + A_1x, \\ C = C_w = C_o + E_1x, \quad N = N_w = N_o + H_1x \quad \text{at } y = 0, \\ u \longrightarrow 0, \quad T \longrightarrow T_\infty = T_o + A_2x, \\ C \longrightarrow C_\infty = C_o + E_2x, \quad N \longrightarrow N_\infty = N_o + H_2x \quad \text{as } y \longrightarrow \infty, \end{aligned} \right\} \quad (5.5)$$

where A_1, A_2, E_1, E_2, H_1 and H_2 are the dimensional constants. The following similarity transformation[127] has been adopted to convert of Eqs.(5.1)–(5.4) to the ordinary differential equations.

$$\left. \begin{aligned} \eta = \left(\frac{a}{\nu} \right)^{0.5} y, \quad \psi = -(a\nu)^{0.5} x f(\eta), \quad \theta = \frac{T - T_\infty}{T_w - T_0}, \\ \phi = \frac{C - C_\infty}{C_w - C_0}, \quad \chi = \frac{N - N_\infty}{N_w - N_0}, \end{aligned} \right\} \quad (5.6)$$

where $\eta, f, \theta, \phi, \chi$ and ψ are similarity variable, dimensionless stream function, dimensionless temperature, dimensionless concentration of nanoparticles, dimensionless concentration of microorganisms and stream function obeying $u = \frac{\partial \psi}{\partial y}$ and $v = -\frac{\partial \psi}{\partial x}$. As a result, we get the same expressions of u and v as in Eq.(3.10). Now, through the use of transformations from Eqs. (3.10) and (5.6), we obtain the subsequent set of

non-linear ODEs:

$$f'''' - (1 + \lambda_1) [(f')^2 - f f''] + \beta [(f'')^2 - f f^{iv}] - (1 + \lambda_1) M f' + Gr[\theta - Nr\phi - Rb\chi] = 0, \quad (5.7)$$

$$\theta'' - Pr f' \theta - Pr St f' + Pr f \theta' + Pr Nb \phi' \theta' + Pr Nt (\theta')^2 + Ec Pr M (f')^2 + Pr Ec \left((f'')^2 + \lambda_2 f'' (f' f'' - f f''') \right) = 0, \quad (5.8)$$

$$\phi'' - Pr Le f' \phi - Pr Le Sc f' + Pr Le f \phi' + \frac{Nt}{Nb} \theta'' = 0, \quad (5.9)$$

$$\chi'' - Lb f' \chi - Lb Sm f' + Lb f \chi' - Pe (\chi' \phi' + \phi'' (\sigma + \chi)) = 0. \quad (5.10)$$

The set of boundary conditions turns into the following form:

$$\left. \begin{aligned} f(0) = 0, \quad f'(0) = 1, \quad \theta(0) = 1 - St, \quad \phi(0) = 1 - Sc, \quad \chi(0) = 1 - Sm \text{ at } \eta = 0, \\ f'(\eta) \rightarrow 0, \quad f''(\eta) \rightarrow 0, \quad \theta(\eta) \rightarrow 0, \quad \phi(\eta) \rightarrow 0, \quad \chi(\eta) \rightarrow 0 \text{ as } \eta \rightarrow \infty. \end{aligned} \right\} \quad (5.11)$$

Dimensionless parameters appearing in Eqs. (5.7)-(5.10) have been illustrated below:

$$\left. \begin{aligned} Pe &= \frac{bW_c}{D_m} \text{ (bioconvection Peclet number)}, \quad M = \frac{\sigma_f B_0^2}{a\rho} \text{ (magnetic parameter)}, \\ Ec &= \frac{c^2 x^2}{c_p (T_w - T_o)} \text{ (Eckert number)}, \quad Lb = \frac{\nu}{D_b} \text{ (bioconvection Lewis number)}, \\ Nt &= \frac{(\rho c)_p D_T (T_w - T_o)}{T_\infty \nu (\rho c)_f} \text{ (thermophoresis parameter)}, \\ Nb &= \frac{(\rho c)_p D_B (C_w - C_o)}{\nu (\rho c)_f} \text{ (Brownian motion parameter)}, \\ Sm &= \frac{H_2}{H_1} \text{ (motile density stratification parameter)}, \quad \beta = a\lambda_2 \text{ (Deborah number)}, \\ St &= \frac{A_2}{A_1} \text{ (thermal stratification parameter)}, \quad Le = \frac{\alpha}{D_B} \text{ (Lewis number)}, \\ Sc &= \frac{E_2}{E_1} \text{ (mass stratification parameter)}, \quad Pr = \frac{\nu}{\alpha} \text{ (Prandtl number)}, \\ \sigma &= \frac{N_\infty}{N_w - N_0} \text{ (microorganisms concentration difference parameter)}, \\ Gr &= \frac{\beta^* \gamma^* (1 - C_\infty) (T_w - T_o)}{aU_o} \text{ (mixed convection parameter)}, \\ Nr &= \frac{(\rho_p - \rho_f) (C_w - C_o)}{\beta^* \rho_f (T_w - T_o)} \text{ (buoyancy ratio parameter)}, \\ Rb &= \frac{\gamma^* (N_w - N_o) (\rho_m - \rho_f)}{\beta^* \rho_f (1 - C_\infty) (T_w - T_o)} \text{ (bioconvection Rayleigh number)}. \end{aligned} \right\} \quad (5.12)$$

The valuable physical quantities in this research are the local shear stress coefficient C_f , Nusselt number Nu_x , Sherwood number Sh_x and density number

Nn_x that are specified by:

$$C_f = \frac{2\tau_w}{\rho_f U_w^2}, \quad Nu_x = \frac{xq_w}{k(T_w - T_0)}, \quad Sh_x = \frac{xq_m}{D_B(C_w - C_0)}, \quad Nn_x = \frac{xq_n}{D_m(N_w - N_0)}, \quad (5.13)$$

where

$$\tau_w = \left| \mu \frac{\partial u}{\partial y} \right|_{y=0}, \quad q_w = \left| -k \frac{\partial T}{\partial y} \right|_{y=0}, \quad q_m = \left| -D_B \frac{\partial C}{\partial y} \right|_{y=0}, \quad q_n = \left| -D_m \frac{\partial N}{\partial y} \right|_{y=0}. \quad (5.14)$$

Using the similarity transformation presented above, (5.13) can be described as:

$$\left. \begin{aligned} \frac{1}{2} C_f Re_x^{0.5} = f''(0), \quad Nu_x Re_x^{-0.5} = -\theta'(0), \\ Sh_x Re_x^{-0.5} = -\phi'(0), \quad Nn_x Re_x^{-0.5} = -\chi'(0), \end{aligned} \right\} \quad (5.15)$$

in which the local Reynolds number is written as $Re_x = \frac{xU_w}{\nu}$.

5.3 Numerical Solution by Keller Box Method

To obtain the numerical solution of the nonlinear ODEs (5.7) - (5.10) alongside the end point conditions (5.12), the Keller-box method [114, 115] have been employed for different values of the concerned parameters. The following steps are the main components of this numerical scheme:

1. To convert the momentum, energy, concentration and microorganisms equations to the first order set of differential equations.
2. To achieve the difference equations with the help of the central finite differences.
3. To linearize the non-linear difference equations by using the Newton's method.
4. To implement the block tri-diagonal elimination scheme to get the solution of the linear system iteratively.

The new variables $\check{u}_1, \check{u}_2, \check{u}_3, \check{t}, \check{c}$ and \check{g} have been introduced to get a system of first order ODEs such that

$$\frac{df}{d\eta} = \check{u}_1, \quad \frac{d\check{u}_1}{d\eta} = \check{u}_2, \quad \frac{d\check{u}_2}{d\eta} = \check{u}_3, \quad \frac{d\theta}{d\eta} = \check{t}, \quad \frac{d\phi}{d\eta} = \check{c}, \quad \frac{d\chi}{d\eta} = \check{g}. \quad (5.16)$$

The resulting system of first order ODEs is then written as:

$$\begin{aligned}
& -\beta f \frac{d\check{u}_3}{d\eta} + \check{u}_3 - (1 + \lambda_2)[\check{u}_1^2 - f\check{u}_2] + \beta\check{u}_2^2 - (1 + \lambda_2)M\check{u}_1 \\
& + Gr[\theta - Nr\phi - Rb\chi] = 0,
\end{aligned} \tag{5.17}$$

$$\begin{aligned}
& \frac{d\check{t}}{d\eta} - PrSt\check{u}_1 - Pr\check{u}_1\theta + Prf\check{t} + PrNt(\check{t})^2 + PrNb\check{c}\check{t} + MPrEc\check{u}_1^2 \\
& + PrEc\left((\check{u}_2)^2 + \lambda_2\check{u}_2(\check{u}_1\check{u}_2 - f\check{u}_3)\right) = 0,
\end{aligned} \tag{5.18}$$

$$\frac{d\check{c}}{d\eta} - PrLe\check{u}_1\phi - PrLeSc\check{u}_1 + PrLe\check{f}\check{c} + \frac{Nt}{Nb} \frac{d\check{t}}{d\eta} = 0, \tag{5.19}$$

$$\frac{d\check{g}}{d\eta} - Lb\check{u}_1\chi - LbSm\check{u}_1 + Lbf\check{g} - Pe\left(g\check{c} + (\sigma + \chi)\frac{d\check{c}}{d\eta}\right) = 0. \tag{5.20}$$

The evolved boundary conditions for this study are:

$$\left. \begin{aligned}
& f(0) = 0, \quad \check{u}_1(0) = 1, \quad \theta(0) = 1 - St, \quad \phi(0) = 1 - Sc, \quad \chi(0) = 1 - Sm, \\
& \check{u}_1 \rightarrow 0, \quad \check{u}_2 \rightarrow 0, \quad \theta \rightarrow 0, \quad \phi \rightarrow 0, \quad \chi \rightarrow 0 \quad \text{as } \eta \rightarrow \infty.
\end{aligned} \right\} \tag{5.21}$$

The domain is discretized with the help of the subsequent nodes: $\eta_0 = 0$, $\eta_j = \eta_{j-1} + h_j$, $j = 0, 1, 2, 3, \dots, J$, $\eta_J = \eta_\infty$ where, h_j is the step size. The central difference approximations as pointed out in (2), are as follows:

$$\frac{f_j - f_{j-1}}{h_j} = (\check{u}_1)_{j-\frac{1}{2}}, \tag{5.22}$$

$$\frac{(\check{u}_1)_j - (\check{u}_1)_{j-1}}{2} = (\check{u}_2)_{j-\frac{1}{2}}, \tag{5.23}$$

$$\frac{(\check{u}_2)_j - (\check{u}_2)_{j-1}}{2} = (\check{u}_3)_{j-\frac{1}{2}}, \tag{5.24}$$

$$\frac{\theta_j - \theta_{j-1}}{h_j} = (\check{t})_{j-\frac{1}{2}}, \tag{5.25}$$

$$\frac{\phi_j - \phi_{j-1}}{h_j} = (\check{c})_{j-\frac{1}{2}}, \tag{5.26}$$

$$\frac{\chi_j - \chi_{j-1}}{h_j} = (\check{g})_{j-\frac{1}{2}}, \tag{5.27}$$

$$\left. \begin{aligned}
& \beta \left[\left((\check{u}_2)_{j-\frac{1}{2}} \right)^2 - \left(f_{j-\frac{1}{2}} \right) \left(\frac{(\check{u}_3)_j - (\check{u}_3)_{j-1}}{h_j} \right) \right] - (1 + \lambda_2) \\
& \left[\left((\check{u}_1)_{j-\frac{1}{2}} \right)^2 - \left(f_{j-\frac{1}{2}} \right) \left((\check{u}_2)_{j-\frac{1}{2}} \right) \right] + \left((\check{u}_3)_{j-\frac{1}{2}} \right) \\
& - M(1 + \lambda_2) \left((\check{u}_1)_{j-\frac{1}{2}} \right) + Gr \left[\left(\theta_{j-\frac{1}{2}} \right) - Nr \left(\phi_{j-\frac{1}{2}} \right) - Rb \left(\chi_{j-\frac{1}{2}} \right) \right] = 0,
\end{aligned} \right\} \tag{5.28}$$

$$\left. \begin{aligned}
& \left(\frac{\check{t} - \check{t}_{j-1}}{h_j} \right) - Pr \left((\check{u}_1)_{j-\frac{1}{2}} \right) \left(\theta_{j-\frac{1}{2}} \right) - PrSt \left((\check{u}_1)_{j-\frac{1}{2}} \right) + Pr \left(f_{j-\frac{1}{2}} \right) \left((\check{t})_{j-\frac{1}{2}} \right) \\
& + PrNb \left((\check{c})_{j-\frac{1}{2}} \right) \left((\check{t})_{j-\frac{1}{2}} \right) + PrNt \left((\check{t})_{j-\frac{1}{2}} \right)^2 + MPrEc \left((\check{u}_1)_{j-\frac{1}{2}} \right)^2 \\
& + PrEc \left((\check{u}_2)_{j-\frac{1}{2}}^2 + \lambda_2 (\check{u}_2)_{j-\frac{1}{2}} \left((\check{u}_1)_{j-\frac{1}{2}} (\check{u}_2)_{j-\frac{1}{2}} - f_{j-\frac{1}{2}} (\check{u}_3)_{j-\frac{1}{2}} \right) \right) = 0,
\end{aligned} \right\} \tag{5.29}$$

$$\left. \begin{aligned} & \left(\frac{\check{c} - \check{c}_{j-1}}{h_j} \right) - PrLe \left((\check{u}_1)_{j-\frac{1}{2}} \right) \left(\phi_{j-\frac{1}{2}} \right) - PrLeSc \left((\check{u}_1)_{j-\frac{1}{2}} \right) \\ & + PrLe \left(f_{j-\frac{1}{2}} \right) \left((\check{c})_{j-\frac{1}{2}} \right) + \frac{Nt}{Nb} \left(\frac{t_j - t_{j-1}}{h_j} \right) = 0, \end{aligned} \right\} \quad (5.30)$$

$$\left. \begin{aligned} & \left(\frac{\check{g} - \check{g}_{j-1}}{h_j} \right) - Lb \left((\check{u}_1)_{j-\frac{1}{2}} \right) \left((\check{\chi})_{j-\frac{1}{2}} \right) - LbSm \left((\check{u}_1)_{j-\frac{1}{2}} \right) + \\ & Lb \left(f_{j-\frac{1}{2}} \right) \left((\check{g})_{j-\frac{1}{2}} \right) - Pe \left((\check{g})_{j-\frac{1}{2}} \right) \left((\check{c})_{j-\frac{1}{2}} \right) \\ & - Pe \left(\sigma + f_{j-\frac{1}{2}} \right) \left(\frac{\check{c} - \check{c}_{j-1}}{h_j} \right) = 0. \end{aligned} \right\} \quad (5.31)$$

in which $f_{j-\frac{1}{2}} = \frac{f_j + f_{j-1}}{2}$ etc. To linearize the system of nonlinear Eqs. (5.22)-(5.31) by Newton's method, the following substitutions have been introduced:

$$\left. \begin{aligned} & (\check{u}_1)_j^{n+1} = (\check{u}_1)_j^n + \delta(\check{u}_1)_j^n, (\check{u}_2)_j^{n+1} = (\check{u}_2)_j^n + \delta(\check{u}_2)_j^n, t_j^{n+1} = t_j^n + \delta t_j^n, \\ & f_j^{n+1} = f_j^n + \delta f_j^n, \theta_j^{n+1} = \theta_j^n + \delta \theta_j^n, \phi_j^{n+1} = \phi_j^n + \delta \phi_j^n, \chi_j^{n+1} = \chi_j^n + \delta \chi_j^n, \\ & c_j^{n+1} = c_j^n + \delta c_j^n, g_j^{n+1} = g_j^n + \delta g_j^n, (\check{u}_3)_j^{n+1} = (\check{u}_3)_j^n + \delta(\check{u}_3)_j^n. \end{aligned} \right\} \quad (5.32)$$

Putting these expressions in Eqs. (5.22)-(5.31) and dropping the higher-order terms in δ , the following system is obtained:

$$(\delta f_j - \delta f_{j-1}) - \frac{h_j}{2} (\delta(\check{u}_1)_j + \delta(\check{u}_1)_{j-1}) = (r_1)_j, \quad (5.33)$$

$$(\delta(\check{u}_1)_j - \delta(\check{u}_1)_{j-1}) - \frac{h_j}{2} (\delta(\check{u}_2)_j + \delta(\check{u}_2)_{j-1}) = (r_2)_j, \quad (5.34)$$

$$(\delta(\check{u}_2)_j - \delta(\check{u}_2)_{j-1}) - \frac{h_j}{2} (\delta(\check{u}_3)_j + \delta(\check{u}_3)_{j-1}) = (r_3)_j, \quad (5.35)$$

$$(\delta \theta_j - \delta \theta_{j-1}) - \frac{h_j}{2} (\delta \check{t}_j + \delta \check{t}_{j-1}) = (r_4)_j, \quad (5.36)$$

$$(\delta \phi_j - \delta \phi_{j-1}) - \frac{h_j}{2} (\delta \check{c}_j + \delta \check{c}_{j-1}) = (r_5)_j, \quad (5.37)$$

$$(\delta \chi_j - \delta \chi_{j-1}) - \frac{h_j}{2} (\delta \check{g}_j + \delta \check{g}_{j-1}) = (r_6)_j, \quad (5.38)$$

$$\begin{aligned} & (\xi_1)_j \delta(\check{u}_3)_j + (\xi_2)_j \delta(\check{u}_3)_{j-1} + (\xi_3)_j \delta f_j + (\xi_4)_j \delta f_{j-1} + (\xi_5)_j \delta(\check{u}_2)_j \\ & + (\xi_6)_j \delta(\check{u}_2)_{j-1} + (\xi_7)_j \delta(\check{u}_1)_j + (\xi_8)_j \delta(\check{u}_1)_{j-1} + (\xi_9)_j \delta \theta_j + (\xi_{10})_j \delta \theta_{j-1} \\ & + (\xi_{11})_j \delta \phi_j + (\xi_{12})_j \delta \phi_{j-1} + (\xi_{13})_j \delta \chi_j + (\xi_{14})_j \delta \chi_{j-1} = (r_7)_j, \end{aligned} \quad (5.39)$$

$$\begin{aligned} & (\beta_1)_j \delta \check{t}_j + (\beta_2)_j \delta \check{t}_{j-1} + (\beta_3)_j \delta \check{c}_j + (\beta_4)_j \delta \check{c}_{j-1} + (\beta_5)_j \delta f_j + (\beta_6)_j \delta f_{j-1} \\ & + (\beta_7)_j \delta \theta_j + (\beta_8)_j \delta \theta_{j-1} + (\beta_9)_j \delta(\check{u}_1)_j + (\beta_{10})_j \delta(\check{u}_1)_{j-1} + (\beta_{11})_j \delta(\check{u}_2)_j \\ & + (\beta_{12})_j \delta(\check{u}_2)_{j-1} = (r_8)_j, \end{aligned} \quad (5.40)$$

$$\begin{aligned}
& (\alpha_1)_j \delta \check{c}_j + (\alpha_2)_j \delta \check{c}_{j-1} + (\alpha_3)_j \delta f_j + (\alpha_4)_j \delta f_{j-1} + (\alpha_5)_j \delta (\check{u}_1)_j + (\alpha_6)_j \delta (\check{u}_1)_{j-1} \\
& + (\alpha_7)_j \delta \phi_j + (\alpha_8)_j \delta \phi_{j-1} + (\alpha_9)_j \delta t_j + (\alpha_{10})_j \delta t_{j-1} = (r_9)_j,
\end{aligned} \tag{5.41}$$

$$\begin{aligned}
& (\gamma_1)_j \delta \check{c}_j + (\gamma_2)_j \delta \check{c}_{j-1} + (\gamma_3)_j \delta \chi_j + (\gamma_4)_j \delta \chi_{j-1} + (\gamma_5)_j \delta f_j + (\gamma_6)_j \delta f_{j-1} \\
& + (\gamma_7)_j \delta \check{g}_j + (\gamma_8)_j \delta \check{g}_{j-1} = (r_{10})_j,
\end{aligned} \tag{5.42}$$

where

$$\left. \begin{aligned}
(\xi_1)_j &= \frac{h_j}{2} - \frac{\beta}{2}(f_j + f_{j-1}), & (\xi_2)_j &= \frac{h_j}{2} + \frac{\beta}{2}(f_j + f_{j-1}), \\
(\xi_3)_j &= \frac{h_j(1 + \lambda_1)}{4}((\check{u}_2)_j + (\check{u}_2)_{j-1}) - \frac{\beta}{2}((\check{u}_3)_j - (\check{u}_3)_{j-1}) = (\xi_4)_j, \\
(\xi_5)_j &= \frac{h_j(1 + \lambda_1)}{4}(f_j + f_{j-1}) + \frac{h_j \beta}{2}((\check{u}_2)_j + (\check{u}_2)_{j-1}) = (\xi_6)_j, \\
(\xi_7)_j &= \frac{-1}{2}h_j M(1 + \lambda_1) - \frac{h_j(1 + \lambda_1)}{2}((\check{u}_1)_j + (\check{u}_1)_{j-1}) = (\xi_8)_j, \\
(\xi_9)_j &= \frac{h_j}{2}Gr = (\xi_{10})_j, & (\xi_{11})_j &= -\frac{h_j}{2}GrNr = (\xi_{12})_j, \\
(\xi_{13})_j &= -\frac{h_j}{2}GrRb = (\xi_{14})_j, & (r_7)_j &= \frac{h_j}{2}M(1 + \lambda_1)(\check{u}_1)_{j-\frac{1}{2}} + \frac{h_j}{4}(1 + \lambda_1) \\
& (\check{u}_1)_{j-\frac{1}{2}}^2 - \frac{h_j}{4}(1 + \lambda_1)f_{j-\frac{1}{2}}(\check{u}_2)_{j-\frac{1}{2}} - \frac{1}{4}h_j(\check{u}_2)_{j-\frac{1}{2}}^2 - \frac{1}{2}(\check{u}_3)_{j-\frac{1}{2}} + \frac{1}{2}\beta f_{j-\frac{1}{2}} \\
& ((\check{u}_3)_j - (\check{u}_3)_{j-1}) - Grh_j\theta_{j-\frac{1}{2}} + GrNr h_j\phi_{j-\frac{1}{2}} + GrRbh_j\chi_{j-\frac{1}{2}},
\end{aligned} \right\} \tag{5.43}$$

$$\left. \begin{aligned}
(\beta_1)_j &= 1 + \frac{h_j N_b Pr}{4}(\check{c} + \check{c}_{j-1}) + \frac{h_j Pr}{4}(f_j + f_{j-1}) + \frac{h_j N_t Pr}{2}(\check{t} + \check{t}_{j-1}), \\
(\beta_2)_j &= (\beta_1)_j - 2, & (\beta_3)_j &= \frac{h_j N_b Pr}{4}(\check{t} + \check{t}_{j-1}) = (\beta_4)_j, \\
(\beta_5)_j &= \frac{h_j Pr}{4}(\check{t}_j + \check{t}_{j-1}) = (\beta_6)_j, & (\beta_7)_j &= -Prh_j \frac{((\check{u}_2)_j + (\check{u}_2)_{j-1})}{2} = (\beta_8)_j, \\
(\beta_9)_j &= \frac{h_j M Pr Ec}{2}((\check{u}_1)_j + (\check{u}_1)_{j-1}) - \frac{Prh_j}{2}(\theta_j + \theta_{j-1}) = (\beta_{10})_j, \\
(r_8)_j &= (\check{t}_{j-1} - \check{t}_j) - h_j N_b Pr(\check{c})_{j-\frac{1}{2}}(\check{t})_{j-\frac{1}{2}} - h_j Pr(\check{t})_{j-\frac{1}{2}}f_{j-\frac{1}{2}} \\
& - h_j N_t Pr(\check{t})_{j-\frac{1}{2}}^2 - h_j M Pr Ec(\check{u}_1)_{j-\frac{1}{2}}^2 - h_j Pr Ec(\check{u}_2)_{j-\frac{1}{2}}^2 \\
& - 2h_j Pr(\check{u}_1)_{j-\frac{1}{2}}\theta_{j-\frac{1}{2}},
\end{aligned} \right\} \tag{5.44}$$

$$\left. \begin{aligned}
(\alpha_1)_j &= 1 + \frac{h_j Sc}{4}(f_j + f_{j-1}), & (\alpha_2)_j &= (\alpha_1)_j - 2, \\
(\alpha_3)_j &= \frac{h_j Sc}{4}(\check{c} + \check{c}_{j-1}) = (\alpha_4)_j, & (\alpha_5)_j &= \frac{h_j Sc}{2}(\phi_j + \phi_{j-1}) = -(\gamma_6)_j, \\
(\alpha_7)_j &= -\frac{h_j Sc}{2}((\check{u}_1)_j + (\check{u}_1)_{j-1}) = (\alpha_8)_j, \\
(\alpha_9)_j &= -Sr = -(\alpha_{10})_j, \\
(r_9)_j &= (\check{c}_{j-1} - \check{c}_j) + Sr(\check{t}_{j-1} - \check{t}_j) - \frac{h_j Sc}{4}\check{c}_{j-\frac{1}{2}}f_{j-\frac{1}{2}} + \frac{h_j Sc}{2}(\check{u}_1)_{j-\frac{1}{2}}\phi_{j-\frac{1}{2}},
\end{aligned} \right\} \tag{5.45}$$

$$[A_j] = \begin{bmatrix} -0.5h_j & 0 & 0 & 0 & 0 & 1 & 0 & 0 & 0 & 0 \\ -1 & -0.5h_j & 0 & 0 & 0 & 0 & 0 & 0 & 0 & 0 \\ 0 & -1 & 0 & 0 & 0 & 0 & -0.5h_j & 0 & 0 & 0 \\ 0 & 0 & -1 & 0 & 0 & 0 & 0 & -0.5h_j & 0 & 0 \\ 0 & 0 & 0 & -1 & 0 & 0 & 0 & 0 & -0.5h_j & 0 \\ 0 & 0 & 0 & 0 & -1 & 0 & 0 & 0 & 0 & -0.5h_j \\ (\xi_8)_j & (\xi_6)_j & 0 & 0 & 0 & (\xi_3)_j & (\xi_1)_j & 0 & 0 & 0 \\ (\beta_{10})_j & (\beta_{12})_j & (\beta_8)_j & 0 & 0 & (\beta_5)_j & 0 & (\beta_1)_j & (\beta_3)_j & 0 \\ (\alpha_6)_j & 0 & 0 & (\alpha_8)_j & 0 & (\alpha_3)_j & 0 & (\alpha_9)_j & (\alpha_1)_j & 0 \\ 0 & 0 & 0 & 0 & (\gamma_4)_j & (\gamma_5)_j & 0 & 0 & (\gamma_1)_j & (\gamma_7)_j \end{bmatrix}, 2 \leq j \leq J$$

$$[B_j] = \begin{bmatrix} 0 & 0 & 0 & 0 & 0 & -1 & 0 & 0 & 0 & 0 \\ 0 & 0 & 0 & 0 & 0 & 0 & 0 & 0 & 0 & 0 \\ 0 & 0 & 0 & 0 & 0 & 0 & -0.5h_j & 0 & 0 & 0 \\ 0 & 0 & 0 & 0 & 0 & 0 & 0 & -0.5h_j & 0 & 0 \\ 0 & 0 & 0 & 0 & 0 & 0 & 0 & 0 & -0.5h_j & 0 \\ 0 & 0 & 0 & 0 & 0 & 0 & 0 & 0 & 0 & -0.5h_j \\ 0 & 0 & 0 & 0 & 0 & (\xi_4)_j & (\xi_2)_j & 0 & 0 & 0 \\ 0 & 0 & 0 & 0 & 0 & (\beta_6)_j & 0 & (\beta_2)_j & (\beta_4)_j & 0 \\ 0 & 0 & 0 & 0 & 0 & (\alpha_4)_j & 0 & (\alpha_{10})_j & (\alpha_2)_j & 0 \\ 0 & 0 & 0 & 0 & 0 & (\gamma_6)_j & 0 & 0 & (\gamma_2)_j & (\gamma_8)_j \end{bmatrix}, 2 \leq j \leq J$$

$$[C_j] = \begin{bmatrix} -0.5h_j & 0 & 0 & 0 & 0 & 0 & 0 & 0 & 0 & 0 \\ 1 & -0.5h_j & 0 & 0 & 0 & 0 & 0 & 0 & 0 & 0 \\ 0 & 1 & 0 & 0 & 0 & 0 & 0 & 0 & 0 & 0 \\ 0 & 0 & 1 & 0 & 0 & 0 & 0 & 0 & 0 & 0 \\ 0 & 0 & 0 & 1 & 0 & 0 & 0 & 0 & 0 & 0 \\ 0 & 0 & 0 & 0 & 1 & 0 & 0 & 0 & 0 & 0 \\ (\xi_7)_j & (\xi_5)_j & 0 & 0 & 0 & 0 & 0 & 0 & 0 & 0 \\ (\beta_9)_j & (\beta_{11})_j & (\beta_7)_j & 0 & 0 & 0 & 0 & 0 & 0 & 0 \\ (\alpha_5)_j & 0 & 0 & (\alpha_7)_j & 0 & 0 & 0 & 0 & 0 & 0 \\ 0 & 0 & 0 & 0 & 0 & (\gamma_3)_j & 0 & 0 & 0 & 0 \end{bmatrix}, 1 \leq j \leq J-1.$$

Now we factorize A as

$$A = LU, \quad (5.48)$$

where

$$L = \begin{bmatrix} [a_1] & & & & \\ [b_2] [a_2] & & & & \\ & \ddots & & & \\ & & \ddots & [a_{J-1}] & \\ & & & [b_J] [a_J] & \end{bmatrix},$$

$$U = \begin{bmatrix} [I] [c_1] & & & & \\ & [I] [c_2] & & & \\ & & \ddots & \ddots & \\ & & & [I] [c_{J-1}] & \\ & & & & [I] \end{bmatrix}.$$

Here $[a_i]$, $[b_i]$ and $[c_i]$ are 10×10 matrices and $[I]$ is the unit matrix of order 10. Eq. (5.47) provides the solution for δ by the LU factorization method. The grid of size $h_j = 0.001$ is employed to achieve the numerical solution using $\eta_{max} = 12$ and an error tolerance of 10^{-6} for all instances. To ascertain the accurateness of the adopted numerical strategy, a highly convincing comparison of the present results with those reported by Ishak et al. [116] and Pal and Mondal [117] for $\theta'(0)$ is conducted and findings are quite similar to those presented in Table 3.2.

5.4 Results and Discussions

The evolved Eqs. (5.7)-(5.10) of momentum, energy, concentration and motile microorganisms density along with the boundary condition (5.11) are solved

numerically and the computational analysis is carried out for some appropriate choices of the physical parameters. Figs 5.2-5.18 are illustrated to scrutinize the dynamics in the velocity profile $f'(\eta)$, temperature $\theta(\eta)$, concentration of nanoparticles $\phi(\eta)$ and motile micro-organisms density $\chi(\eta)$ of the nanofluid for various values of some important physical parameters like Deborah number β , magnetic number M , Prandtl number Pr , Eckert number Ec , thermophoresis Nt , Brownian motion Nb , Peclet number Pe , bioconvection Lewis number Lb , thermal stratification St , motile density stratification Sm , Lewis number Le , micro-organisms concentration difference σ and concentration stratification Sc . In addition Figs. 5.19-5.24 are drawn to examine the essential and relevant quantities of physical interest, specifically the local drag coefficient, Nusselt number, Sherwood number and motile microorganisms density rate.

Fig. 5.2 demonstrates the impact of magnetic number M on the velocity distribution profile $f'(\eta)$. It is found that the presence of M reduces the boundary-layer thickness as well as the velocity profile. Physically, the magnetic field generates the Lorentz force that gives a resistance to the fluid flow and slows down the fluid velocity. The impact of Deborah number β on velocity profile $f'(\eta)$ is presented in Fig. 5.3. It is noticed that the velocity and the boundary layer thickness are enhanced with the rising values of β . As β depends on the stretching rate a , an enhancement in β causes a rise in the fluid movement in the boundary-layer close to the surface. Consequently, it rises the velocity as well as thickness of the boundary layer. Fig. 5.4 reveals the impact of values of the relaxation over retardation time λ_1 on the velocity profile. The velocity $f'(\eta)$ is observed to reduce for a rise in λ_1 . The velocity boundary layer thickness is also boosts whenever λ_1 enhances. It has been observed that boundary layer(momentum) diminishes for greater values of λ_1 . Because λ_1 is inversely related to the time of retardation of the non-Newtonian fluid therefore by raising λ_1 we have decrease in time of retardation and subsequently the fluid flow decreases.

Fig. 5.5 demonstrates the influence of Pr on the thermal profile $\theta(\eta)$. As the Prandtl number is enhanced, the temperature profile reduces. It is simply because that for larger values of Pr , the thermal diffusivity of the liquid is reduced. Consequently, the temperature profile of the fluid is reduced. Fig. 5.6 demonstrates the impact of Ec on the thermal profile θ . From Fig. 5.6, it is seen that an escalation in Ec boosts the

temperature field θ just because heat is accumulated in the fluid caused by a frictional heating. Further close to the surface, thermal profile overshoots with an increment in Ec . From Fig. 5.7, it is obvious that temperature is dropped down for rising values of β . In physical sense, β is directly related to the time of retardation, therefore the retardation time is boosted whenever β is raised. This rise in retardation time contributes to reduce the temperature as well as the thermal boundary layer thickness.

Through Fig. 5.8, it is noticed that for growing values of Nt , the temperature profile shows an increasing trend. Physically, the thermophoretic parameter enhances the density of the thermal boundary layer, as a consequence of which the temperature profile is increased. Fig. 5.9 shows the impact of Nb on θ . The dimensionless temperature is increased with the escalating values of the Brownian motion parameter Nb . It is just because a rise in Nb strengthens the random movement of the particles as a result of which an additional heat is generated. Consequently the temperature of the fluid enhanced. Fig. 5.10 highlights the influence of the thermal stratification parameter St on $\theta(\eta)$. In general, in case of St rises, the temperature difference between heated sheet and ambient is reduced. Consequently, the fluid temperature is experienced to decline.

Fig. 5.11 reveals the effect of Nb on the concentration profile $\phi(\eta)$. It is noticed that an enhancement in the values of Nb reduces $\phi(\eta)$. Generally, an increment in the Brownian motion parameter speeds up the collision among the fluid particles, resulting in an additional heat. As a result, the concentration profile $\phi(\eta)$ is reduced. Figs. 5.12 suggests the influence of Nt on the mass fraction function $\phi(\eta)$. It can be observed that an intensification in the thermophoresis parameter boosts up the concentration profile. It manifests that bigger values of Nt will result in an enlargement of the thermophoresis force within the boundary-layer region that accelerates the mass fraction of the nanoparticles. Fig. 5.13 presents the concentration profile $\phi(\eta)$ for various values of Le . The concentration profile is reduced for the escalating values of the Lewis number Le . Because the ratio of thermal diffusivity over mass diffusivity is defined as the Lewis number, therefore the larger values of Le lessen the mass fraction function. Consequently, the concentration profile is reduced by enhancing the value of Le . An influence of the solutal stratification parameter Sc on the mass fraction

function $\phi(\eta)$ is reflected in Fig. 5.14. It can be clearly viewed that the concentration distribution $\phi(\eta)$ shows a diminishing behavior for an enhancement in the values of the solutal stratification parameter Sc .

Fig. 5.15 is sketched to observe the behaviour of the gyro-tactic microorganism density profile $\chi(\eta)$ for different choices of the values of the Peclet number Pe . Peclet number is defined by advective over diffusive transport rate. It is noticed from the figure that a rise in Peclet number Pe leads to a decrement in the motile microorganism density profile, because a rise in Pe produces an advancement in the motion of the fluid particles which induces a decline in the thickness of gyro-tactic micro-organism. Fig. 5.16 is sketched to highlight the effect of the bio-convection number Lb on the motile density. It is analyzed that for bigger values of the bio-convection number, the diffusivity of micro-organisms is reduced as a result of which the density of the gyro-tactic micro-organisms is seen to deteriorate. Fig. 5.17 shows that the concentration of microorganisms $\chi(\eta)$ suffers a decreasing trend for an increment in the micro-organism concentration difference parameter σ . It can be depicted from Fig. 5.18 that an enhancement in Sm considerably lessens the concentration difference of the micro-organisms between the sheet and far from the sheet and so a reduction in the density profile is observed.

Fig. 5.19 presents the behaviour of the local skin friction coefficient $f''(0)$ for various values of Deborah number β and magnetic parameter M . It can be perceived from the figure that for rising values of the Deborah number, the skin friction coefficient shows an enhancement. Additionally, the skin friction coefficient reveals a decreasing behavior for enhancing values of the magnetic parameter M . Fig. 5.20 exhibits the heat transfer rate $-\theta'(0)$ affected by the Eckert number Ec for a variety of values of β . It is noted that a rise in β boosts the heat transfer rate which is observed to be reduced for larger values of Ec . Fig. 5.21 shows the variations in the mass transfer rate $-\phi'(0)$ versus the Brownian motion parameter Nb and the thermophoresis parameter Nt . It has been concluded that $-\phi'(0)$ is increased with an augmentation in Nb while it is decreased for bigger Nt . Fig. 5.22 describes that the mass transfer rate $-\phi'(0)$ is enhanced with a rise in the Brownian motion parameter Nb and Lewis number Le . The impact of the bioconvection Lewis number Lb on the local

micro-organism transfer rate $-\chi'(0)$ for different values of Pe is presented in Fig. 5.23. It can be noticed that $-\chi'(0)$ is enhanced with a boost of Lb . It is due to the reason that the convection of the motile microorganism is amplified with a rise of the bioconvection Lewis number Lb . The local micro-organism transfer rate $-\chi'(0)$ is reduced for the rising values of the bioconvection Peclet number Pe . From Fig. 5.24, it is found that the local micro-organism transfer rate $-\chi'(0)$ is reduced for the greater micro-organisms concentration difference parameter σ , however the greater values of Lb are observed to cause an increment in the $-\chi'(0)$.

Table 5.1 is furnished with the numerical values of Nusselt number, Sherwood number and motile microorganisms density rate for various values of the relevant parameters. From this table, it is noticed that a boost in the magnetic number M , Brownian motion parameter Nb , thermophoresis parameter Nt , Eckert number Ec , relaxation to the retardation time λ_1 and Lewis number Le tends to reduce the Nusselt number at surface, though it increases for the escalating values of the Deborah number β and Prandtl number Pr . An intensification in the Brownian motion Nb , thermophoresis Nt , Deborah number β and Prandtl number Pr leads to diminish the Sherwood number while it is enhanced for the raising values of the magnetic number M , Lewis number Le , relaxation to the retardation time λ_1 and Eckert number Ec . Additionally, a growth in the magnetic number M , Lewis number Le , Eckert number Ec , Peclet number Pe , bioconvection Lewis number Lb , relaxation to the retardation times λ_1 and micro-organisms concentration difference parameter σ is noticed to raise the motile micro-organisms density rate, however it is reduced for the enhancing values of the Brownian motion Nb , thermophoresis Nt , Deborah number β , relaxation to the retardation time λ_1 and Prandtl number Pr .

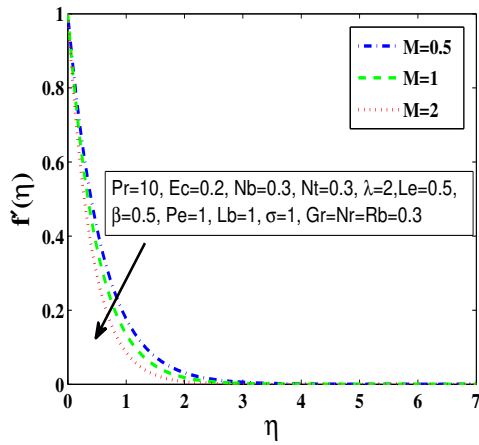


FIG. 5.2: Influence of M on $f'(\eta)$.

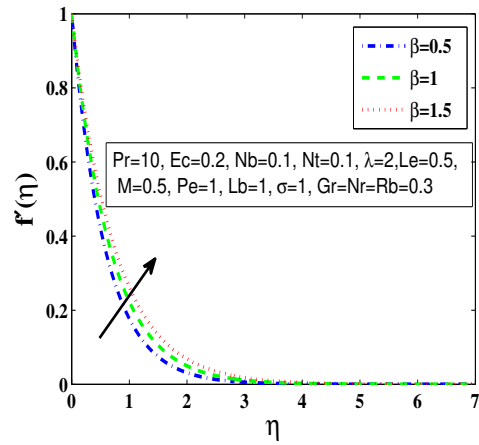


FIG. 5.3: Influence of β on $f'(\eta)$.

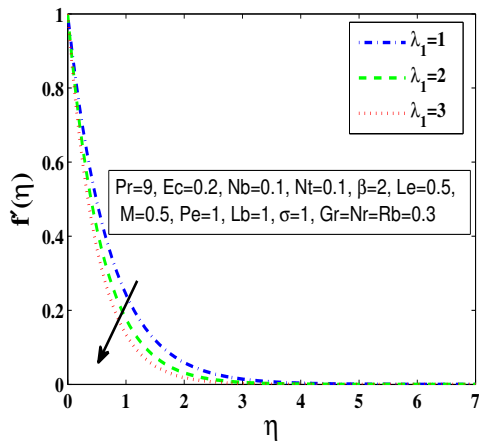


FIG. 5.4: Influence of λ_1 on $f'(\eta)$.

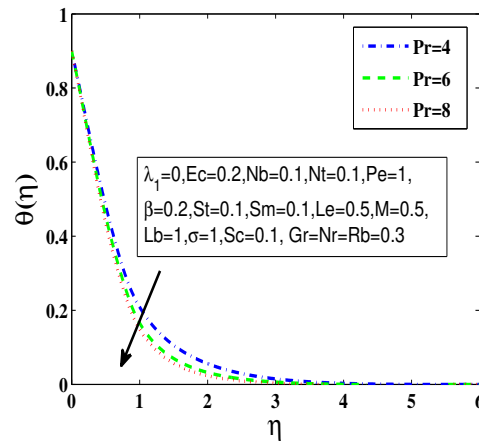


FIG. 5.5: Influence of Pr on $\theta(\eta)$.

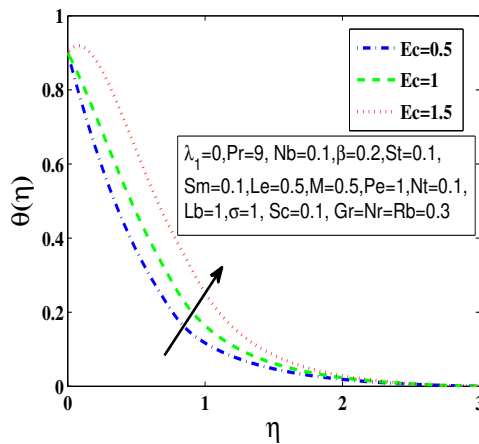


FIG. 5.6: Influence of Ec on $\theta(\eta)$.

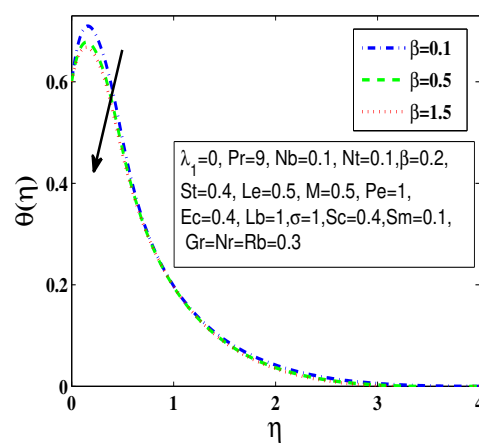


FIG. 5.7: Influence of β on $\theta(\eta)$.

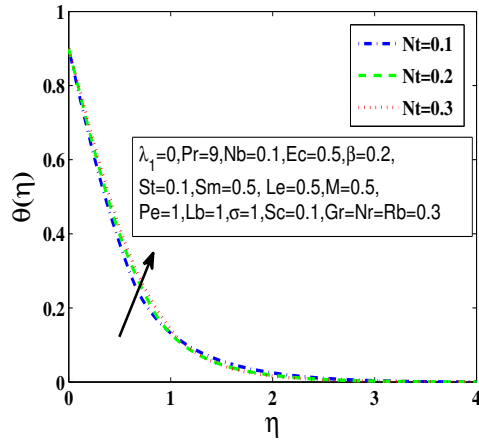


FIG. 5.8: Influence of Nt on $\theta(\eta)$.

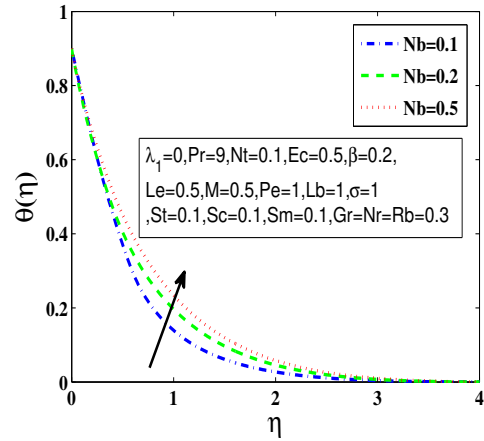


FIG. 5.9: Influence of Nb on $\theta(\eta)$.

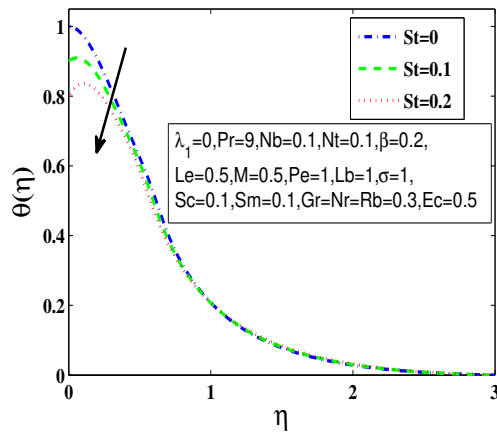


FIG. 5.10: Influence of St on $\theta(\eta)$.

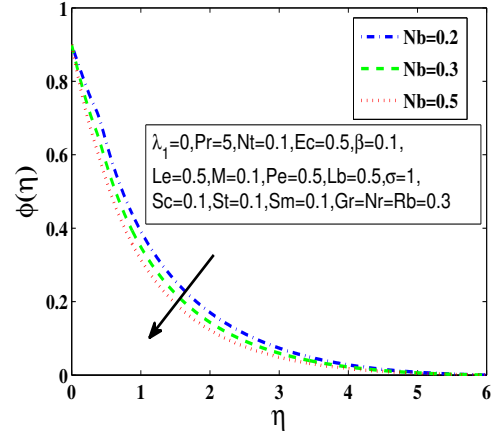


FIG. 5.11: Influence of Nb on $\phi(\eta)$.

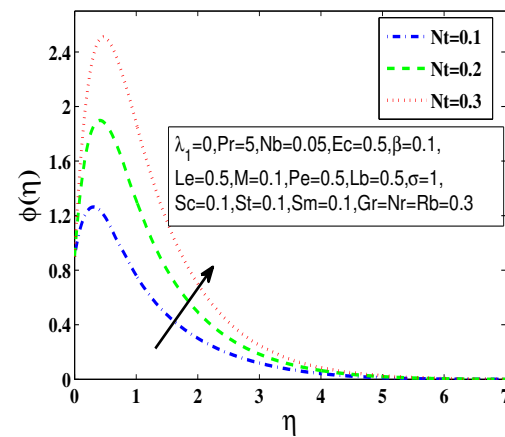


FIG. 5.12: Influence of Nt on $\phi(\eta)$.

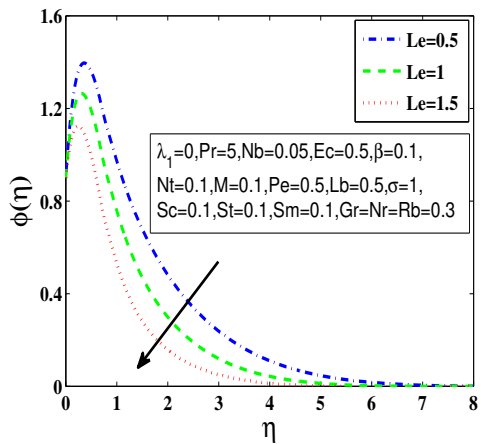


FIG. 5.13: Influence of Le on $\phi(\eta)$.

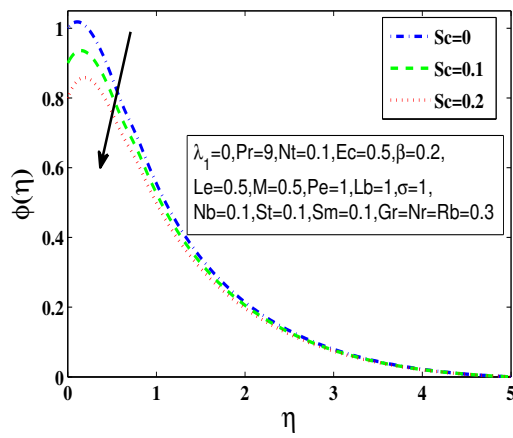


FIG. 5.14: Influence of Sc on $\phi(\eta)$.

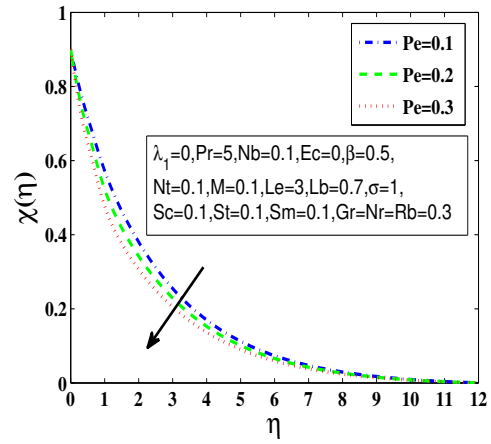


FIG. 5.15: Influence of Pe on $\chi(\eta)$.

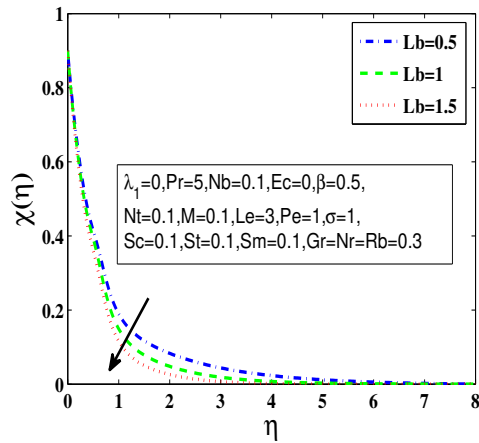


FIG. 5.16: Influence of Lb on $\chi(\eta)$.

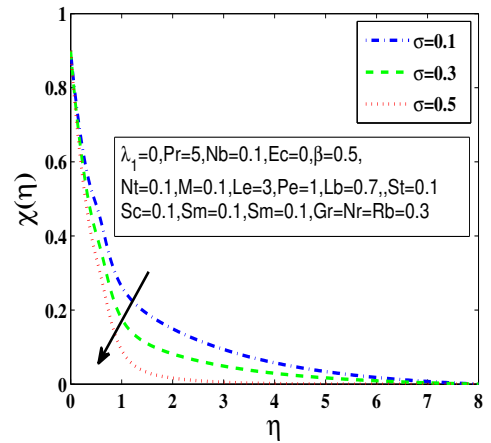


FIG. 5.17: Influence of σ on $\chi(\eta)$.

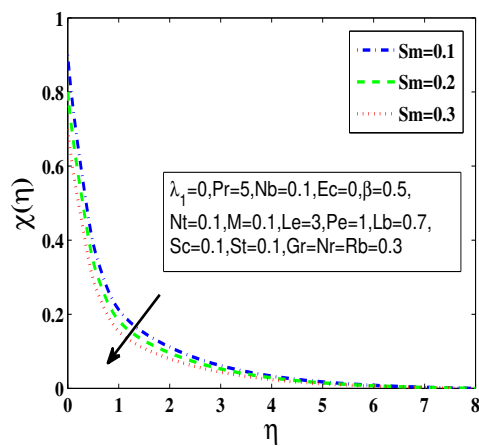


FIG. 5.18: Influence of Sm on $\chi(\eta)$.

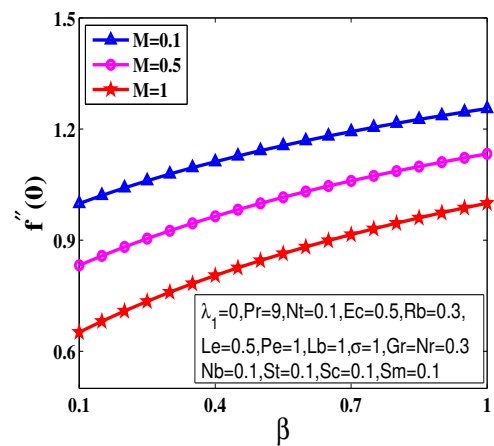


FIG. 5.19: Influence of β on $f''(0)$ for different values of M .

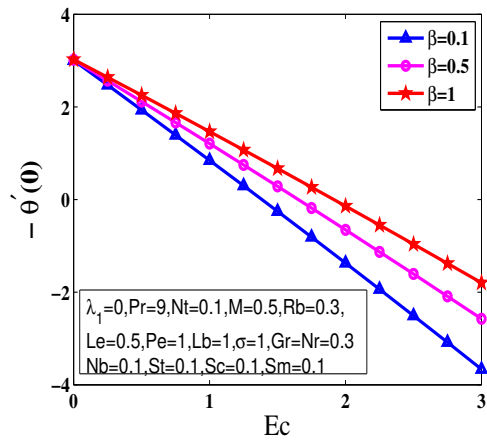


FIG. 5.20: Influence of Ec on $-\theta'(0)$ for different values of β .

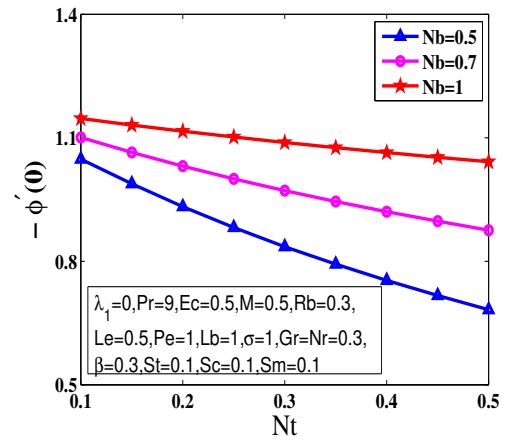


FIG. 5.21: Influence of Nt on $-\phi'(0)$ for different values of Nb .

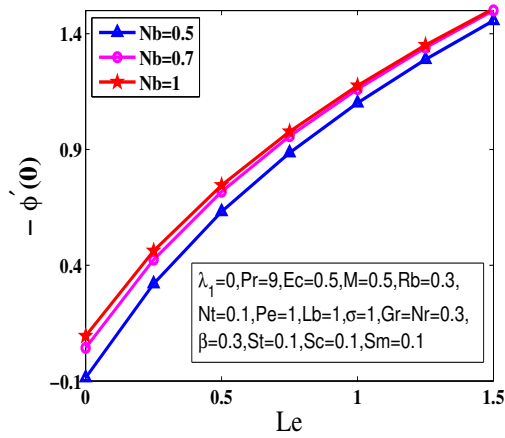


FIG. 5.22: Influence of Le on $-\phi'(0)$ for different values of Nb .

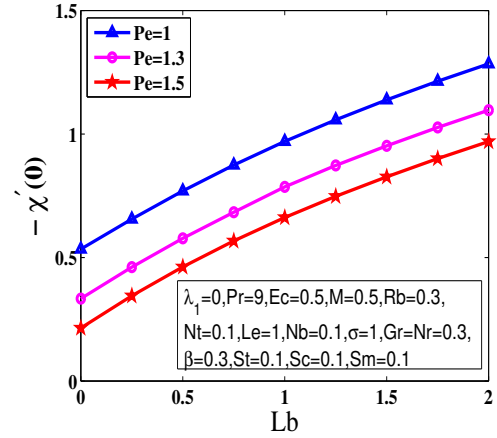


FIG. 5.23: Variation of $-\chi'(0)$ against Lb for different values of Pe .

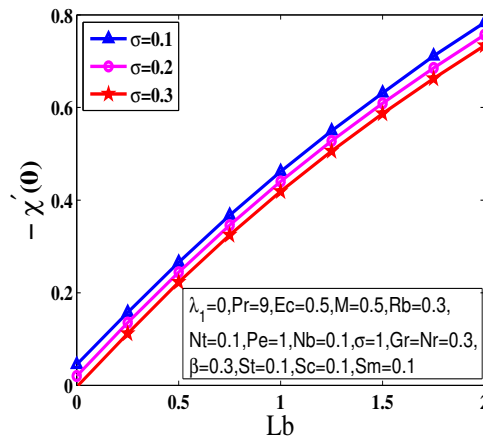


FIG. 5.24: Variation of $-\chi'(0)$ against Lb for different values of σ .

TABLE 5.1: Variation of $-\theta'(0)$, $-\phi'(0)$ and $-\chi'(0)$ for different sorts of parameters in flow.

M	Le	Nt	Nb	β	Ec	Pr	Pe	Lb	σ	λ_1	$-\theta'(0)$	$-\phi'(0)$	$-\chi'(0)$
0.5	1	0.1	0.1	0.5	0.5	10	1	1	1	2	1.48542	0.00685	0.46113
											0.74877	0.59253	1.55852
											0.05718	1.16240	2.64117
											0.76777	1.34107	2.96743
											0.64896	2.44760	5.07854
											0.58940	3.22067	6.57480
		0.1									0.89215	0.47672	1.34053
		0.2									0.79296	0.15883	0.86705
		0.3									0.72259	0.00386	0.72025
			0.1								0.89215	0.47672	1.34053
			0.2								0.79296	0.15883	0.86705
			0.3								0.72259	0.00386	0.72025
				0.1							0.29784	0.92415	2.17335
				0.5							0.89215	0.47672	1.34053
				1							1.32571	0.17185	0.77225
					0.4						1.18143	0.20785	0.81387
					0.5						0.60226	0.74615	1.86842
					0.6						0.02007	1.28732	2.93496
						1					0.49346	0.69420	1.66729
						2					0.65966	0.57279	1.41428
						3					0.77451	0.49256	1.22175
							1				0.89215	0.47672	1.34053
							2				0.89260	0.47648	2.23952
							3				0.89269	0.47649	3.15047
								0.5			0.89215	0.47672	1.15028
								1			0.89215	0.47672	1.34053
								1.5			0.89215	0.47672	1.50766
									0.2		0.89194	0.47689	1.01249
									0.4		0.89215	0.47672	1.17366
									0.6		0.89215	0.47672	1.34053
										1	1.47589	0.07142	0.57956
										2	0.89215	0.47672	1.34053
										3	0.34586	0.88690	2.10581

5.5 Concluding Remarks

The main outcomes in this research have been listed below:

- The concentration of the motile micro-organisms is a reducing function of the bioconvection Peclet number, bioconvection Lewis number and micro-organisms concentration difference.

- An enhancement in the Deborah number results in an augmentation in the velocity distribution though the magnetic parameter causes it to reduce.
- The velocity as well as the local nusselt number are diminishing functions of the magnetic number M .
- The skin friction coefficient and the local Nusselt number are increased with a boost in the Deborah number.
- Sherwood number is enhanced with a growth in thermophoresis parameter but suffers a decrement due to the Brownian motion parameter.
- The motile density number of micro-organisms is enhanced with a rise in the bioconvection Lewis number, however it is reduced by enhancing the Peclet number.
- The local Nusselt number and the local density number are noticed to rise with an escalation in the thermophoresis as well as the Brownian motion parameters.
- The thermal, mass and motile density stratification parameters decrease the temperature, concentration of nanoparticles and motile density of the micro-organisms profiles.

Chapter 6

MHD Rotating Flow of Nanofluid past a Stretching Sheet

6.1 Introduction

In this chapter, the flow of a nanofluid with H_2O as the base liquid and Cu and Ag as the nanoparticles has been considered between two rotating plates. The upper plate has been considered porous. In addition, the bottom surface is assumed to move with variable speed to cause the forced convection. Centripetal and Coriolis forces effects on the rotation of the fluid are also considered. The group of non-dimensional ordinary differential equations is obtained by applying some appropriate transformations on the governing partial differential equations. Numerical solution of the set of nonlinear ODEs is obtained through the shooting technique. It is theoretically observed that the nanofluid has a higher heat transfer rate and less drag as compared with the base fluid. Impact of rotation makes the drag rise and diminishes the Nusselt number independent of the various essential parameters used. Streamlines have been displayed to show the effect of injection/suction.

6.2 Mathematical Formulation

We contemplate an incompressible magnetohydrodynamic rotating flow of H_2O based Cu and Ag nanofluids between two plates with angular velocity $\boldsymbol{\Omega} [0, \Omega, 0]$. The upper plate is porous whereas the lower surface is moving with velocity $U_w = a x$ ($a > 0$) and stretching uniformly along the x -axis with the rate a . The time independent velocity field of flow is given as $\mathbf{V} [u, v, w]$, where the velocity components u, v and w are the functions of x, y and z , in the x, y and z directions respectively. A uniform magnetic field of strength B_0 is employed along the y -axis such that the induced magnetic field is ignored under the very small magnetic Reynolds number assumption. The schematic diagram is presented in Fig. 6.1. In case of the rotating flow, the conservative continuity

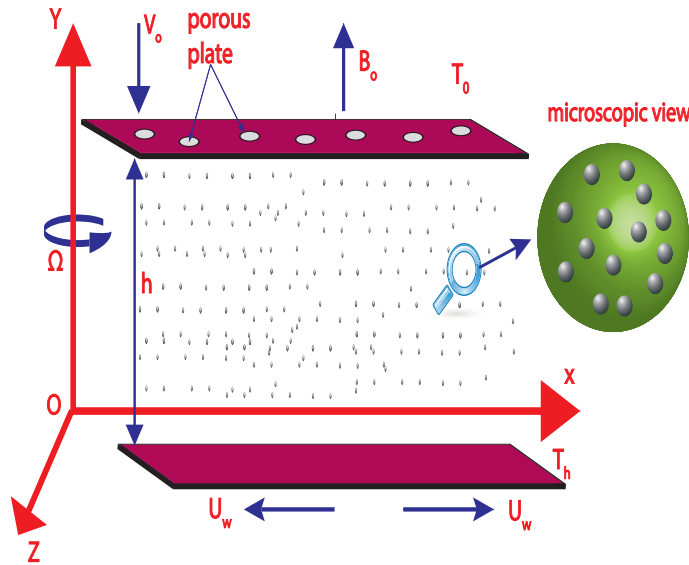


FIG. 6.1: Geometry of the problem.

and momentum equations are given as [128]

$$\nabla \cdot \mathbf{V} = 0, \quad (6.1)$$

$$\rho_{nf} \left(\frac{d\mathbf{V}}{dt} + 2\boldsymbol{\Omega} \times \mathbf{V} + \boldsymbol{\Omega} \times (\boldsymbol{\Omega} \times \mathbf{r}) \right) = \text{div} \mathbf{T} + \mathbf{J} \times \mathbf{B}. \quad (6.2)$$

Direction of Coriolis force $2\boldsymbol{\Omega} \times \mathbf{V}$ is perpendicular to both $\boldsymbol{\Omega}$ and \mathbf{V} . Centripetal force is given by $\boldsymbol{\Omega} \times (\boldsymbol{\Omega} \times \mathbf{r})$, that is perpendicular to $\boldsymbol{\Omega}$ and \mathbf{V} although acts towards the axis of rotation. Here, \mathbf{T} and ρ_{nf} denote the stress tensor and nanofluid density respectively. The governing PDEs in the component form are as follows.

$$\frac{\partial u}{\partial x} + \frac{\partial v}{\partial y} = 0, \quad (6.3)$$

$$\rho_{nf} \left(u \frac{\partial u}{\partial x} + v \frac{\partial u}{\partial y} + 2\Omega w \right) = -\frac{\partial p^*}{\partial x} + \mu_{nf} \left(\frac{\partial^2 u}{\partial x^2} + \frac{\partial^2 u}{\partial y^2} \right) - \sigma_{nf} B_0^2 u, \quad (6.4)$$

$$\rho_{nf} \left(u \frac{\partial v}{\partial x} + v \frac{\partial v}{\partial y} \right) = -\frac{\partial p^*}{\partial y} + \mu_{nf} \left(\frac{\partial^2 v}{\partial x^2} + \frac{\partial^2 v}{\partial y^2} \right), \quad (6.5)$$

$$\rho_{nf} \left(u \frac{\partial w}{\partial x} + v \frac{\partial w}{\partial y} - 2\Omega u \right) = \mu_{nf} \left(\frac{\partial^2 w}{\partial x^2} + \frac{\partial^2 w}{\partial y^2} \right) - \sigma_{nf} B_0^2 w, \quad (6.6)$$

where $p^* = p - \frac{\Omega^2 x^2}{2}$ is the modified pressure, B_0 the applied magnetic field and μ_{nf} the nanofluid effective dynamic viscosity. Mathematical expression for the heat transfer profile, may be expressed as

$$u \frac{\partial T}{\partial x} + v \frac{\partial T}{\partial y} = \alpha_{nf} \left(\frac{\partial^2 T}{\partial x^2} + \frac{\partial^2 T}{\partial y^2} \right), \quad (6.7)$$

where the effective thermal diffusivity $\alpha_{nf} = \frac{k_{nf}}{(\rho c_p)_{nf}}$ is the ratio of the effective thermal conductivity k_{nf} to the effective heat capacity $(\rho c_p)_{nf}$ of the nanofluid. Nanofluid effective density [129] is given by

$$\rho_{nf} = (1 - \phi)\rho_f + \phi\rho_s. \quad (6.8)$$

The effective heat capacity $(\rho c_p)_{nf}$ and the effective dynamic viscosity μ_{nf} of the nanofluid [130] are given as

$$(\rho c_p)_{nf} = (1 - \phi)(\rho c_p)_f + \phi(\rho c_p)_s, \quad \mu_{nf} = \frac{\mu_f}{(1 - \phi)^{2.5}}. \quad (6.9)$$

We consider the Yu and Choi model[130] for the effective thermal conductivity k_{nf} of the nanofluids.

$$\frac{k_{nf}}{k_f} = \frac{(k_s + 2k_f) + 2\phi(k_s - k_f)(1 + \beta)^3}{(k_s + 2k_f) - 2\phi(k_s - k_f)(1 + \beta)^3}, \quad (6.10)$$

in which β is define as the ratio of the nano-layer thickness over the particle radius.

Moreover, the electrical conductivity σ_{nf} of nanofluids [131] is as follows.

$$\frac{\sigma_{nf}}{\sigma_f} = 1 + \frac{3(\sigma_s - \sigma_f)\phi}{(\sigma_s + 2\sigma_f) - (\sigma_s - \sigma_f)\phi}. \quad (6.11)$$

Thermophysical properties of base fluid and different nanoparticles are shown in Table 6.1. In case of uniform injection/suction, the velocity component v at the upper surface is constant because of its porosity. the temperature gradient is produced across the fluid such that the upper surface has less temperature T_0 as compared with the lower surface temperature T_h , i.e. $T_0 < T_h$.

TABLE 6.1: Thermophysical attributes of water, silver and copper nanoparticles[132].

Physical properties	Water	Copper	Silver
ρ (kg/m^3)	997	8933	10,500
k (W/mK)	0.613	401	429
c_p (J/kgK)	4179	385	235
σ (Ωm) ⁻¹	0.05	5.96×10^7	6.30×10^7

The Boundary conditions at the lower and upper surfaces are as follows.

$$\left. \begin{aligned} u = U_w = ax, \quad v = 0, \quad w = 0, \quad T = T_h \quad \text{at} \quad y = 0, \\ u = 0, \quad v = -V_0, \quad w = 0, \quad T = T_0, \quad \text{at} \quad y = h, \end{aligned} \right\} \quad (6.12)$$

where V_0 is the velocity at the upper wall such that $V_0 > 0$ represents the uniform suction and $V_0 < 0$ the uniform injection. Consider the following similarity transformation and eliminate the pressure gradient .

$$\left. \begin{aligned} u = axf'(\eta), \quad v = -ahf(\eta), \quad w = axg(\eta), \\ \theta(\eta) = \frac{T - T_0}{T_h - T_0}, \quad \eta = \frac{y}{h}. \end{aligned} \right\} \quad (6.13)$$

The resulting non-dimensional system of ODEs is given by

$$f'''' - \delta_1 \epsilon_1 (f' f'' - f f''') - 2\lambda_2 \epsilon_1 g' - \left(\frac{\sigma_{nf}}{\sigma_f} \right) \delta_1 \delta_3 f''' = 0, \quad (6.14)$$

$$g'' - \delta_1 \epsilon_1 (g f' - f g') + 2\delta_2 \epsilon_1 f' - \left(\frac{\sigma_{nf}}{\sigma_f} \right) \delta_1 \delta_3 g = 0, \quad (6.15)$$

$$\theta'' + Pr \epsilon_2 \frac{\delta_1}{\epsilon_3} f \theta' = 0, \quad (6.16)$$

with the following dimensionless boundary conditions:

$$\left. \begin{aligned} f(0) = 0, \quad f'(0) = 1, \quad g(0) = 0, \quad \theta(0) = 1, \\ f(1) = S, \quad g(1) = 0, \quad f'(1) = 0, \quad \theta(1) = 0. \end{aligned} \right\} \quad (6.17)$$

Here, prime represents the derivative w.r.t η . The parameters involved in the non-dimensional equations are given[132] by

$$S = \frac{V_0}{ah} \quad (-3 \leq S \leq 5), \quad \delta_1 = \frac{ah^2}{\nu_f} \quad (0 \leq \delta_1 \leq 5), \quad (6.18)$$

$$\delta_2 = \frac{\Omega h^2}{\nu_f} \quad (0 \leq \delta_2 \leq 5), \quad \delta_3 = \frac{\sigma_f}{\rho_f a} B_0^2 (1 - \phi)^{2.5} \quad (0 \leq \delta_3 \leq 5), \quad (6.19)$$

$$Pr = \frac{\mu_f (c_p)_f}{k_f} \quad (Pr = 6.2), \quad \epsilon_1 = \left[(1 - \phi) + \phi \frac{\rho_s}{\rho_f} \right] (1 - \phi)^{2.5}, \quad (0 \leq \phi \leq 0.2) \quad (6.20)$$

$$\epsilon_2 = \left[(1 - \phi) + \phi \frac{(\rho c_p)_s}{(\rho c_p)_f} \right], \quad (6.21)$$

$$\epsilon_3 = \frac{(k_s + 2k_f) + 2\phi(k_s - k_f)(1 + \beta)^3}{(k_s + 2k_f) - 2\phi(k_s - k_f)(1 + \beta)^3}, \quad (6.22)$$

$$\epsilon_4 = \frac{\sigma_{nf}}{\sigma_f} = 1 + \frac{3(\sigma_s - \sigma_f)\phi}{(\sigma_s + 2\sigma_f) - (\sigma_s - \sigma_f)\phi}, \quad (6.23)$$

wherein the physical flow parameters are S (suction/injection parameter), δ_1 (Reynolds number), δ_2 (rotation parameter), δ_3 (magnetic parameter), Pr (Prandtl number), and ϕ (concentration of nanoparticles).

The important physical parameters, the drag coefficient C_f and the local heat transfer rate Nu_x , are represented as

$$C_f = \frac{2\tau_w}{\rho_{nf} U_w^2}, \quad Nu_x = \frac{xq_w}{k_{nf}(T_w - T_\infty)}, \quad (6.24)$$

where $\tau_w = \mu_{nf} \left(\frac{\partial u}{\partial y} \right)$ is the wall shear-stress at $y = 0$ and $q_w = -k_{nf} \left(\frac{\partial T}{\partial y} \right)$ is the heat flux at wall. Using the similarity transform presented above, Eq. (6.24) can be described as:

$$\left. \begin{aligned} C_f Re_x^{0.5} = \frac{(1 - \phi + \phi \frac{\rho_s}{\rho_f})}{(1 - \phi)^{2.5}} f''(0), \quad \frac{Nu_x}{Re_x^{0.5}} = -\theta'(0), \\ C_f Re_x^{0.5} = \frac{(1 - \phi + \phi \frac{\rho_s}{\rho_f})}{(1 - \phi)^{2.5}} f''(1), \quad \frac{Nu_x}{Re_x^{0.5}} = -\theta'(1), \end{aligned} \right\} \quad (6.25)$$

where $Re_x = \frac{U_x}{\nu_f}$ is the local Reynolds number.

6.3 Solution Methodology

The system of nonlinear ordinary differential Eqs. (6.14) - (6.16) alongside the end point conditions (6.17) has been attempted numerically through the shooting method[133] for different variety of values of the involved parameters. We have utilized the subsequent nomenclature for transforming the BVP to the IVP containing eight first-order system of ODEs.

$$\left. \begin{aligned} y_1 = f, y_2 = f', y_3 = f'', y_4 = f''', y_5 = g, \\ y_6 = g', y_7 = \theta, y_8 = \theta'. \end{aligned} \right\} \quad (6.26)$$

The coupled nonlinear flow and energy equations are turned into the subsequent system of eight first order ODEs together with the initial conditions.

$$\left. \begin{aligned} y_1' &= y_2 & y_1(0) &= 0, \\ y_2' &= y_3 & y_2(0) &= 1, \\ y_3' &= y_4 & y_3(0) &= k, \\ y_4' &= \delta_1 \epsilon_1 (y_2 y_3 - y_1 y_4) + 2\lambda_2 \epsilon_1 y_6 + \frac{\sigma_{nf}}{\sigma_f} \delta_1 \delta_3 y_4 & y_4(0) &= l, \\ y_5' &= y_6 & y_5(0) &= 0, \\ y_6' &= \delta_1 \epsilon_1 (y_2 y_5 - y_1 y_6) - 2\lambda_2 \epsilon_1 y_2 + \frac{\sigma_{nf}}{\sigma_f} \delta_1 \delta_3 y_5 & y_6(0) &= m, \\ y_7' &= y_8 & y_7(0) &= 1, \\ y_8' &= -Pr \epsilon_2 \frac{\delta_1}{\epsilon_3} y_1 y_8 & y_8(0) &= n. \end{aligned} \right\} \quad (6.27)$$

We employ the Runge-Kutta method of order four to solve the above IVP. To improve the values of k, l, m and n , we apply the Newton's method till the following criteria is met $\max\{|y_1(1) - S|, |y_2(1) - 0|, |y_5(1) - 0|, |y_7(1) - 0|\} < \varepsilon$, where $\varepsilon > 0$ is a small positive real number. All of the numerical results in this paper, are accomplished with $\varepsilon = 10^{-6}$. For code verification, the problem of non-stretching is taken into account first. Table 6.2 illustrates a comparison between our outcomes as well as those of Turkyilmazoglu[134] for varying values of Ω . An excellent agreement could be noticed. The accuracy of the present study can also be measured from comparison of the local Nusselt number and the local skin-friction with those reported by Hussain et al. [135]

provided in Table 6.3 for $S=-1, 0, 1$ and $\phi = 0$.

TABLE 6.2: Variation of $-g'(0)$ for different values of Ω at $Re = 1$ in case of $S_1 = S_2 = 0$.

	Ω	Turkyilmazoglu[134]	Present study
1	-1.0	2.00095215	2.01638636
2	-0.8	1.80258847	1.81545510
3	-0.3	1.30442355	1.31866340
4	0.0	1.00427756	1.02386401
5	0.50	0.50261351	0.53678812

TABLE 6.3: Values of skin friction coefficient and Nusselt number for the different values of rising parameters at lower/upper surface.

S	ϕ	$C_f Re_x^{1/2}$ at $\eta = 0$		$Re_x^{-1/2} Nu_x$ at $\eta = 0$		$C_f Re_x^{1/2}$ at $\eta = 1$		$Re_x^{-1/2} Nu_x$ at $\eta = 1$	
		Present study	Hussain et al. [135]	Present study	Hussain et al. [135]	Present study	Hussain et al. [135]	Present study	Hussain et al. [135]
-1	0	-9.54155	-9.54155	0.39001	0.39001	8.85752	8.85752	4.82296	4.82296
0	0	-4.09595	-4.09595	1.33610	1.33610	1.95289	1.95289	0.80249	0.80249
1	0	2.23565	2.23565	2.19498	2.19498	-3.81099	-3.81099	0.05776	0.05776

6.4 Results and Discussion

The numerical estimations of the local Nusselt number and local skin-friction for assorted values of the injection/suction parameter S , nanoparticle volume fraction ϕ , Reynolds number δ_1 , rotation parameter δ_2 and magnetic parameter δ_3 are presented in Tables 6.4 – 6.7. From Table 6.4, it is noted that an increase of ϕ tends to decrease the local skin friction at lower surface and the same trend is seen for the upper surface in case of Table 6.5. Table 6.6 illustrates that an increment in the ϕ tends to enhance the local Nusselt number for $S = -1$ and decrease the local Nusselt number for $S = 0, 1$ at the lower surface, while an opposite trend is observed for the upper surface in case of Table 6.7.

To examine the fluid flow and heat transport, outcomes are displayed in Figs. 6.2-6.16, portraying the variations in $f'(\eta)$, $g(\eta)$ and $\theta(\eta)$ inside the confined domain. Figs.

TABLE 6.4: Values of C_f for the different values of rising parameters at lower surface.

		$C_f Re_x^{1/2}$ at $\eta = 0$							
		$\delta_2 = 0, \delta_3 = 0$		$\delta_2 = 1, \delta_3 = 0$		$\delta_2 = 0, \delta_3 = 1$		$\delta_2 = 1, \delta_3 = 1$	
S	ϕ	$\delta_1 = 0.5$	$\delta_1 = 1$	$\delta_1 = 0.5$	$\delta_1 = 1$	$\delta_1 = 0.5$	$\delta_1 = 1$	$\delta_1 = 0.5$	$\delta_1 = 1$
-1	0.0	-9.74691	-9.49301	-9.80870	-9.56547	-9.85538	-9.71522	-9.88613	-9.75298
	0.05	-7.87632	-7.61975	-7.95513	-7.71618	-7.96546	-7.80349	-8.00860	-7.85851
	0.1	-6.98925	-6.73133	-7.07985	-6.84544	-7.06927	-6.89690	-7.12202	-6.96579
0	0.0	-4.04945	-4.09874	-4.05975	-4.10903	-4.10880	-4.21588	-4.14009	-4.24649
	0.05	-3.30091	-3.34892	-3.31357	-3.36160	-3.34915	-3.44399	-3.38022	-3.47432
	0.1	-2.94594	-2.99335	-2.96016	-3.00758	-2.98893	-3.07795	-3.02029	-3.10854
1	0.0	2.10515	2.20944	2.13204	2.23160	2.08947	2.17612	2.13125	2.21246
	0.05	1.73175	1.83608	1.76344	1.86104	1.71889	1.80828	1.76535	1.84748
	0.1	1.55467	1.65895	1.58925	1.68538	1.54315	1.63378	1.59231	1.67442

TABLE 6.5: Values of C_f for the different values of rising parameters at upper surface.

		$C_f Re_x^{1/2}$ at $\eta = 1$							
		$\delta_2 = 0, \delta_3 = 0$		$\delta_2 = 1, \delta_3 = 0$		$\delta_2 = 0, \delta_3 = 1$		$\delta_2 = 1, \delta_3 = 1$	
S	ϕ	$\delta_1 = 0.5$	$\delta_1 = 1$	$\delta_1 = 0.5$	$\delta_1 = 1$	$\delta_1 = 0.5$	$\delta_1 = 1$	$\delta_1 = 0.5$	$\delta_1 = 1$
-1	0.0	8.38930	8.81410	8.43421	8.86200	8.41680	8.86177	8.46777	8.91272
	0.05	6.89818	7.33552	6.95431	7.39634	6.92010	7.37142	6.98370	7.43568
	0.1	6.19185	6.63770	6.25550	6.70739	6.21113	6.66791	6.28318	6.74120
0	0.0	1.97478	1.95008	1.97424	1.94977	1.96053	1.92301	1.95983	1.92251
	0.05	1.60150	1.57724	1.60090	1.57700	1.59000	1.55557	1.58922	1.55511
	0.1	1.42449	1.40046	1.42388	1.40031	1.41430	1.38136	1.41348	1.38096
1	0.0	-3.88685	-3.78563	-3.92744	-3.82318	-3.94514	-3.89753	-3.99173	-3.93904
	0.05	-3.13976	-3.04126	-3.18886	-3.08580	-3.18699	-3.13105	-3.24337	-3.18040
	0.1	-2.78575	-2.68917	-2.84023	-2.73796	-2.82774	-2.76848	-2.89033	-2.82262

6.2-6.4 explain a comparison between the effects of copper and silver nanoparticles for a variety of values of ϕ , on $f'(\eta)$, $g(\eta)$ and $\theta(\eta)$. When the values of ϕ increase in Fig. 6.2, there is an extremely small variation in $f'(\eta)$, but it may be found within the inset of this figure that copper nanoparticles have comparatively low effect on the velocity profile when compared with the silver nanoparticles. Fig. 6.3 illustrates the variation in the dimensionless velocity $g(\eta)$ for various values of ϕ . It is noticed that the copper-water nanofluid has relatively low velocity distribution than silver-water nanofluid. Effect of various values of ϕ on the thermal distribution is presented in Fig. 6.4. It can be observed that with a boost in the ϕ , the thermal profile rises. It can also be detected that the copper nanoparticles have almost the same effect on the temperature profile as that of the silver nanoparticles.

TABLE 6.6: Values of Nu_x for the different values of rising parameters at lower surface.

		$Re_x^{-1/2} Nu_x$ at $\eta = 0$							
		$\delta_2 = 0, \delta_3 = 0$		$\delta_2 = 1, \delta_3 = 0$		$\delta_2 = 0, \delta_3 = 1$		$\delta_2 = 1, \delta_3 = 1$	
S	ϕ	$\delta_1 = 0.5$	$\delta_1 = 1$	$\delta_1 = 0.5$	$\delta_1 = 1$	$\delta_1 = 0.5$	$\delta_1 = 1$	$\delta_1 = 0.5$	$\delta_1 = 1$
-1	0.0	0.67940	0.39037	0.67899	0.38966	0.67819	0.38685	0.67781	0.38622
	0.05	0.76747	0.54608	0.76677	0.54439	0.76647	0.54242	0.76581	0.54096
	0.1	0.82791	0.66160	0.82724	0.65980	0.82712	0.65841	0.82649	0.65685
0	0.0	1.16173	1.33608	1.16149	1.33558	1.16049	1.33092	1.16026	1.33046
	0.05	1.11763	1.24141	1.11731	1.24074	1.11674	1.23777	1.11643	1.23715
	0.1	1.08731	1.17769	1.08703	1.17713	1.08666	1.17504	1.08639	1.17452
1	0.0	1.62883	2.19477	1.62876	2.19463	1.62782	2.19130	1.62775	2.19116
	0.05	1.46776	1.91482	1.46758	1.91438	1.46699	1.91196	1.46682	1.91156
	0.1	1.35106	1.69860	1.35087	1.69812	1.35048	1.69633	1.35030	1.69589

TABLE 6.7: Values of Nu_x for the different values of rising parameters at upper surface.

		$Re_x^{-1/2} Nu_x$ at $\eta = 1$							
		$\delta_2 = 0, \delta_3 = 0$		$\delta_2 = 1, \delta_3 = 0$		$\delta_2 = 0, \delta_3 = 1$		$\delta_2 = 1, \delta_3 = 1$	
S	ϕ	$\delta_1 = 0.5$	$\delta_1 = 1$	$\delta_1 = 0.5$	$\delta_1 = 1$	$\delta_1 = 0.5$	$\delta_1 = 1$	$\delta_1 = 0.5$	$\delta_1 = 1$
-1	0.0	2.43038	4.82219	2.43070	4.82380	2.43193	4.83048	2.83646	5.41024
	0.05	1.95588	3.41809	1.95632	3.42072	1.95699	3.42487	2.20927	3.78109
	0.1	1.66702	2.60322	1.66740	2.60549	1.66780	2.60803	1.83377	2.83182
0	0.0	0.89872	0.80217	0.89898	0.80284	0.89964	0.80560	0.88051	0.78792
	0.05	0.92519	0.85343	0.92550	0.85415	0.92587	0.85600	0.91183	0.84300
	0.1	0.94385	0.88970	0.94411	0.89029	0.94436	0.89165	0.93383	0.88185
1	0.0	0.26551	0.05769	0.26568	0.05780	0.26592	0.05810	0.19871	0.04228
	0.05	0.38434	0.12991	0.38465	0.13020	0.38476	0.13055	0.31289	0.10419
	0.1	0.49491	0.22600	0.49524	0.22640	0.49529	0.22679	0.42635	0.19279

Figs. 6.5-6.7 demonstrate the influence of S (injection/suction parameter) on the velocities and temperature. Figs 6.5 and 6.6 reveal the velocity distribution. For injection/suction case, the velocity profile $f'(\eta)$ and $g(\eta)$ get bigger. Additionally, it may be seen that a deviation in the velocities is more prominent at the mean place of the channel as compared to the proximity of the top and bottom walls of the channel. Additionally, the extreme value of the velocity moves a little towards the lower surface for positive S although for negative S it moves towards the upper surface. For different values of the injection/suction parameter S , Fig. 6.7 represents the temperature

distribution profile. It could be figured out that escalating injection/suction parameter S , resists the thermal distribution and so it provides a drop in the thermal field.

Fig. 6.8 shows two distinct behaviors of the velocity profile for the parameter δ_1 and it is observed that velocity profile swaps its behavior at the mean position from increasing to decreasing for different values of δ_1 . This result is generally a consequence of the stretching of the bottom wall. The velocity distribution $g(\eta)$ in Fig. 6.9 demonstrates a uniform diminishing behavior for higher values of δ_1 . When the lower plate is stationary, velocity shows symmetrical behavior at central position. However the maximum value of velocity profile moves towards the lower plate, as the value of δ_1 increases. The temperature profile $\theta(\eta)$ shows a diminishing behavior with an increase in the values of δ_1 (see Fig. 6.10). In case of the lower plate at rest (i.e. $\delta_1 = 0$), the temperature profile exhibits a linear lessening behavior. Whereas nonlinear decreasing behavior is shown for the rest of the values of δ_1 .

For different values of δ_2 , Figs. 6.11-6.13 reflect the dynamics of the velocities $f'(\eta)$, $g(\eta)$ and temperature field $\theta(\eta)$. In Fig. 6.11, it is determined that $f'(\eta)$ inside the confined domain shows a dual nature behavior. It is detected that the flow profile $f'(\eta)$ shows a reducing behavior inside the domain $0 \leq \eta \leq 0.5$, although these outcomes are entirely different inside the region $0.5 \leq \eta \leq 1$. At the upper half of the channel more dominant variation for velocity field provided by the rotating parameter δ_2 . In Fig. 6.12, it is noticed that no variation in vertical velocity component when $\delta_2 = 0$, so the problem is reduced to the steady 2D flow in the absence of the rotation parameter. Nevertheless, it is evident that an increase in the values of δ_2 decreases the velocity distribution $g(\eta)$. Additionally, a disturbance in the velocity is greater at the central position, as compared to that near the upper and the lower surfaces. Fig. 6.13 indicates that the temperature $\theta(\eta)$ increases slightly as the rotation parameter δ_2 rises.

Figs. 6.14-6.16 are shown for $f'(\eta)$, $g(\eta)$ and $\theta(\eta)$ for variety of values of the magnetic parameter δ_3 . Fig. 6.14 exhibits dual nature behavior for $f'(\eta)$ inside the confined domain. It can be seen that $f'(\eta)$ shows a reducing behavior for increasing values of the magnetic parameter δ_3 inside the domain $0 \leq \eta < 0.4$, whereas an opposite

behavior can be seen in the domain $0.4 \leq \eta \leq 1$. In Fig. 6.15, it is found that the velocity field $g(\eta)$ has the escalating behavior for the increasing values of δ_3 . Moreover it can be noted that variation in the velocity is greater at the central position, as compared to that near the upper and lower surfaces. Fig. 6.16 suggests a slight growing tendency in the temperature profile $\theta(\eta)$ w.r.t the magnetic parameter δ_3 . Streamlines variations are plotted in Figs. 6.17-6.19 for different values of injection/suction parameter S . It is noticed from the Figs. 6.17-6.19 that the gaps between stream lines decrease with rising the magnitude of S . Injection/Suction parameter S thus significantly alters the fluid dynamics of the stretching sheet region.

The drag coefficient of the nanofluid is examined at the lower plate of the channel and results are plotted for various parameters for both copper and silver. In Fig. 6.20, for the injection/suction parameter S and particles volume fraction ϕ , the drag coefficient is plotted. It is revealed that the drag coefficient absolute values increases as ϕ increase for $S=0,-1$, but it decreases for $S=1$. Also copper nanoparticles are found to greater drag coefficient when compared with the silver nanoparticles. Figs. 6.21-6.23 depict the drag coefficient w.r.t. the nanoparticles volume fraction ϕ . The results indicate that it increases with an increment in δ_1 and δ_2 however it diminishes with an increment of the magnetic parameter δ_3 . Figs. 6.24-6.27 show the variation of the drag coefficient caused by the forced convection at the lower wall and the rotation at the upper wall. Largely, friction coefficient exhibits rise w.r.t ϕ regardless of the other relevant parameters. It is found that drag coefficient at the upper wall decreases with the increase of δ_1 , δ_2 and δ_3 .

Figs. 6.28-6.31 reflect the impact of various physical parameters on the heat transfer coefficient. In Fig. 9(a), it is observed that for $S=0$ and $S=1$, there is a decreasing behavior in the transfer of heat w.r.t ϕ . But the effect of $S=-1$ is opposite in nature w.r.t ϕ . The effect of δ_1 , δ_2 and δ_3 along with ϕ on the Nusselt number is plotted in Figs. 6.29-6.31. It is seen that there is a rise in Nu_x with the growth in the ϕ . Moreover it is determined that the silver nanoparticles have high rate of heat flow as compared with the copper nanoparticles. Figs. 6.32-6.35 exhibit the dynamics of Nu_x at the top surface for various vales of the ϕ . Figs. 6.33-6.35 display the decrease in the Nu_x with the increase in volume fraction of nanoparticles ϕ .

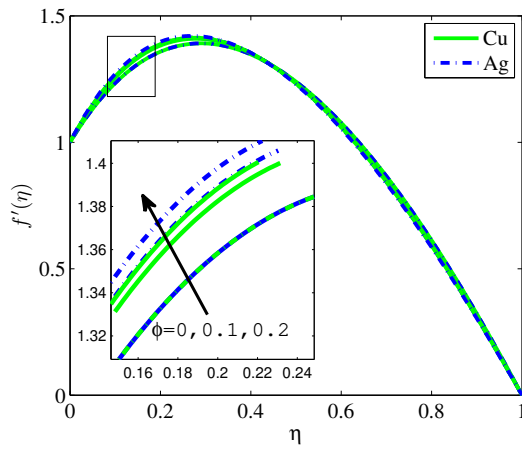


FIG. 6.2: Impact of ϕ on $f'(\eta)$ when $\delta_1 = \delta_2 = \delta_3 = 2, S = 1$.

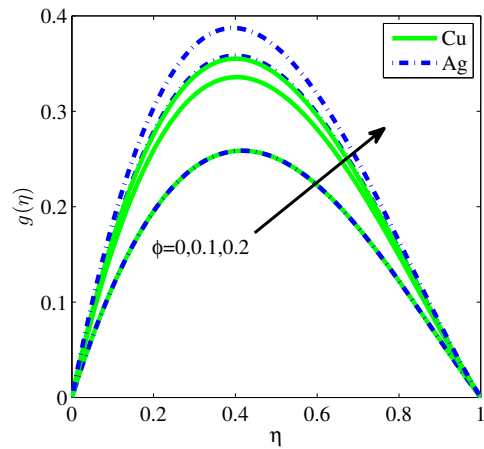


FIG. 6.3: Impact of ϕ on $g(\eta)$ when $\delta_1 = \delta_2 = \delta_3 = 2, S = 1$.

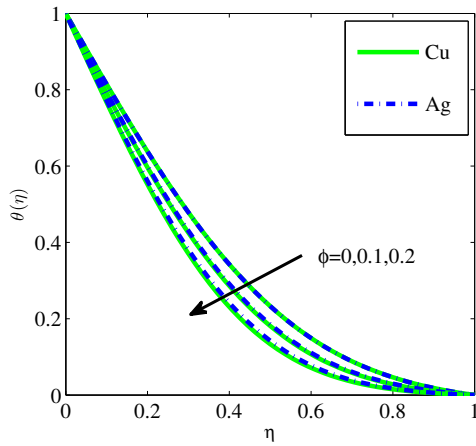


FIG. 6.4: Impact of ϕ on $\theta(\eta)$ when $\delta_1 = \delta_2 = \delta_3 = 2, S = 1$.

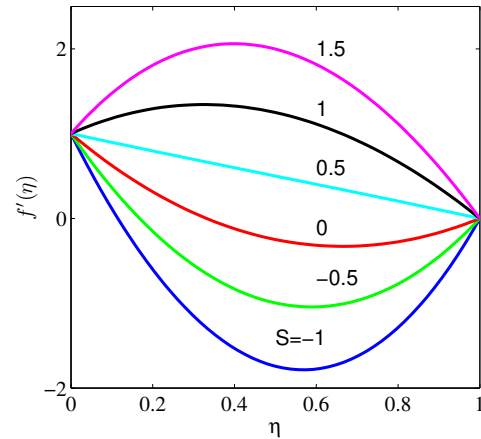


FIG. 6.5: Impact of S on $f'(\eta)$ for copper-water nanofluid when $\delta_1 = \delta_2 = \delta_3 = 2, \phi = 0.2$.

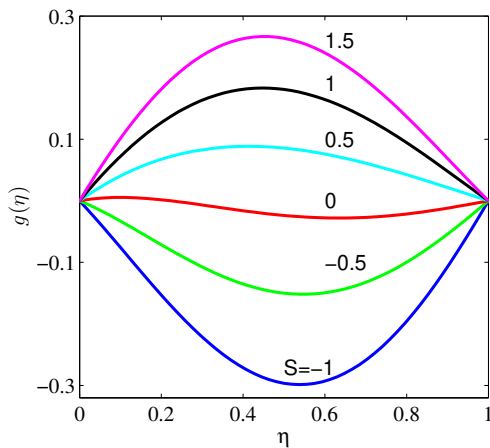


FIG. 6.6: Impact of S on $g(\eta)$ for copper-water nanofluid when $\delta_1 = \delta_2 = \delta_3 = 2, \phi = 0.2$.

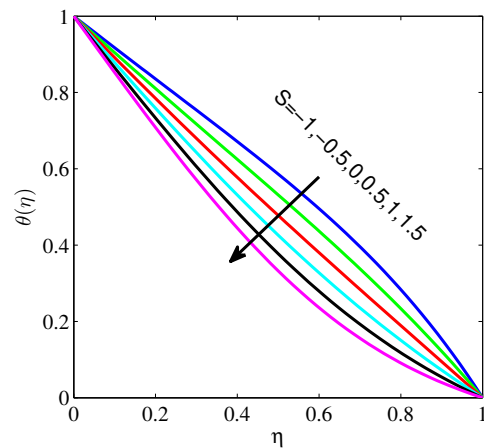


FIG. 6.7: Impact of S on $\theta(\eta)$ for copper-water nanofluid when $\delta_1 = \delta_2 = \delta_3 = 2, \phi = 0.2$.

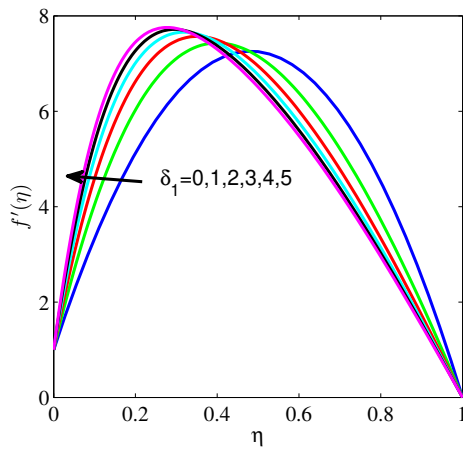


FIG. 6.8: Impact of δ_1 on $f'(\eta)$ for copper-water nanofluid when $\delta_2 = 0.2, \delta_3 = 0, \phi = 0.2, S = 5$.

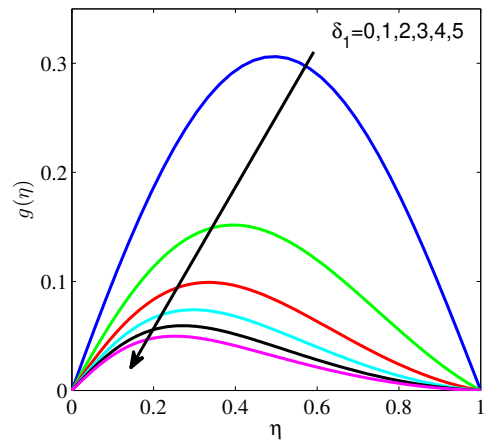


FIG. 6.9: Impact of δ_1 on $g(\eta)$ for copper-water nanofluid when $\delta_2 = 0.2, \delta_3 = 0, \phi = 0.2, S = 5$.

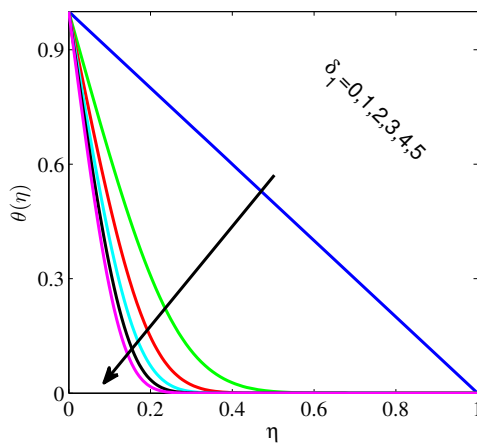


FIG. 6.10: Impact of δ_1 on $\theta(\eta)$ for copper-water nanofluid when $\delta_2 = 0.2, \delta_3 = 0, \phi = 0.2, S = 5$.

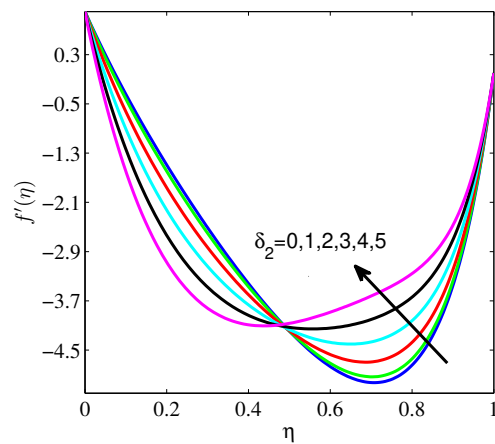


FIG. 6.11: Impact of δ_2 on $f'(\eta)$ for copper-water nanofluid when $\delta_1 = 0.2, \delta_3 = 0, \phi = 0.2, S = -3$.

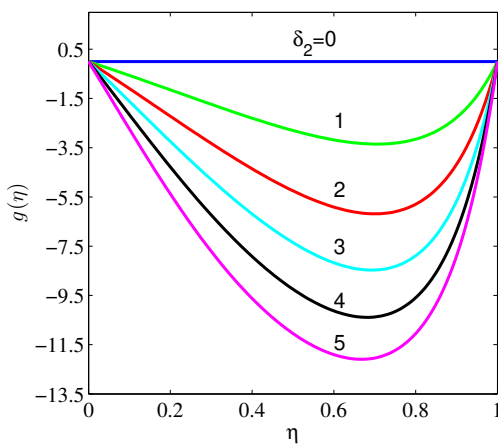


FIG. 6.12: Impact of δ_2 on $g(\eta)$ for copper-water nanofluid when $\delta_1 = 0.2, \delta_3 = 0, \phi = 0.2, S = -3$.

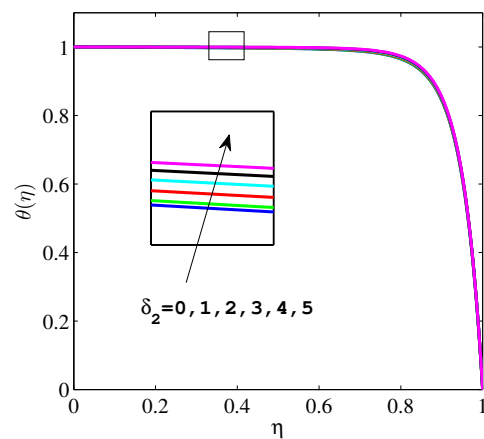


FIG. 6.13: Impact of δ_2 on $\theta(\eta)$ for copper-water nanofluid when $\delta_1 = 0.2, \delta_3 = 0, \phi = 0.2, S = -3$.

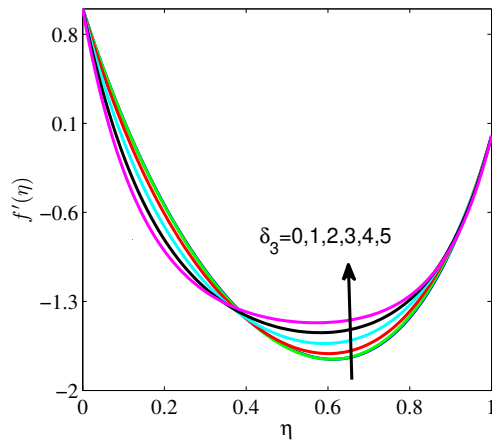


FIG. 6.14: Impact of δ_3 on $f'(\eta)$ for copper-water nanofluid when $\delta_1 = 2, \delta_2 = 2, \phi = 0.2, S = -1$.

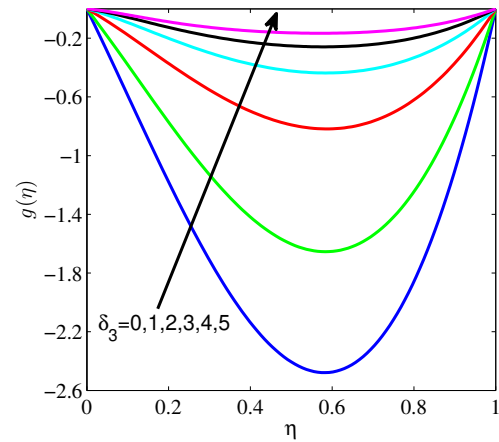


FIG. 6.15: Impact of δ_3 on $g(\eta)$ for copper-water nanofluid when $\delta_1 = 2, \delta_2 = 2, \phi = 0.2, S = -1$.

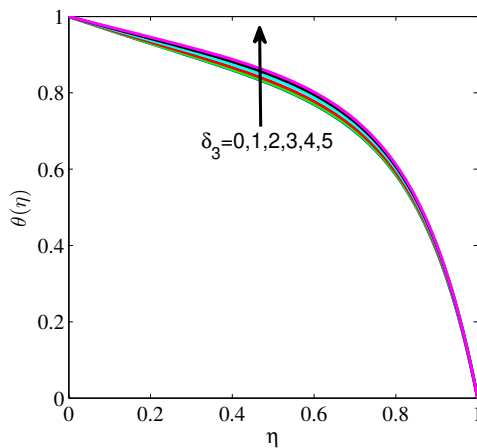


FIG. 6.16: Impact of δ_3 on $\theta(\eta)$ for copper-water nanofluid when $\delta_1 = 2, \delta_2 = 2, \phi = 0.2, S = -1$.

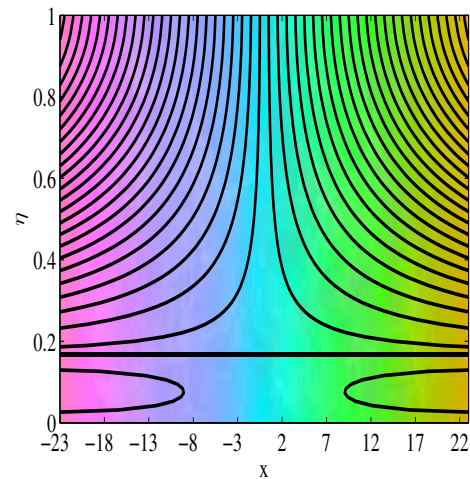


FIG. 6.17: Streamlines plot when $S = -1$.

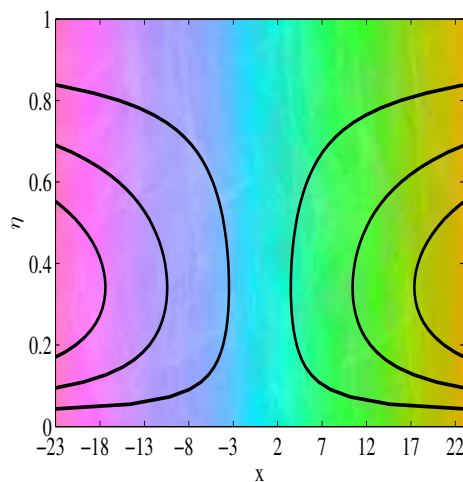


FIG. 6.18: Streamlines plot when $S = 0$.

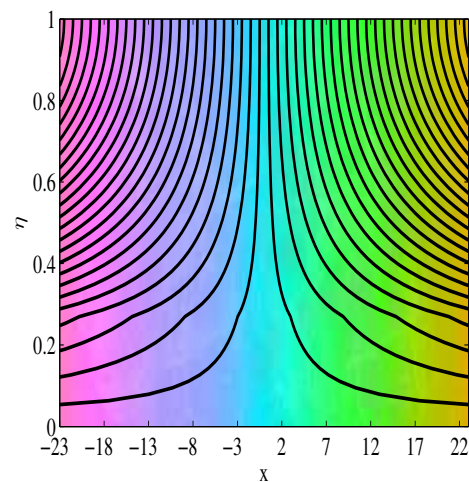


FIG. 6.19: Streamlines plot when $S = 1$.

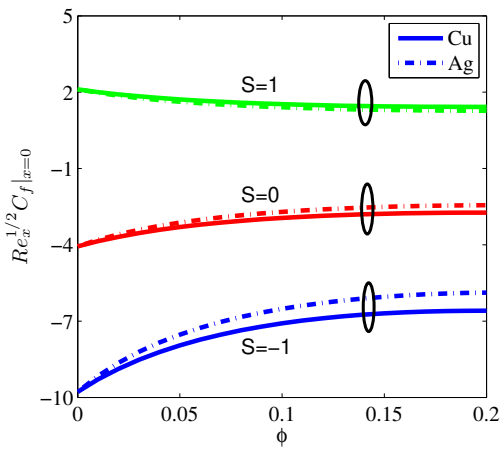


FIG. 6.20: Effects of ϕ and S on C_f at $\eta = 0$ when $\delta_1 = \delta_2 = \delta_3 = 0.5$.

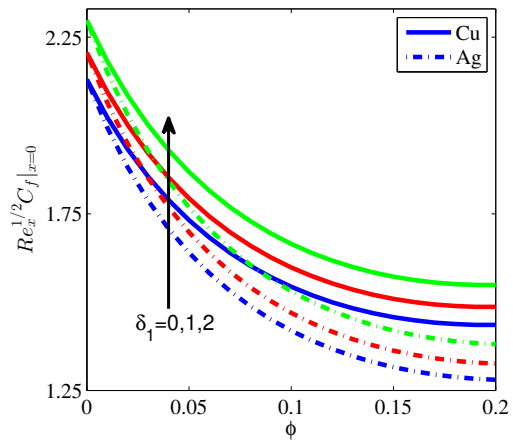


FIG. 6.21: Effects of ϕ and δ_1 on C_f at $\eta = 0$ when $\delta_2 = \delta_3 = 1.5, S = 1$.

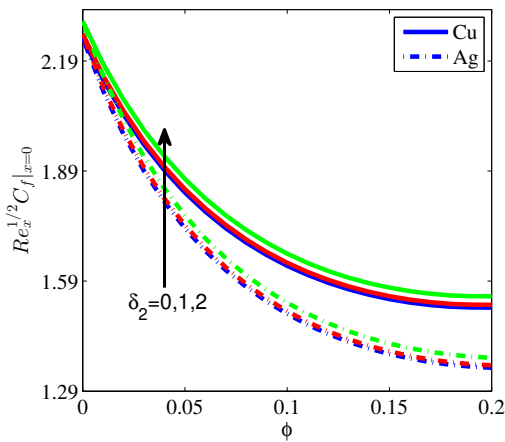


FIG. 6.22: Effects of ϕ and δ_2 on C_f at $\eta = 0$ when $\delta_1 = 2, \delta_3 = 1.5, S = 1$.

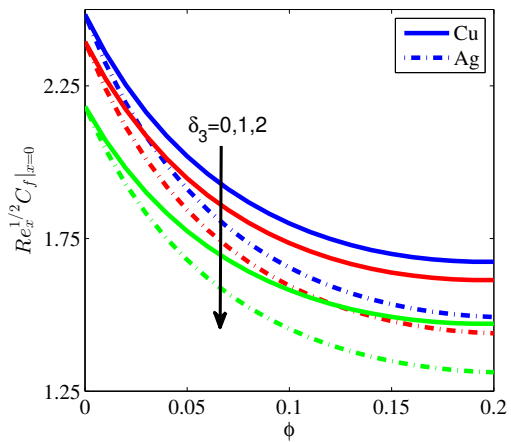


FIG. 6.23: Effects of ϕ and δ_3 on C_f at $\eta = 0$ when $\delta_1 = 2, \delta_2 = 1, S = 1$.

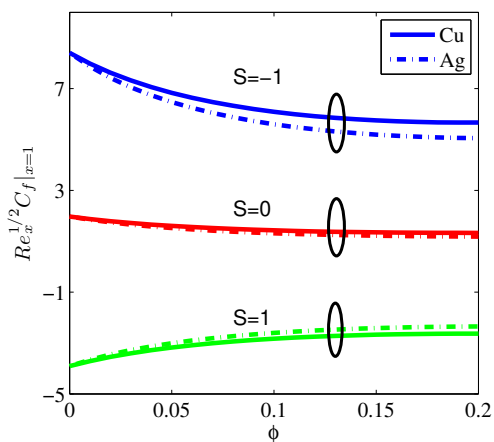


FIG. 6.24: Effects of ϕ and S on C_f at $\eta = 1$ when $\delta_1 = \delta_2 = \delta_3 = 0.5$.

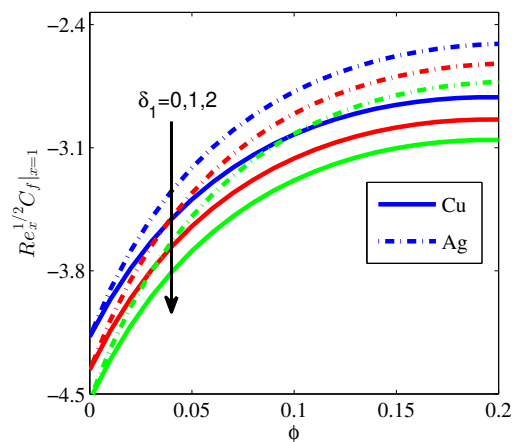


FIG. 6.25: Effects of ϕ and δ_1 on C_f at $\eta = 1$ when $\delta_2 = \delta_3 = 1.5, S = 1$.

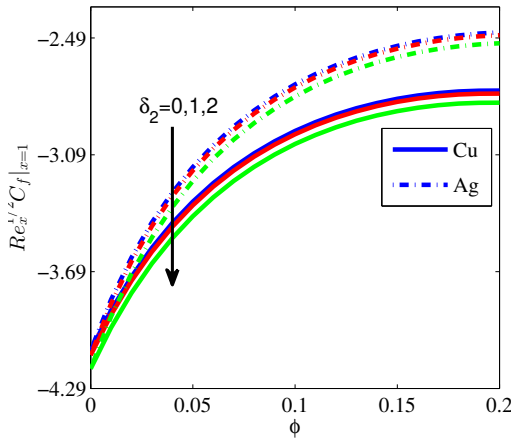


FIG. 6.26: Effects of ϕ and δ_2 on C_f at $\eta = 1$ when $\delta_1 = 2, \delta_3 = 1.5, S = 1$.

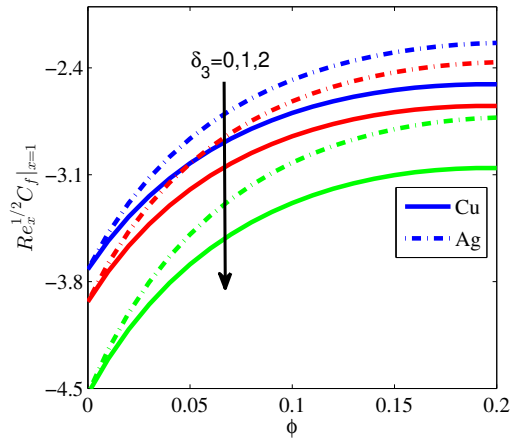


FIG. 6.27: Effects of ϕ and δ_2 on C_f at $\eta = 1$ when $\delta_1 = 2, \delta_3 = 1, S = 1$.

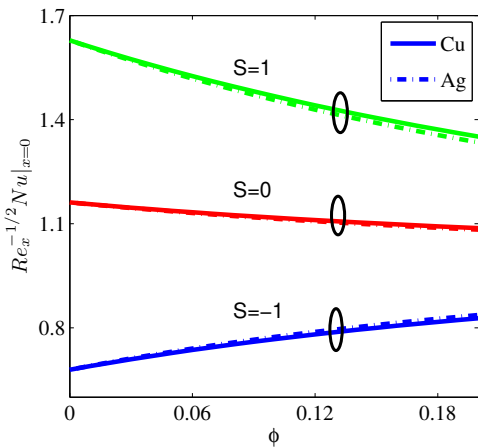


FIG. 6.28: Effects of ϕ and S on Nu_x at $\eta = 0$ when $\delta_1 = \delta_2 = \delta_3 = 0.5$.

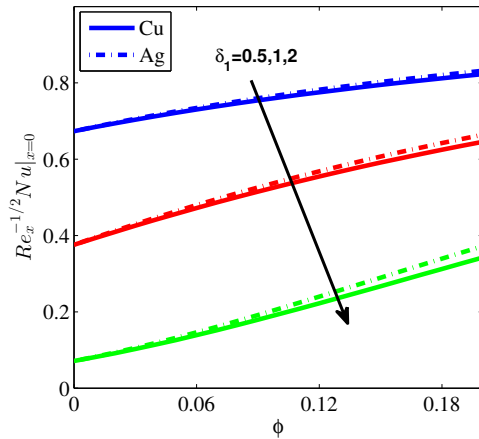


FIG. 6.29: Effects of ϕ and δ_1 on Nu_x at $\eta = 0$ when $\delta_2 = \delta_3 = 2, S = -1$.

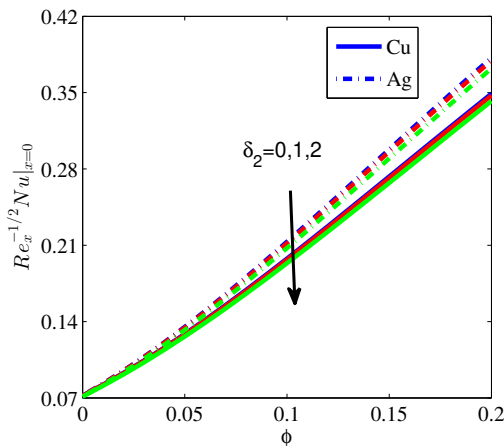


FIG. 6.30: Effects of ϕ and δ_2 on Nu_x at $\eta = 0$ when $\delta_1 = \delta_3 = 2, S = -1$.

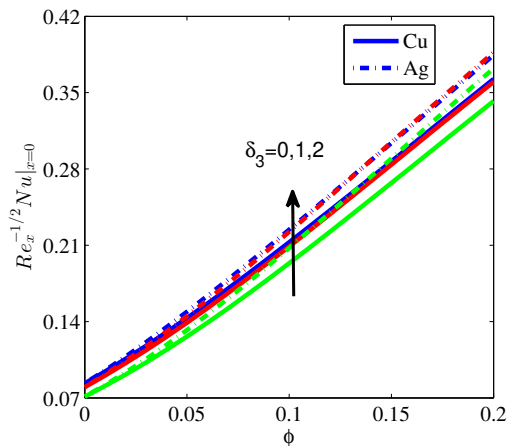


FIG. 6.31: Effects of ϕ and δ_3 on Nu_x at $\eta = 0$ when $\delta_1 = \delta_2 = 2, S = -1$.

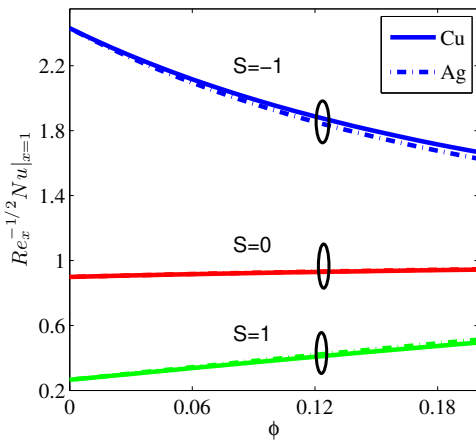


FIG. 6.32: Effects of ϕ and S on Nu_x at $\eta = 1$ when $\delta_1 = \delta_2 = \delta_3 = 0.5$.

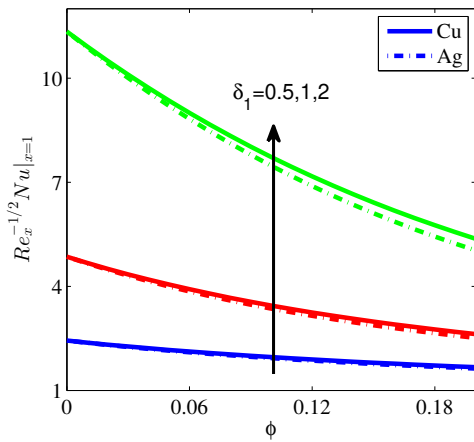


FIG. 6.33: Effects of ϕ and δ_1 on Nu_x at $\eta = 1$ when $\delta_2 = \delta_3 = 2, S = -1$.

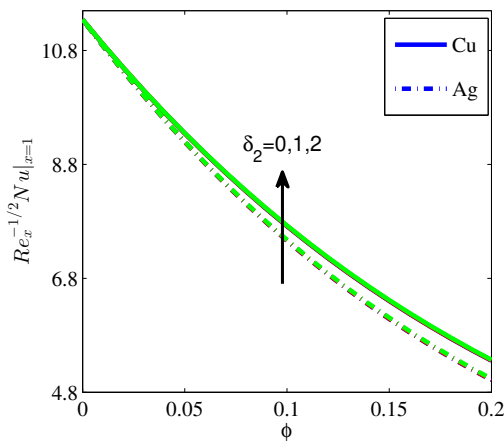


FIG. 6.34: Effects of ϕ and δ_2 on Nu_x at $\eta = 1$ when $\delta_1 = \delta_3 = 2, S = -1$.

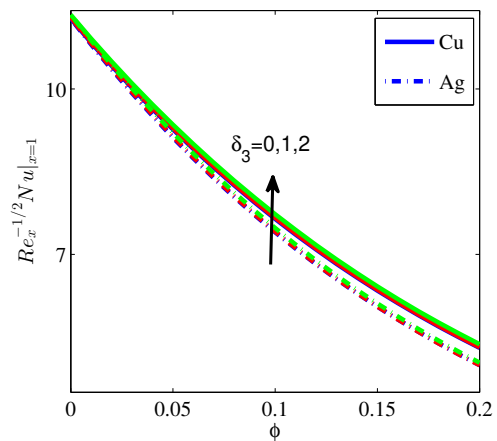


FIG. 6.35: Effects of ϕ and δ_3 on Nu_x at $\eta = 1$ when $\delta_1 = \delta_2 = 2, S = -1$.

6.5 Conclusions

Rotating flow and heat transfer of copper-water and silver-water nanofluid flow over a stretching sheet is examined using their thermophysical properties. With the help of graphs, effects of copper and silver nanoparticles on the skin friction and the Nusselt number are discussed. The main findings of this investigation are as follows:

-
- The volume fraction of nanoparticles increases the velocities and temperature of the nanofluid for both copper and silver nanoparticles.
 - The flow field is strongly influenced by the injection/suction parameter. In most of the cases, the position of the extreme value of the velocity is effected by these parameters.
 - A rise in the magnetic and rotational parameter leads to an increase in the temperature and f' velocity profiles.
 - The skin friction coefficient is higher for the copper-water nanofluid as compared to the silver-water nanofluid against the nanoparticles volume fraction at the lower surface while opposite trend is observed for the upper surface.
 - The rate of heat transfer increases for the silver-water nanofluid as compared to that for the copper-water nanofluid against the nanoparticles volume fraction at the lower surface while opposite trend is observed for the upper surface.
 - The magnetic parameter decreases the skin friction coefficient whereas it increases the Nusselt number.

Chapter 7

Conclusion

7.1 Conclusion

Within this dissertation, a study of the boundary layer flows for viscous, Jeffrey and tangent hyperbolic fluids over various kinds of geometries is introduced. Scale analysis is employed to obtain the mathematically modeled equations centered on the laws of conservations. By imparting appropriate similarity transformation, mathematically modeled set of the boundary layer equations together with the boundary conditions are turned into a group of ordinary differential equations. Out of the four problems discussed in this thesis, three are solved by Keller-box method whereas the fourth one by the shooting method. The effect of different physical parameters on the relevant variable, is displayed in tabular as well as graphical form. The outcomes so attained are compared with those of the already published articles for limiting cases. In Chapter 3, the heat transfer flow of MHD Jeffrey nanofluid flow due to a stretching surface is studied under the effects of Joule heating and viscous dissipation. In Chapter 4, MHD tangent hyperbolic nanofluid flow due to a stretching sheet is analyzed. In Chapter 5 stratified MHD Jeffrey nanofluid flow with gyrotactic microorganisms past a stretching surface is investigated. Chapter 6 focuses on the heat transfer MHD flow of a rotating nanofluid induced by a stretching sheet. The following significant outcomes are noticed out of this dissertation:

- For the Jeffrey and tangent hyperbolic nanofluids, the velocity field is diminished for the escalating values of the magnetic parameter while opposite behavior is noted for the Newtonian nanofluid.
- The velocity of the silver-ethylene glycol Jeffrey nanofluid is less than that of the base fluid although there is an opposite finding regarding the temperature.
- An enhancement in the Deborah number causes an augmentation in the velocity though the Weissenberg number and magnetic parameter cause it to reduce.
- The flow field is strongly influenced by the injection/suction parameter. In most of the cases, the position of the extreme value of the velocity is effected by these parameters.
- The temperature field is an increasing function of the concentration of nanoparticles, Brownian motion parameter, magnetic parameter, thermophoresis parameter and Eckert number.
- The temperature profile of $Ag - H_2O$ Jeffrey nanofluid is higher than those of $Al_2O_3 - C_2H_6O_2$ and $TiO_2 - C_2H_6O_2$ nanofluids and a contrary behavior is noted in the velocity profile.
- The concentration is decreasing function of Brownian motion parameter while it behaves the other way round for the thermophoresis parameter.
- The drag coefficient and the heat transfer rate are increased with a boost in the Deborah number however the drag coefficient diminishes by enhancing the solid volume fraction as well as the magnetic parameter.
- The motile density number of micro-organisms is enhanced with a rise in the bioconvection Lewis number, however it is reduced by enhancing the Peclet number.
- The thermal, mass and motile density stratification parameters decrease the temperature, volume fraction of nanoparticles and motile density of the micro-organisms profiles.
- The concentration distribution shows an opposite trend with chemical reaction parameter for both destructive reaction ($\gamma > 0$) and constructive reaction ($\gamma < 0$) case.

7.2 Future Recommendations

The research study performed in the present dissertation has covered some problems related to the heat and mass transport of steady flow for viscous, Jeffrey and tangent hyperbolic fluids with nanoparticles past a stretching surface. However a number of problems related to these scenarios are still open for additional inspection. Some of these cases are listed below.

- This study can be extended to nanofluids for turbulent flow regimes.
- The impacts of Joule heating and viscous dissipation with nanoparticles involving the two rotating disks and over a wedge are remained lacking in the literature. Therefore the problem discussed in third chapter could be extended for the wedge as well as rotating disks with various other well-known effects like non-linear thermal radiation, Hall and ion-slip.
- Chapter 6 could also be extended to non-Newtonian nanofluid models for instance Carreau-Yasuda naofluid, Oldroyd-B nanofluid, second grade nanofluid etc.
- These models could be solved for the non-linear stretching sheets, shrinking sheets, vertical sheets, stretching cylinders and exponential stretching sheets.

Bibliography

- [1] K. V. Wong and O. D. Leon. Applications of nanofluids: current and future. *Advances in Mechanical Engineering*, 2:1–11, 2010.
- [2] M. Kostic. Critical issues in nanofluids research and application potentials. In *Nanofluids: Research, Development and Applications*. Nova Science Publishers, Inc., 2013.
- [3] J. C. Maxwell. *A Treatise on Electricity and Magnetism*. Clarendon Press Oxford UK, 1873.
- [4] J. A. Eastman, S. U. S. Choi, S. Li, W. Yu, and L. J. Thompson. Anomalously increased effective thermal conductivities of ethylene glycol based nanofluids containing copper nanoparticles. *Applied Physics*, 78:718–720, 2001.
- [5] J. A. Eastman, S. U. S. Choi, S. Li, L. J. Thompson, and S. Lee. Enhanced thermal conductivity through the development of nanofluids. *MRS Online Proceedings Library Archive*, 457, 1996.
- [6] S. U. S. Choi. Enhancing thermal conductivity of fluids with nanoparticles. *ASME Fluid Engineering*, 231:99–105, 1995.
- [7] J. Buongiorno. Convective transport in nanofluids. *Journal of Heat Transfer*, 128:240–250, 2006.
- [8] R. K. Tiwari and M. K . Das. Heat transfer augmentation in a two-sided lid-driven differentially heated square cavity utilizing nanofluids. *International Journal of Heat and Mass Transfer*, 50(9-10):2002–2018, 2007.

- [9] S. Lee, S. U. S. Choi, S. Li, and J. A. Eastman. Measuring thermal conductivity of fluids containing oxide nanoparticles. *Journal of Heat Transfer*, 121:280–289, 1999.
- [10] S. K. Das, N. Putra, P. Thiesen, and W. Roetzel. Temperature dependence of thermal conductivity enhancement for nanofluids. *Journal of Heat Transfer*, 125:567–574, 2003.
- [11] M. M. Rashidi, N. V. Ganesh, A. K. Hakeemi, and B. Ganga. Buoyancy effect on MHD flow of nanofluid over a stretching sheet in the presence of thermal radiation. *Journal of Molecular Liquids*, 198:234–238, 2014.
- [12] S. M. S. Murshed, K. C. Leong, and C. Yang. Investigations of thermal conductivity and viscosity of nanofluids. *International Journal of Thermal Sciences*, 47:560–568, 2008.
- [13] M. Turkyilmazoglu. Unsteady convection flow of some nanofluids past a moving vertical flat plate with heat transfer. *Journal of Heat Transfer*, 136:1–7, 2014.
- [14] S. Dinarvand, R. Hosseini, and I. Pop. Unsteady convective heat and mass transfer of a nanofluid in Howarth’s stagnation point by Buongiorno’s model. *International Journal of Numerical Methods for Heat and Fluid Flow*, 25:1176–1197, 2015.
- [15] S. Das and R. N. Jana. Natural convective magneto-nanofluid flow and radiative heat transfer past a moving vertical plate. *Alexandria Engineering Journal*, 54:55–64, 2015.
- [16] L. Nakharintr and P. Naphon. Magnetic field effect on the enhancement of nanofluids heat transfer of a confined jet impingement in mini-channel heat sink. *International Journal of Heat and Mass Transfer*, 110:753–759, 2017.
- [17] M. Lomascolo, G. Colangelo, M. Milanese, and A. Risi. Review of heat transfer in nanofluids: Conductive, convective and radiative experimental results. *Renewable and Sustainable Energy Reviews*, 43:1182–1198, 2015.
- [18] R. L. Panton. *Incompressible Flow*. John Wiley & Sons, 2013.
- [19] N. P. Thien and N. M. Duy. *Understanding Viscoelasticity: An Introduction to Rheology*. Springer, 2017.

- [20] M. A. Abbas, Y. Q. Bai, M. M. Bhatti, and M. M. Rashidi. Three dimensional peristaltic flow of hyperbolic tangent fluid in non-uniform channel having flexible walls. *Alexandria Engineering Journal*, 55(1):653 – 662, 2016.
- [21] W. Ibrahim. Magnetohydrodynamics (MHD) flow of a tangent hyperbolic fluid with nanoparticles past a stretching sheet with second order slip and convective boundary condition. *Results in Physics*, 7:3723–3731, 2017.
- [22] M. Kothandapani and J. Prakash. Influence of heat source, thermal radiation, and inclined magnetic field on peristaltic flow of a hyperbolic tangent nanofluid in a tapered asymmetric channel. *IEEE Transactions on NanoBioscience*, 14(4):385–392, 2015.
- [23] A. Shafiq, Z. Hammouch, and N. Sindhu. Bioconvective MHD flow of tangent hyperbolic nanofluid with Newtonian heating. *International Journal of Mechanical Sciences*, 133:759–766, 2017.
- [24] B. Mahanthesh, S. Kumar, J. Gireesha, S. Manjunatha, and R. Gorla. Nonlinear convective and radiated flow of tangent hyperbolic liquid due to stretched surface with convective condition. *Results in Physics*, 7:2404–2410, 2017.
- [25] S. A. Gaffar, V. R. Prasad, and O. A. Beg. Numerical study of flow and heat transfer of non-Newtonian tangent hyperbolic fluid from a sphere with Biot number effects. *Alexandria Engineering Journal*, 54(4):829 – 841, 2015.
- [26] K. G. Kumar, B. J. Gireesha, M. R. Krishnamurthy, and N. G. Rudraswamy. An unsteady squeezed flow of a tangent hyperbolic fluid over a sensor surface in the presence of variable thermal conductivity. *Results in Physics*, 7:3031 – 3036, 2017.
- [27] V. Nagendramma, A. Leelarathnam, K. Raju, A. Shehzad, and T. Hussain. Doubly stratified MHD tangent hyperbolic nanofluid flow due to permeable stretched cylinder. *Results in Physics*, 9:23–32, 2018.
- [28] L. Nagaraja, M. S. Reddy, and M. S. Reddy. Magnetic field effect on tangent hyperbolic fluid towards porous plate with suction/injection. *Research Journal of Science and Technology*, 9(4):592–596, 2017.

- [29] U. Zakir and Z. Gul. Lie group analysis of magnetohydrodynamic tangent hyperbolic fluid flow towards a stretching sheet with slip conditions. *Heliyon*, 3(11):e00443, 2017.
- [30] N. Sandeep and C. Sulochana. Momentum and heat transfer behaviour of Jeffrey, Maxwell and Oldroyd-B nanofluids past a stretching surface with non-uniform heat source/sink. *Ain Shams Engineering Journal*, 2016.
- [31] H. I. Andersson, K. H. Bech, and B. S. Dandapat. Magnetohydrodynamic flow of a power-law fluid over a stretching sheet. *International Journal of Non-Linear Mechanics*, 27(6):929–936, 1992.
- [32] K. Ahmad, Z. Hanouf, and A. Ishak. Mixed convection Jeffrey fluid flow over an exponentially stretching sheet with magnetohydrodynamic effect. *AIP Advances*, 6(3):035024, 2016.
- [33] P. V. Narayana, D. Babu, and B. Venkateswarlu. Soret and Dufour effects on MHD radiative heat and mass transfer flow of a Jeffrey fluid over a stretching sheet. *Frontiers in Heat and Mass Transfer*, 8, 2017.
- [34] S. Jena, S. R. Mishra, and G. C. Dash. Chemical reaction effect on MHD Jeffery fluid flow over a stretching sheet through porous media with heat generation/absorption. *International Journal of Applied and Computational Mathematics*, 3(2):1225–1238, 2017.
- [35] L. Crane. Flow past a stretching plate. *Journal of Applied Mathematics and Physics*, 21:645–647, 1970.
- [36] B. C. Sakiadis. Boundary layer behavior on continuous solid flat surfaces. *American Institute of Chemical Engineers Journal*, 7:26–28, 1961.
- [37] F. K. Tsou, E. M. Sparrow, and R. J. Goldstein. Flow and heat transfer in the boundary layer on a continuous moving surface. *International Journal of Heat and Mass Transfer*, 10:219–235, 1967.
- [38] L. E. Erickson, L. T. Fan, and V. G. Fox. Heat and mass transfer on moving continuous flat plate with suction or injection. *Industrial and Engineering Chemistry Fundamentals*, 5:19, 1966.

- [39] D. Srinivasacharya and M. Uppendar. Thermal radiation and chemical reaction effects on MHD mixed convection heat and mass transfer in a micropolar fluid. *Mechanica*, 19:518–525, 2013.
- [40] R. C. Bataller. Viscoelastic fluid flow and heat transfer over a stretching sheet under the effects of a non-uniform heat source, viscous dissipation and thermal radiation. *International Journal of Heat and Mass Transfer*, 50:3152–3162, 2007.
- [41] B. Venkateswarlu and P. V. Narayana. Influence of variable thermal conductivity on MHD Casson fluid flow over a stretching sheet with viscous dissipation, Soret and Dufour effects. *Frontiers in Heat and Mass Transfer*, 7:16, 2016.
- [42] F. M. Noor, S. A. Kechil, and I. Hashim. Simple nonperturbative solution for MHD viscous flow due to a shrinking sheet. *Communications in Nonlinear Science and Numerical Simulation*, 15:144–148, 2010.
- [43] B. C. Prasannakumara, G. K. Ramesh, and B. J. Gireesha. Melting and radiation effects on stagnation point Jeffrey fluid flow over a stretching sheet in the presence of nanoparticles. *Journal of Nanofluids*, 5(6):993–999, 2016.
- [44] M. Bilal, S. Hussain, and M. Sagheer. Boundary layer flow of magneto-micropolar nanofluid flow with Hall and ion-slip effects using variable thermal diffusivity. *Bulletin of the Polish Academy of Sciences : Technical Sciences*, 65(2):383–390, 2017.
- [45] T. Sarpakaya. Flow of non-Newtonian fluids in a magnetic field. *American Institute of Chemical Engineers*, 7(2):324–328, 1961.
- [46] J. Anderson and F. Wendt. *Computational Fluid Dynamics*. Springer, 1995.
- [47] T. C. Jue. Analysis of combined thermal and magnetic convection ferrofluid flow in a cavity. *International Communications in Heat and Mass Transfer*, 33:846–852, 2006.
- [48] C. E. Nanjundappa, I. S. Shivakumara, and M. M. Ravisha. The onset of ferro convection in a horizontal ferrofluid saturated porous layer heated from below and cooled from above with constant heat flux subject to MHD viscosity. *International Communications in Heat and Mass Transfer*, 37:1246–1250, 2010.

- [49] E. M. A. Elbashbeshy, T. G. Emam, and K. M. Abdelgaber. Effects of thermal radiation and magnetic field on unsteady mixed convection flow and heat transfer over an exponentially stretching surface with suction in the presence of internal heat generation/ absorption. *Journal of the Egyptian Mathematical Society*, 20:215–222, 2012.
- [50] I. L. Animasaun. Effects of thermophoresis, variable viscosity and thermal conductivity on free convective heat and mass transfer of non-Darcian MHD dissipative Casson fluid flow with suction and n th order of chemical reaction. *Journal of the Nigerian Mathematical Society*, 30:187–195, 2013.
- [51] M. Turkyilmazoglu. Nanofluid flow and heat transfer due to a rotating disk. *Computer & Fluids*, 94:139–146, 2014.
- [52] M. Bahiraei, S. Hosseinalipour, and M. Hangi. Numerical study and optimization of hydrothermal characteristics of manganese-zinc ferrite nanofluid within annulus in the presence of magnetic field. *Journal of Superconductivity and Novel Magnetism*, 27:527–534, 2014.
- [53] M. Sheikholeslami, M. G. Bandy, R. Ellahi, and A. Zeeshan. Simulation of MHD copper oxide - water nanofluid flow and convective heat transfer considering Lorentz forces. *Journal of Magnetism and Magnetic Materials*, 369:69–80, 2014.
- [54] R. Azizian, E. Doroodch, T. McKrell, J. Buongiorno, W. Hu, and B. Moghtaderi. Effect of magnetic field on laminar convective heat transfer of magnetite nanofluids. *International Journal of Heat and Mass Transfer*, 68:94–109, 2014.
- [55] A. Malvandi and D. Ganji. Magnetic field effect on nanoparticles migration and heat transfer of water-alumina nanofluid in a channel. *Journal of Magnetism and Magnetic Materials*, 362:172–179, 2014.
- [56] X. Zhang and H. Huang. Effect of magnetic obstacle on fluid flow and heat transfer in a rectangular duct. *International Communications in Heat and Mass Transfer*, 51:31–38, 2014.
- [57] M. K. Nayak, N. S. Akbar, V. S. Pandey, Z. H. Khan, and D. Tripathi. 3D free convective MHD flow of nanofluid over permeable linear stretching sheet with thermal radiation. *Powder Technology*, 315:205–215, 2017.

- [58] T. L. Stewart and H. S. Fogler. Biomass plug development and propagation in porous media. *Biotechnology and Bioengineering*, 72(3):353–363, 2001.
- [59] O. Polyansky and R. Vladimir. Fluid convection in sediment-hosted reservoirs due to thermal action of dikes and sills. *Russian Geology and Geophysics*, 43:25–39, 01 2002.
- [60] A. V. Kuznetsov. Bio-thermal convection induced by two different species of microorganisms. *International Communications in Heat and Mass Transfer*, 38(5):548–553, 2011.
- [61] W. A. Khan and O. D. Makinde. MHD nanofluid bioconvection due to gyrotactic microorganisms over a convectively heat stretching sheet. *International Journal of Thermal Sciences*, 81:118–124, 2014.
- [62] O. D. Makinde and I. L. Animasaun. Bioconvection in MHD nanofluid flow with nonlinear thermal radiation and quartic autocatalysis chemical reaction past an upper surface of a paraboloid of revolution. *International Journal of Thermal Sciences*, 109:159–171, 2016.
- [63] S. Xun, J. Zhao, L. Zheng, and X. Zhang. Bioconvection in rotating system immersed in nanofluid with temperature dependent viscosity and thermal conductivity. *International Journal of Heat and Mass Transfer*, 111:1001–1006, 2017.
- [64] S. Mosayebidorcheh, M. A. Tahavori, T. Mosayebidorcheh, and D. D. Ganji. Analysis of nano-bioconvection flow containing both nanoparticles and gyrotactic microorganisms in a horizontal channel using modified least square method. *Journal of Molecular Liquids*, 227:356–365, 2017.
- [65] M. Ibrahim and K. Suneetha. Heat source and chemical effects on MHD convection flow embedded in a porous medium with Soret, viscous and Joules dissipation. *Ain Shams Engineering Journal*, 7(2):811–818, 2016.
- [66] S. Shah, S. Hussain, and M. Sagheer. MHD effects and heat transfer for the UCM fluid along with Joule heating and thermal radiation using Cattaneo-Christov heat flux model. *AIP Advances*, 6(8):085103, 2016.

- [67] D. Gopal, N. Kishan, and K. Raju. Viscous and Joule's dissipation on Casson fluid over a chemically reacting stretching sheet with inclined magnetic field and multiple slips. *Informatics in Medicine Unlocked*, 9:154 – 160, 2017.
- [68] D. Jing, Y. Pan, and X. Wang. Joule heating, viscous dissipation and convective heat transfer of pressure-driven flow in a microchannel with surface charge-dependent slip. *International Journal of Heat and Mass Transfer*, 108:1305 – 1313, 2017.
- [69] M. Ferdows, A. A. Afify, and E. E. Tzirtzilakis. Hall current and viscous dissipation effects on boundary layer flow of heat transfer past a stretching sheet. *International Journal of Applied and Computational Mathematics*, pages 1–17, 2017.
- [70] S. Goud and R. Shekar. Finite element solution of viscous dissipative effects on unsteady MHD flow past a parabolic started vertical plate with mass diffusion and variable temperature. *i-Manager's Journal on Mathematics*, 7(1):18–25, 2018.
- [71] T. Thumma and R. Mishra. Effect of viscous dissipation and Joule heating on magnetohydrodynamic Jeffery nanofluid flow with and without multi slip boundary conditions. *Journal of Nanofluids*, 7(3):516–526, 2018.
- [72] R. Kumar, R. Kumar, A. Shehzad, and M. Sheikholeslami. Rotating frame analysis of radiating and reacting ferro-nanofluid considering Joule heating and viscous dissipation. *International Journal of Heat and Mass Transfer*, 120:540–551, 2018.
- [73] M. Hafidzuddin and R. Nazar. Numerical solutions of MHD rotating flow and heat transfer over a permeable shrinking sheet. *ScienceAsia*, 40:58–62, 2014.
- [74] C. Y. Wang. Stretching a surface in a rotating fluid. *Zeitschrift für angewandte Mathematik und Physik ZAMP*, 39(2):177–185, 1988.
- [75] R. Nazar, N. Amin, and I. Pop. Unsteady boundary layer flow due to a stretching surface in a rotating fluid. *Mechanics Research Communications*, 31(1):121–128, 2004.
- [76] H. Rosali, A. Ishak, R. Nazar, and I. Pop. Rotating flow over an exponentially shrinking sheet with suction. *Journal of Molecular Liquids*, 211:965–969, 2015.

- [77] C. Sulochana, P. Samrat, and N. Sandeep. Magneto hydrodynamic radiative nanofluid flow over a rotating surface with Soret effect. *Multidiscipline Modeling in Materials and Structures*, 14(1):168–188, 2018.
- [78] S. Seth, R. Kumar, and A. Bhattacharyya. Entropy generation of dissipative flow of carbon nanotubes in rotating frame with Darcy-Forchheimer porous medium: A numerical study. *Journal of Molecular Liquids*, 268:637 – 646, 2018.
- [79] J. Gireesha, G. Kumar, R. Krishnamurthy, and G. Rudraswamy. Enhancement of heat transfer in an unsteady rotating flow for the aqueous suspensions of single wall nanotubes under nonlinear thermal radiation: a numerical study. *Colloid and Polymer Science*, pages 1–8, 2018.
- [80] R. N. Bearon and D. Grunbaum. Bioconvection in a stratified environment: experiments and theory. *Physics of Fluids*, 18(12):127102, 2006.
- [81] K. Kameswaran, B. Vasu, N. Murthy, and R. Gorla. Mixed convection from a wavy surface embedded in a thermally stratified nanofluid saturated porous medium with non-linear Boussinesq approximation. *International Communications in Heat and Mass Transfer*, 77:78–86, 2016.
- [82] V. Madhu and S. Reddy. Influence of thermal stratification on MHD heat transfer flow over an exponentially stretching surface. *International Journal of Scientific Research in Science and Technology*, 4:832–838, 2018.
- [83] Y. S. Daniel, Z. A. Aziz, Z. Ismail, and F. Salah. Thermal stratification effects on MHD radiative flow of nanofluid over nonlinear stretching sheet with variable thickness. *Journal of Computational Design and Engineering*, 5(2):232–242, 2018.
- [84] K. Jagan, S. Sivasankaran, M. Bhuvanewari, and S. Rajan. Effect of non-linear radiation on 3D unsteady MHD nanoliquid flow over a stretching surface with double stratification. *Applied Mathematics and Scientific Computing*, pages 109–116, 2019.
- [85] S. M. Atif, S. Hussain, and M. Sagheer. Magneto hydrodynamic stratified bioconvective flow of micropolar nanofluid due to gyrotactic microorganisms. *AIP Advances*, 9(2):025208, 2019.

- [86] M. Ijaz and M. Ayub. Nonlinear convective stratified flow of Maxwell nanofluid with activation energy. *Heliyon*, 5(1):e01121, 2019.
- [87] R. K. Bansal. *A Textbook of Fluid Mechanics and Hydraulic Machines*. Laxmi Publications (P) LTD, 2005.
- [88] M. Deville and T. B. Gatski. *Mathematical Modeling for Complex Fluids and Flows*. Springer Science & Business Media, 2012.
- [89] J. D. Anderson. Ludwig Prandtl's boundary layer. *Physics Today*, 58(12):42–48, 2005.
- [90] D. C. Ipsen. *Units, Dimensions and Dimensionless Numbers*. McGraw-Hill, London, 1960.
- [91] S. Sattar and S. Rana. Significance of Dimensionless Numbers in the Fluid Mechanics. In *MDSRIC*. University of Wah, Pakistan, November 2019.
- [92] R. Remsburg. *Convection Heat Transfer in Electronic Equipment*, pages 241–395. Springer US, Boston, MA, 1998.
- [93] R. J. Poole. The Deborah and Weissenberg numbers. *British Society of Rheology, Rheology Bulletin.*, 53(2):32–39, 2012.
- [94] J. P. Holman. *Heat Transfer*. McGraw-Hill Education, 2009.
- [95] E. A. Brujan. *Cavitation in Non-Newtonian Fluids: With Biomedical and Bioengineering Applications*. Springer Science & Business Media, 2010.
- [96] V. Bianco, K. Vafai, O. Manca, and S. Nardini. *Heat Transfer Enhancement with Nanofluids*. CRC press, 2015.
- [97] A. Belmiloudi. *Heat Transfer: Mathematical Modelling, Numerical Methods and Information Technology*. BoD–Books on Demand, 2011.
- [98] H. Yan and H. Wu. *Joule Heating and Chip Materials*, pages 1–15. Springer US, Boston, MA, 2013.
- [99] G. W. Sutton and A. Sherman. *Engineering Magnetohydrodynamics*. Courier Dover Publications, 2006.

-
- [100] S. M. Peker and S. S. Helvacı. *Solid-Liquid Two Phase Flow*. Elsevier, 2011.
- [101] Y. A. Cengel and A. Ghajar. *Heat and Mass Transfer: A Practical Approach*. McGraw-Hill Education, 2011.
- [102] C. Dafermos, J. L. Ericksen, and D. Kinderlehrer. *Amorphous Polymers and Non-Newtonian Fluids*, volume 6. Springer Science & Business Media, 2012.
- [103] D. Joseph. *Fluid Dynamics of Viscoelastic Liquids*, volume 84. Springer Science & Business Media, 2013.
- [104] S. Thomas and W. Yang. *Advances in Polymer Processing: From Macro-to Nano-Scales*. Elsevier, 2009.
- [105] P. Elyas and P. Shateri. MHD boundary layer flow and heat transfer of Newtonian nanofluids over a stretching sheet with variable velocity and temperature distribution. *Transport Phenomena in Nano and Micro Scales*, 4(2):28–40, 2016.
- [106] T. Y. Na. *Computational Methods in Engineering Boundary Value Problems*, volume 145. Academic Press, 1980.
- [107] A. Nakayama. *PC-Aided Numerical Heat Transfer and Convective Flow*. CRC press, 1995.
- [108] S. N. Ha. A nonlinear shooting method for two-point boundary value problems. *Computers & Mathematics with Applications*, 42(10-11):1411–1420, 2001.
- [109] K. Das, N. Acharya, and P. K. Kundu. Radiative flow of MHD Jeffrey fluid past a stretching sheet with surface slip and melting heat transfer. *Alexandria Engineering Journal*, 54(4):815–821, 2015.
- [110] H. Brinkman. The viscosity of concentrated suspensions and solutions. *Journal of Chemical Physics*, 20:571–581, 1952.
- [111] K. Khanafer, K. Vafai, and M. Lightstone. Buoyancy driven heat transfer enhancement in a two dimensional enclosure utilizing nanofluids. *International Journal of Heat and Mass Transfer*, 46:3639–3653, 2003.
- [112] J. Maxwell. *A Treatise on Electricity and Magnetism*. Cambridge Oxford University Press London, 1904.

- [113] J. V. Ramana Reddy, V. Sugunamma, N. Sandeep, and C. Sulochana. Influence of chemical reaction, radiation and rotation on MHD nanofluid flow past a permeable flat plate in porous medium. *Journal of the Nigerian Mathematical Society*, 35(1):48 – 65, 2016.
- [114] H. B. Keller. *Numerical Methods for Two-Point Boundary Value Problems*. Dover Publications New York, 1992.
- [115] T. Cebeci and P. Bradshaw. *Physical and Computational Aspects of Convective Heat Transfer*. Springer New York, 1988.
- [116] A. Ishak, R. Nazar, and I. Pop. Hydromagnetic flow and heat transfer adjacent to a stretching vertical sheet. *Heat and Mass Transfer*, 44(8):921, 2008.
- [117] D. Pal and H. Mondal. Hydromagnetic non-Darcy flow and heat transfer over a stretching sheet in the presence of thermal radiation and Ohmic dissipation. *Communications in Nonlinear Science and Numerical Simulation*, 15(5):1197–1209, 2010.
- [118] K. Ahmad and A. Ishak. MHD flow and heat transfer of a Jeffrey fluid over a stretching sheet with viscous dissipation. *Malaysian Journal of Mathematical Sciences*, 10:311–323, 2016.
- [119] A. V. Kuznetsov and D. A. Nield. Natural convective boundary-layer flow of a nanofluid past a vertical plate. *International Journal of Thermal Sciences*, 49(2):243–247, 2010.
- [120] S. A. Gaffar, V. R. Prasad, E. K. Reddy, and O. A. Bég. Free convection flow and heat transfer of non-Newtonian tangent hyperbolic fluid from an isothermal sphere with partial slip. *Arabian Journal for Science and Engineering*, 39(11):8157–8174, 2014.
- [121] M. K. Nayak, N. S. Akbar, V. S. Pandey, Z. H. Khan, and D. Tripathi. 3D free convective MHD flow of nanofluid over permeable linear stretching sheet with thermal radiation. *Powder Technology*, 315:205 – 215, 2017.
- [122] H. B. Keller and T. Cebeci. Accurate numerical methods for boundary-layer flows. *AIAA Journal*, 10(9):1193–1199, 1972.

- [123] J. P. Croisille. Keller's box-scheme for the one-dimensional stationary convection-diffusion equation. *Computing*, 68(1):37–63, 2002.
- [124] T. Cebeci and P. Bradshaw. *Physical and Computational Aspects of Convective Heat Transfer*. Springer Science & Business Media, 2012.
- [125] W. Ibrahim. Magnetohydrodynamics (MHD) flow of a tangent hyperbolic fluid with nanoparticles past a stretching sheet with second order slip and convective boundary condition. *Results in Physics*, 7:3723–3731, 2017.
- [126] M. Ali, R. Nazar, N. Arifin, and I. Pop. MHD boundary layer flow and heat transfer over a stretching sheet with induced magnetic field. *Heat and Mass Transfer*, 47(2):155–162, 2011.
- [127] M. Ijaz, M. Waqas, T. Hayat, M. Imran, and A. Alsaedi. Behavior of stratification phenomenon in flow of Maxwell nanomaterial with motile gyrotactic microorganisms in the presence of magnetic field. *International Journal of Mechanical Sciences*, 131-132:426 – 434, 2017.
- [128] R. Ahmad and M. Mustafa. Model and comparative study for rotating flow of nanofluids due to convectively heated exponentially stretching sheet. *Journal of Molecular Liquids*, 220:635–641, 2016.
- [129] R. Tiwari and M. Das. Heat transfer augmentation in a two sided lid driven differentially heated square cavity utilizing nanofluids. *International Journal of Heat and Mass Transfer*, 50:2002–2018, 2007.
- [130] H. Brinkman. The viscosity of concentrated suspensions and solutions. *Journal of Chemical Physics*, 20:571–581, 1952.
- [131] S. A . Angayarkanni and J. Philip. Review on thermal properties of nanofluids: recent developments. *Advances in Colloid and Interface Science*, 225:146–176, 2015.
- [132] M. Sheikholeslami, D. Ganji, and M. Hatami. Nanofluid flow and heat transfer in a rotating system in the presence of a magnetic field. *Journal of Molecular Liquids*, 190:112–120, 2014.

-
- [133] S. N. Ha. A nonlinear shooting method for two-point boundary value problems. *Computers and Mathematics with Applications*, 42(10-11):1411–1420, 2001.
- [134] M. Turkyilmazoglu. Flow and heat simultaneously induced by two stretchable rotating disks. *Physics of Fluids*, 28(4):043601, 2016.
- [135] S. T. Hussain, R. Haq, Z. H. Khan, and S. Nadeem. Water driven flow of carbon nanotubes in a rotating channel. *Journal of Molecular Liquids*, 214:136–144, 2016.